Institut für Geowissenschaften
Mathematisch-Naturwissenschaftliche Fakulität
Universität Potsdam

Tectonic and Climatic Controls on Orogenic Processes:

The Northwest Himalaya, India

Dissertation

zur Erlangung des akademischen Grades
Doktor der Naturwissenschaften
"*doctor rerum naturalium*"
in der Wissenschaftsdisziplin "*Geologie*"

eingereicht an der
Mathematisch-Naturwissenschaftlichen Fakultät
der Universität Potsdam

von
Dipl.-Geol. Rasmus Christoph Thiede
Geb. 12.01.1972 in Kiel

Potsdam, November 2004

Abstract

The role of feedback between erosional unloading and tectonics controlling the development of the Himalaya is a matter of current debate. The distribution of precipitation is thought to control surface erosion, which in turn results in tectonic exhumation as an isostatic compensation process. Alternatively, subsurface structures can have significant influence in the evolution of this actively growing orogen.

Along the southern Himalayan front new $^{40}Ar/^{39}Ar$ white mica and apatite fission track (AFT) thermochronologic data provide the opportunity to determine the history of rock-uplift and exhumation paths along an approximately 120-km-wide NE-SW transect spanning the greater Sutlej region of the northwest Himalaya, India. $^{40}Ar/^{39}Ar$ data indicate, consistent with earlier studies that first the High Himalayan Crystalline, and subsequently the Lesser Himalayan Crystalline nappes were exhumed rapidly during Miocene time, while the deformation front propagated to the south. In contrast, new AFT data delineate synchronous exhumation of an elliptically shaped, NE-SW-oriented ~80 x 40 km region spanning both crystalline nappes during Pliocene-Quaternary time. The AFT ages correlate with elevation, but show within the resolution of the method no spatial relationship to preexisting major tectonic structures, such as the Main Central Thrust or the Southern Tibetan Fault System. Assuming constant exhumation rates and geothermal gradient, the rocks of two age vs. elevation transects were exhumed at ~1.4 ±0.2 and ~1.1 ±0.4 mm/a with an average cooling rate of ~50-60 °C/Ma during Pliocene-Quaternary time. The locus of pronounced exhumation defined by the AFT data coincides with a region of enhanced precipitation, high discharge, and sediment flux rates under present conditions. We therefore hypothesize that the distribution of AFT cooling ages might reflect the efficiency of surface processes and fluvial erosion, and thus demonstrate the influence of erosion in localizing rock-uplift and exhumation along southern Himalayan front, rather than encompassing the entire orogen.

Despite a possible feedback between erosion and exhumation along the southern Himalayan front, we observe tectonically driven, crustal exhumation within the arid region behind the orographic barrier of the High Himalaya, which might be related to and driven by internal plateau forces. Several metamorphic-igneous gneiss dome complexes have been exhumed between the High Himalaya to the south and Indus-Tsangpo suture zone to the north since the onset of Indian-Eurasian collision ~50 Ma ago. Although the overall tectonic setting is characterized by convergence the exhumation of these domes is accommodated by extensional fault systems.

Along the Indian-Tibetan border the poorly described Leo Pargil metamorphic-igneous gneiss dome (31-34°N/77-78°E) is located within the Tethyan Himalaya. New field mapping, structural, and geochronologic data document that the western flank of the Leo Pargil dome was formed by extension along temporally linked normal fault systems. Motion on a major detachment system, referred to as the Leo Pargil detachment zone (LPDZ) has led to the

juxtaposition of low-grade metamorphic, sedimentary rocks in the hanging wall and high-grade metamorphic gneisses in the footwall. However, the distribution of new $^{40}Ar/^{39}Ar$ white mica data indicate a regional cooling event during middle Miocene time. New apatite fission track (AFT) data demonstrate that subsequently more of the footwall was extruded along the LPDZ in a brittle stage between 10 and 2 Ma with a minimum displacement of ~9 km. Additionally, AFT-data indicate a regional accelerated cooling and exhumation episode starting at ~4 Ma.

Thus, tectonic processes can affect the entire orogenic system, while potential feedbacks between erosion and tectonics appear to be limited to the windward sides of an orogenic systems.

Kurzfassung

Welche Rolle Wechselwirkungen zwischen der Verteilung des Niederschlags, Erosion und Tektonik während der Entwicklung des Himalayas über geologische Zeiträume gespielt haben bzw. heute spielen, ist umstritten. Dabei ist von besonderem Interesse, ob Erosion ausschliesslich in Folge tiefkrustaler Hebungsprozesse entsteht und gesteuert wird, oder ob Regionen besonders effektiver Erosion, bedingt durch isostatische Kompensation, die Lokation tektonischer Deformation innerhalb aktiver Orogene beeinflussen können.

Entlang der südlichen Himalayafront ermöglichen neue thermochronologische $^{40}Ar/^{39}Ar$-Hellglimmer- und Apatite-Spaltspur-Alter die Bestimmung der Exhumationspfade entlang eines 120-km-langen NE-SW-gerichteten Profils, dass quer durch die gesamte Sutlej-Region des nordwestlichen, indischen Himalayas verläuft. Dabei deuten die $^{40}Ar/^{39}Ar$-Daten in übereinstimmung mit früheren Studien darauf hin, dass zuerst das Kristallin des Hohen Himalayas und anschliessend, südwärts propagierend, das Kristallin des Niederen Himalayas während des Miozäns exhumiert worden ist. Im Gegensatz dazu weisen die neuen Apatit-Spaltspur-Alter auf eine gleichmässige und zeitgleiche Exhumation beider kristallinen Decken entlang des Sutlejflusses. Dieser 80x40 km weite Bereich formt einen elliptischen, nordost-südwest orientierten Sektor erhöhter Exhumationsraten während des Pliozäns und Quartärs. Innerhalb des Fehlerbereichs der Spaltspurmethode zeigen die Alter eine gute Korrelation mit der Höhe, zeigen aber gleichzeitig keine Abhängigkeit zu bedeutenden tektonischen Störungen, wie die „Main Central Thrust“ oder dem „Southern Tibetan Fault System“. Unter der vereinfachten Annahme konstanter Exhumationsraten deuten zwei verschiedene Höhenprofile auf Exhumationraten in der Grössenordnung von ~1,4 ±0,2 und ~1,1 ±0,4 mm/a bei einer durchschnittlichen Abkühlrate von ~50-60 °C/m.y. während des Pliozäns bzw. Quartärs hin. Der anhand von Spaltspuraltern bestimmte Sektor verstärkter Exhumation korreliert mit dem Gebiet, das während des Holozäns hohen Niederschlags-, Erosion- bzw. Sedimenttransportraten ausgesetzt ist. Daher vermuten wir, dass die Verteilung von jungen Spaltspuraltern den regionalen Grad der Effiziens von Oberflächenprozessen und fluviatiler Erosion wiederspiegelt. Dies deutet auf einen Zusammenhang zwischen Erosion und der

Lokalisierung von Hebung und Exhumation entlang der südlichen Front des Himalayas hin, und zeigt gleichzeitig, dass die Exhumation nicht einfach über die gesamte Front gleichmässig verteilt ist.

Trotz der Wechselwirkungen zwischen Exhumation und Erosion, die möglicherweise die Entwicklung der südlichen Himalayafront beeinflussen, beobachten wir auch tiefkrustale tektonische Exhumation in ariden Gebieten nördlich des Hohen Himalayas, die vermutlich im Zusammenhang mit plateauinternenen Deformationsprozessen steht. So haben sich zum Beispiel mehrere metaplutonische Gneissdomkomplexe zwischen dem Hohen Himalaya im Süden und der Indus-Tsangpo Suturzone im Norden seit der Indien-Asien Kollision vor ca. 50 Millionen Jahren entwickelt. Obwohl die Dome sich grossräumig in einem kommpressiven Spannungsfeld befinden, werden sie lokal entlang von Extensionsstrukturen exhumiert. Bis heute sind die Ursachen für die Entstehung dieser Prozesse umstritten.

Entlang der Indisch-Tibetischen Grenze erstreckt sich der fast vollkommen unbeschriebene Leo-Pargil-Gneissdomkomplex (31-34°N/77-78°E) innerhalb des Tethyschen Himalayas. Neue Geländekartierungen, strukturelle und geochronologische Daten der westliche Flanke des Leo Pargil Domes dokumentieren, dass dieser sich entlang zeitlich verbundener Abschiebungssysteme in einem extensionalen Regime entwickelt hat. Im Gelände wird der Dome von einem mächtigen Störungssystem begrenzt, die “Leo Pargil Detachment Zone” (LPDZ). Durch den tektonischen Versatz entlang der LPDZ liegen heute niedriggradig metamorphe Sedimentgesteine im Hangenden neben hochgradigen Gneisen in Liegenden. Unabhängig von der Probenlokation entlang des aufgeschlossenen Störungssystemes ergeben alle neuen $^{40}Ar/^{39}Ar$-Hellglimmeralter um die 15 Ma und deuten auf ein regional wichtiges Abkühlungsereignis hin. Im Gegensatz dazu deuten die neuen Apatit-Spaltspuralter (AFT) auf eine kontinuierliche Exhumation der hochmetamorphen Einheiten im Liegenden der LPDZ unter sprödtektonischen Bedingungen zwischen 10 und 2 Ma hin, bei einem minimalen Versatz von ungefähr 9 km. Desweiteren deuten die Apatit-Spaltspur-Daten auf überregionale beschleunigte Abkülhlungs- bzw Exhumationsphase seit 4 Ma.

Daraus kann gefolgert werden, dass die tektonischen Prozesse die Entwicklung des gesamten Gebirges beflussen können, während potenzielle Wechselwirkungen zwischen Erosion und Tektonik auf die luvwärtigen Gebirgsflanken beschränkt zu bleiben scheinen.

Table of Contents

Table of Figures

Table of Tables

Preface

When I first visited India in 1997 as a field assistant to a field campaign of my Austrian friends and colleagues from Vienna, I immediately fell in love with both India and the Himalaya. We worked for six weeks in the remote and highly elevated Spiti and Lahaul, the northern districts of Himachal Pradesh, north of the High Himalaya. Working in the beautiful Pin Valley was the highlight of our trip, and at the end I was particularly impressed by the friendliness of local spiti-people who lived under the simplest of conditions, for hundreds of years in this breathtaking, mountainous landscape. My experiences and adventures in both the Himalaya and India, and having the opportunity to meet these people both in the low and highlands of India, have left a deep impression and fascination for this region of our wonderful planet. I will treasure these memories for the rest of my life. However, at that time I had never dreamed of having the opportunity to return to India, and work in the Himalayas for my PhD.

On our return journey we had to stay in Delhi for several days. In one of the many bookshops around the Connaught Place I found a 700 hundred page thick biography of Mahatma Gandhi, reprinted in India and written in English. The people, who know me, know that I am still to a degree, struggling with the English language. However, I realized that there is no way to get around English and so I decided that I would do my best to learn it. This book has accompanied me during my entire graduate studies. My plan was to have finished reading this book, which I did during my last field season in 2002, before the end of my PhD.

Acknowledgements

I thank my close friend and colleague Bodo Bookhagen for the great time we had together when carrying out this project. Thanks for the endless discussions, support and enormous motivation he gave me to do all my work and to go through all highs and lows of the last three years.

I am especially grateful to Manfred Strecker, my thesis advisor for all his sustained support and encouragement to help us carry out all parts of our PhD, sharing his great knowledge and enthusiasm in all kinds of fields of geology.

I thank Ramon Arrowsmith for his support and friendship. Thanks for inviting me not only to work at ASU but also for his great hospitality and for shearing his house with me for six months. Thanks for providing these opportunities and allowing me to have a deep detailed look into his country during difficult times.

I would like to thank Edward Sobel for his patient teaching of the fission track method, Anke Friedrich for discussion and support, Mike McWilliams for introducing Ar/Ar-Method and Ken Farley for U/Th-He.

I owe a great deal to conversations and discussions with Arvid Jain, Sandeep Singh from the IIT Roorkee, India, and all my other Indian friends. My thanks go also to Tashi Tsering and Ram Singh Slathia, the greatest Indian mountain guides, who made our field time extremely effective and successful.

Thanks to Bernhard Grasemann, “Jambo” (Christoph) Janda, Christian Hager, Erich Draganitz for introducing us to the spectacular geology of the Himalaya and joining fieldwork.

I offer my gratitude to Miriam Dühnforth, Estelle Mortimer, Barbara Carrapa, Lindsey Schoenbohm, Peter Blisniuk, Monica Vasques-Parra, Britta Bookhagen, Michel Knigge, Elina Zwickert and Angela Landgraf, Esther Hintersberger, Nadja Insel, Jörn Hauer, for help during fieldwork; to Birgit Fabian, Christine Fischer, Antje Müller and Volkmar, Annette, Silvia and all the other friends.

I am very grateful to my parents Sigrid und Jörn, all my brothers Hannes, Fridtjof and Morten, and the rest of my family for their sustained support and help during all phases of this work.

Finally, I thank the German Research Foundation (DFG) for the financial support (Grant #STR-11/4) for this project.

1. INTRODUCTION

It had long been established that erosion responds to any deformational change. However, one of the most important findings over the past two decades has been recognition of a dynamic coupling between climatically-driven erosion and tectonic processes, which perhaps can take a first order role during orogen evolution (Beaumont et al., 1992; Beaumont et al., 1996b; e.g., Koons, 1989; Koons, 1990; Masek et al., 1994; Willett et al., 1993). As a consequence of collisional tectonics, topography grows and forms orographic barriers, which then possibly enhance and/or divert global atmospheric circulation and precipitation patterns (e.g., Dahlen and Suppe, 1988; Hoffman and Grotzinger, 1993; Molnar and England, 1990; Willett, 1999). Recent field studies in New Zealand's Southern Alps (Tippet and Hovius, 2000), Taiwan (e.g., Dadson et al., 2003; Willett et al., 2003), the Olympic and Cascade Mountains in North America (e.g., Brandon et al., 1998; Reiners et al., 2003), the Tien Shan (Pavlis et al., 1997; Strecker et al., 2003), and the Himalayas (Burbank et al., 2003; Hodges et al., 2004; Thiede et al., 2004; Wobus et al., 2003; Zeitler et al., 2001a) have documented a correlation between regions affected by high erosion and exhumation rates. In addition, analog and numerical simulations using coupled tectonic and surface process models (e.g., Beaumont et al., 1992; Beaumont et al., 2001; Hoth et al., revised; Koons, 1989; Koons, 1990; Koons et al., 2002; Whipple and Meade, 2004; Willett, 1999) have demonstrated that the mechanics of orogens can be powerfully influenced by surface processes. Thereby the location of erosion with respect to the convergence geometry acts as a first-order parameter controlling pro-wedge and/or retro-wedge evolution (Beaumont et al., 1992; Willett et al., 1993; Willett, 1999).

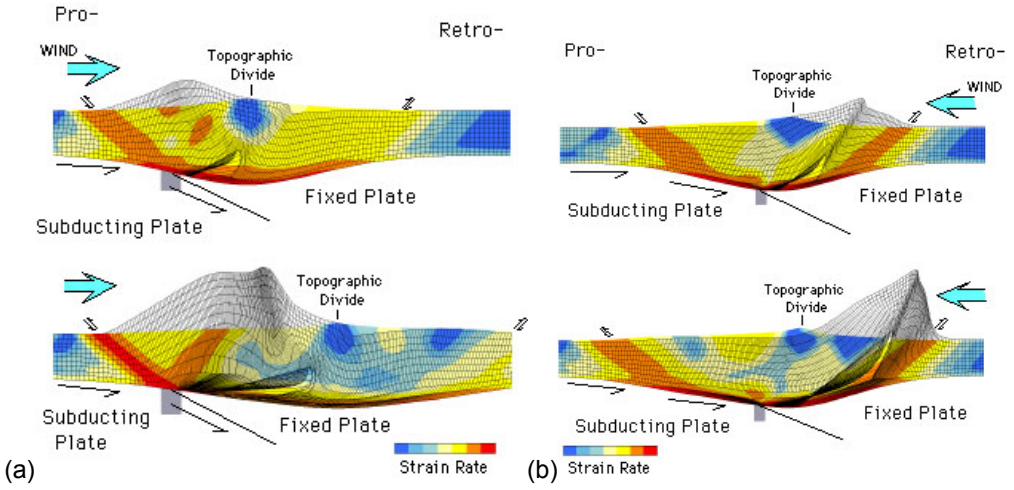

Fig. 1. Coupled finite element model for deformation and erosion of an orogenic mountain range (after Willett, 1999). (a) Pro-wedge erosion: precipitation and erosion are focused on the orogenic wedge above the subducting plate (the pro-wedge). (b) Retrowedge erosion; precipitation and erosion are focused on the orogenic wedge above the overriding plate (the retro-wedge). Colors show distribution of strain within the overriding plate; red high strain, blue low strain, grey eroded upper plate.

Accordingly, any asymmetry of erosion would have a pronounced influence on the distribution of deformation and exhumations rates within the wedge (Hoth et al., revised; Whipple and Meade, 2004). These models have indicated that erosion can control the distribution and propagation of deformation as well as exhumation within orogenic wedges (Hoth et al., revised; Whipple and Meade, 2004).

The linkage and feedback between erosion and tectonic setting depends on the efficiency of erosion (Whipple and Meade, 2004), which is a function of the amount and distribution of precipitation regulating the fluvial discharge and the tectonic setting producing and sustaining high topography, steep relief, and longitudinal river profiles over geologic time. On a continental scale the amount and distribution of precipitation is determined by the relationship and interaction between orientation of the orogen, the global atmospheric circulation pattern, and source area of the moisture such as oceans. Regionally, the distribution of topography and elevation strongly influence the precipitation pattern (Barros and Lettenmaier, 1993; Barros and Lettenmaier, 1994; Bookhagen et al., in review) and generally erosion processes are concentrated on the windward slopes of a mountainous region (Willett, 1999). Thus in conclusion, this wide range of possible preconditions and settings illustrates the high variability of the efficiency of erosion and tectonic interaction, and the wide range of possible effects on the evolution of an orogenic system.

Dahlen and Suppe (1988) demonstrated that erosion rate can control the width of a steady state orogenic wedge, and that deformation patterns are largely influenced by surface erosion. Analytic solutions for the steady state orogen demonstrate that width, orogen-scale strain partitioning, and rock-uplift rates are controlled by the mass balance within an orogenic wedge at flux steady state (Willett and Brandon, 2002). This solution combines the geometric constraints of the critical taper theory and erosion consistent with this topography to find the wedge width required to satisfy the mass balance conditions. As an oversimplification for their models, they assume that erosion is homogenously distributed across the range. However, several studies have demonstrated that bedrock channels play a key role in determining the erosion pattern because they dictate much of the relief structure of mountainous regions, communicate signals of tectonic, climate and eustatic changes across landscapes, and set regional rates of denudation (Burbank et al., 1996b; Whipple and Tucker, 1999). This implies that erosion depends on local circumstances rather then regional conditions.

Many geomorphologists assume that erosion rates is controlled by the stream-power model of bedrock-channel incision (e.g., Hack, 1957; Howard et al., 1994; Howard and Kerby, 1983; Whipple and Tucker, 2002), however the stream-power model should be considered as a simple, empirical, and incomplete approximation to the behavior of a complex suite of processes controlling erosion (Hancock et al., 1998; Sklar and Dietrich, 1998; Whipple et al., 2000; Whipple and Tucker, 2002).

Therefore, if over geologic time a mountain front is affected by sustained high erosion rates, an orogen can develop towards a flux and topographic steady state where the accretion

influx is balanced by the erosional removal of material, thus controlling the orogen width, the distribution of rock-uplift and exhumation rates, as well as the strain partitioning within the orogen (Beaumont et al., 1996a; Beaumont et al., 1992; Dahlen and Suppe, 1988; Hoth et al., revised; Whipple and Meade, 2004; Willett, 1999).

Climatic, topographic and thermochronologic data from New Zealand's Southern Alps, Taiwan's Central Range, the Olympics and Cascade mountains in North and the Andes in South America suggest the existence of a link between the distribution of erosion and rock-uplift rates (Brandon et al., 1998; Koons, 1995; Montgomery et al., 2001; Willett and Brandon, 2002; Willett et al., 2001). Indeed, for example, the dramatic along-strike variability in orogen width, depth of exhumation, and rock uplift rate that characterize the Andes has been attributed to along-strike differences in climate (Dahlen and Suppe, 1988; Hilley and Strecker, 2004; Horton, 1999; Masek et al., 1994; Montgomery et al., 2001). Orogen-scale rock uplift rates are dictated by the erosion rate rather than vice versa, as commonly assumed (Whipple and Tucker, 1999; Willgoose et al., 1991).

The Himalayan orogen today is the highest, and probably one of the most dynamic orogens on Earth. It provides outstanding opportunities to improve and test hypothesizes describing the interaction and feedback between erosion and tectonics. Since the beginning of continental collision between India and Eurasia, approximately 50 m.y. ago, India has continued to move northwards relative to a stable Eurasia (e.g., Lefort, 1975; Molnar and Tapponier, 1975). A convergence rate of approximately 50 mm/yr has resulted in approximately 2500 km of convergence since the onset of collision (Klootwijk et al., 1985; Patriat and Achache, 1984), causing continental deformation throughout central and south-east Asia and forming the Himalayan orogenic wedge along the southern termination of the Tibetan Plateau.

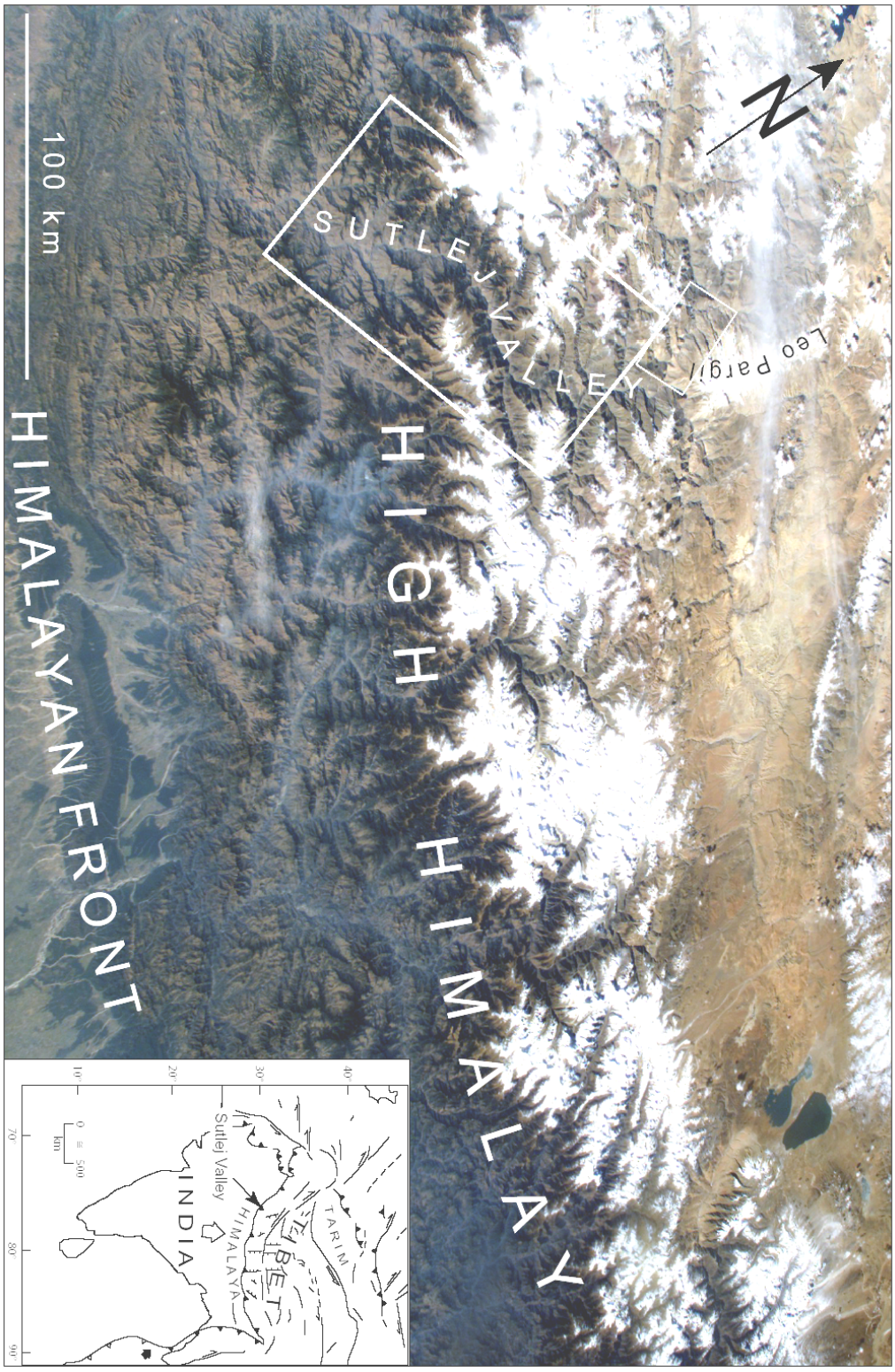

Fig. 2. (a) Terra satellite image of the Himalaya looking towards the N from the Nasa (Astronaut Photography of Earth ISS007_ISS007-E-16052). To the south humid and vegetated southern Himalayan front (dark colors) and the norht, arid and unvegetated sectors (light colors) to the north of the Himalayan orographic barrier. White boxes show study arias.

As a consequence of extended continual deformation and formation of Tibetan Plateau, the atmospheric global circulation pattern was modified, and the Asian monsoon was established in the late Miocene (Dettman et al., 2003; Dettman et al., 2001). However, vast sedimentary basins have been filled since the Miocene, such as the Himalayan foreland basin (Burbank et al., 1996a), the Bengal and Indus fan, respectively, (Clift et al., 2002; Einsele et al., 1996; Metivier et al., 1999). Thus, the Himalaya must have formed an important orographic barrier, which has been affected by sustained high precipitation, erosion, and sediment-flux rates since that time. Previously, any erosional impact on the evolution of the Himalayan orogen had been neglected, and researchers assumed that erosion responds primarily to deformational change, such as the establishment of new thrust systems (e.g., Meigs et al., 1995). However, more recent Himalayan orogen-scale studies assume a close feedback between erosion and exhumation although the effects of erosion on the geodynamic evolution of the southern Himalayan front remain highly controversial (Burbank et al., 2003; Hodges et al., 2004; Thiede et al., 2004; Vannay et al., 2004; Wobus et al., 2003; Zeitler et al., 2001a). This controversy between the role of tectonics, erosion, exhumation and climate constitutes the fundamental motivation for undertaking this thesis. Raising the following open questions formed the framework to my work.

1. Do we find constraints to role out any erosional impact on the geodynamic evolution of the Himalaya?
2. Are erosion rates homogeneously distributed throughout the entire southern Himalayan front, or if not, what kind of consequences on the kinematic evolution of the orogen are expected?
3. How well can deformation compensate a regionally focused distribution of erosion?
4. How and where is the erosion in an orogen most efficient and concentrated?
5. Is rock uplift rate more strongly controlled by erosional efficiency or by accretionary flux?
6. It has remained unclear whether the details of the erosion processes (e.g., climatic variablity controlling erosion processes on different time scales between 10^0 and 10^5 years) are important to the geodynamic evolution of the orogen?
7. How localized can erosion be while still having an effect on the uplift rates, or how localized can exhumation be compensate for localized erosion, on a 10^0, 10^1, or 10^2 km scale?
8. What is the primary control on the evolution of the orogen: the architecture of the orogenic wedge or the distribution of precipitation and erosion?

In order to address these questions I used low-temperature thermochronology such as apatite fission track (AFT), $^{40}Ar/^{39}Ar$ also U/Th-He to constrain the average long-term cooling rates of a rock column relative to the thermal isograde. Thereby I used the circumstance that

the different geochronometers have different closure temperatures (Dodson, 1973) to place constraints on the temporal movement of the rocks passing specific temperatures on their cooling pass through the upper crust. Using low-temperature thermochronology provides the opportunity to date the youngest rock-exhumation and thus potentially cooling affected by surface processes such as river incision. Even if these methods do not provide any direct measurement or constraints on regional surface uplift rates, they provide age data that may be related to relative rock-uplift and exhumation via the concept of closure temperatures (Dodson, 1973). In my study rock-uplift and exhumation rates were analyzed across a 120-km-long SW-NE transect normal to the strike of the NW-Himalayan orogen in India. As a second study, the poorly known Leopargil metamorphic gneiss dome and its structural evolution and exhumation was documented with help of new geologic mapping, collected structural data, and AFT and $^{40}Ar/^{39}Ar$-analysis constraining the timing of exhumation. My results and conclusions are subdivided into three publications presented here in the form of three chapters.

First, I investigated whether along the southern front of the High Himalaya a correlation between areas of rapid rock-uplift and exhumation and recent focused precipitation exists. As discussed above, the recent global atmospheric circulation pattern was established during the late Miocene (Dettman et al., 2003; Dettman et al., 2001), and I therefore assumed a sustained distribution of precipitation and erosion over geologic time. As a consequence of sustained focused erosion affecting the Himalaya, the orogenic wedge is compensating the erosional removal by high rock-uplift and exhumation rates indicating that erosion guides the exhumation along the southern Himalayan front (chapter 5).

Second, the compilation of my own and published thermochronology data and exhumation paths reveals important implications for the geodynamic evolution of the Himalayan orogenic wedge, and suggests a transition from a growing and propagating to a semi-stagnating orogenic wedge (chapter 6).

The third study describes the geodynamic evolution and exhumation of the Leopargil metamorphic gneiss dome. There, I was able to demonstrate that the Leopargil dome developed as a consequence of sustained E-W extension since middle Miocene time. Our results have important implications for testing models that are trying to explain the observed deformation pattern of the southern Tibetan Plateau (chapter 7).

2. THE HIMALAYA-TIBETAN OROGEN

The Himalayan fold and thrust-belt is situated between the Indian shield to the south and the Indus-Tsangpo suture zone to the north (Fig. 2). Since the onset of collision between Eurasia and India, four major north-dipping thrust systems have primarily controlled the evolution of the Himalayan orogenic wedge: the Southern Tibetan Fault System (STFS), Main Central Thrust (MCT), Main Boundary Thrust (MBT), and the Main Frontal Thrust (MFT; Fig. 3). Balanced cross-sections and seismicity data indicate that the MFT and MBT fault systems are rooted in a low angle, basal detachment, referred to as the Main Himalayan Thrust (MHT), which has detached all major Himalayan tectonostratigraphic domains from the underthrusting Indian plate and incorporated them into the orogen (Brunel, 1986; DeCelles et al., 2001; Molnar and Lyon-Caen, 1989; Schelling, 1992; Schelling and Arita, 1991; Srivastava and Mitra, 1994). Whether or not the Main Central Thrust and Southern Tibetan Fault system also root into this basal detachment system, as previously assumed, has been called into question (Searle and Godin, 2003; Searle et al., 2003).

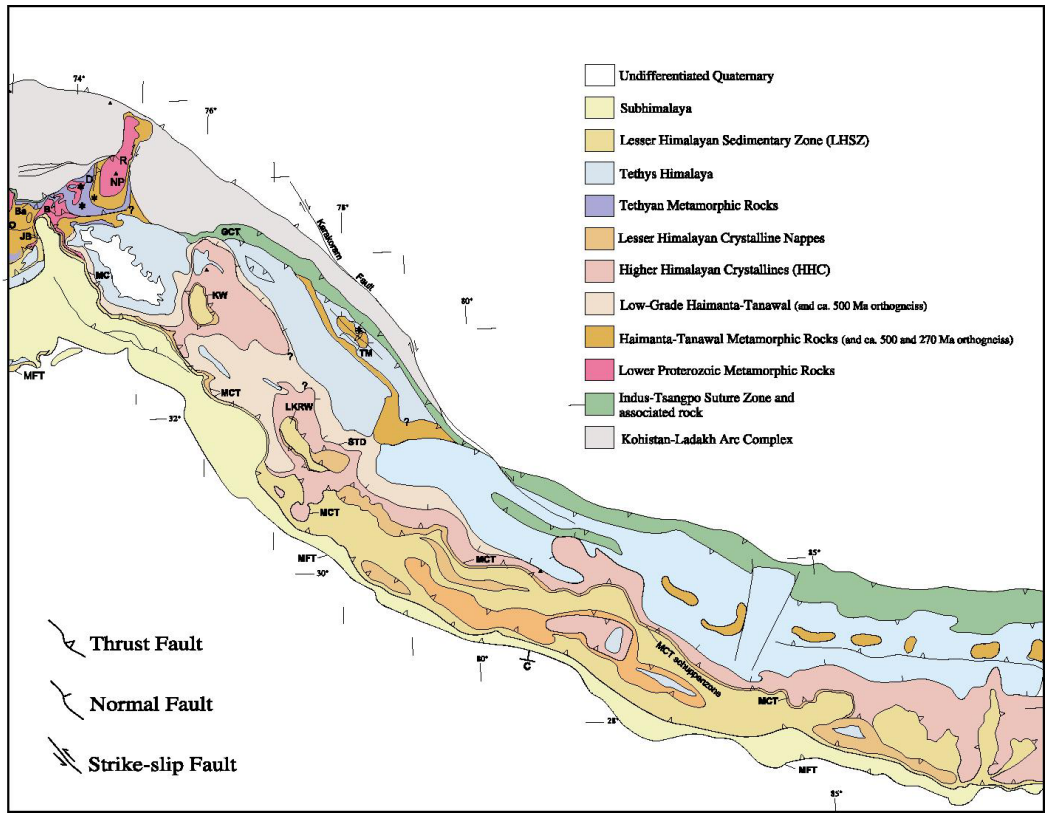

Fig. 3 Simplified tectonic map of the central and western Himalaya (after DiPietro and Pogue, 2004 and ref. therein). Major faults from south to north are Main Frontal Thrust (MFT), Main Boundary Thrust (MBT), Main Central Thrust (MCT), Southern Tibetan Faults System (STFS), Great Counter Thrust System (GCT). Other faults and location from east to west are Indus Syntaxis (IS), Oghi Fault (O), Banna Fault (Ba), Jhelum-Balakot Fault (JB), Batal Fault (B), Diamir Fault (D), Raikot Fault (R), Nanga Parbat (NP), Jammu Thrust (JT), Tso Morari region (TM), Kishtwar Window (KW), Larji-Kulu-Rampur-Window (LKRW).

The crustal faults bound the Himlayan tectonostratigraphic domains that are exposed along the entire length of Himalayan chain (Fig. 3): (a) Indus-Yarlung suture zone (b) Tethyan Himalaya (c) the Himalayan crystalline core, (d) Lesser or Lower Himalaya (LH), (e) the Sub-Himalaya (SubH).

2.1 Indus-Yalu suture zone

The Indus-Yalu suture zone forms the geologic boundary between rocks related to the Indian plate to the south and the Eurasian plate to the north, and contains ophiolites and associated rocks of the Neo-Tethys Ocean. Where the suture zone is preserved, it is bounded by two Cenozoic thrusts. Along the northern side, the north-dipping Gangdese thrust (Harrison et al., 1992; Yin et al., 1994) is juxtaposes the Gangdese batholith over suture-zone rocks or the Xigaze forearc strata. Between 30 Ma and 24 Ma the displacement along the Gangdese thrust caused extensive denudation of the Gangdese batholith in its hanging wall, and underthrusting of the Xigaze forearc strata in its footwall (Yin et al., 1999; Yin et al., 1994). Along the southern side, the younger south-dipping Great Counter Thrust is juxtaposing the Tethyan Himalaya over the melange complex associated with the suture zone (Heim and Gansser, 1939; Ratschbacher et al., 1994). The thrust was active at least during the Miocene, although its timing is still poorly constrained (Quidelleur et al., 1997; Yin et al., 1999).

2.2 The Tethyan Himalaya

To the south follows the Tethyan Himalaya situated between the Southern Tibetan Fault System and the Great Counter Thrust. The Tethyan Himalaya consists of late Precambrian to lower Paleozoic sedimentary and metasedimentary rocks (Burchfiel et al., 1992; Gansser, 1964; Steck et al., 1993) and a thick Permian to Eocene continental-margin sequences (e.g., Brookfield, 1993; Steck, 2003 and ref. therein). The entire sequence is commonly referred to as the Tethyan Sedimentary Sequence. These sediments were generally affected by only very low-grade metamorphic conditions as a consequence of thin-skinned tectonics forming the Tethyan fold-and-thrust belt early, Eo-Himalayan stages of shortening (e.g., Ratschbacher et al., 1994; Wiesmayr and Grasemann, 2002). The age of deformation generally decreases from north to south, from the late Eocene to the early Oligocene. At least three major SW directed nappe structures developed in the NW-Himalaya due to upper crustal deformation during underthrusting (i.e., the Tso Morari, Tetraogal, and Mata Nappes) (Steck et al., 1998). The appearance of schists and gneisses in the Tethyan Himalaya are interpreted to be associated with tectonic displacement and exhumation on syn-collisional extensional structures such as the Gurla Mandhata (Murphy et al., 2002), Kangmar Dome (Chen et al., 1990; Lee et al., 2000), and the Leo Pargil Dome (this study), which postdate the Tethyan fold-and-thrust belt. Gneiss domes have been interpreted as representing the footwall ramp of the Main Central Thrust (Wu et al., 1998). Along the Sutlej section, the base of the Tethyan Himalaya consists mainly of metapelites and metapsammites derived from a thick and homogeneous sequence of upper Proterozoic to lower Cambrian siltstones and sandstones

that are intruded by the Kinnaur Kailash Granite, which yielded Rb-Sr ages of 453 ± 9 Ma and 477 ± 29 Ma (Kwatra et al., 1999).

2.3 The Himalayan crystalline core

The Himalayan crystalline core is exposed between the Southern Tibetan Fault System and the Munsiari Thrust, a thrust system in the footwall of the Main Central Thrust. In the NW-Himalaya the Himalayan crystalline core is composed of two distinct lithotectonic gneiss units that are characterized by different cooling histories (Srivastava and Mitra, 1994; Valdiya, 1980b; Vannay and Grasemann, 1998, 2001b) (Fig. 3). The upper unit corresponds to the High Himalaya Crystalline Sequence (HHCS), a thick, NE-dipping sequence of highly deformed, amphibolite facies to migmatitic ortho- and para-gneisses. The HHCS is bounded at its base by the MCT (Catlos et al., 2001; Coleman, 1998; Hubbard and Harrison, 1989) and at its top by the STDS (Burchfiel et al., 1992; Burg et al., 1984a; Dezes et al., 1999). Toward the foreland, the MCT becomes a shallow-dipping thrust, separating the HHCS from the low- to medium-grade metamorphic sediments of the Lesser Himalaya. However, in some Himalayan sections, a gradual metamorphic transition is observed between the HHCS and the base of the Tethyan Himalaya (Frank et al., 1995), and these units are characterized by comparable Sr, Nd and O isotopic signatures (Ahmad et al., 2000; Robinson et al., 2001). Thus it has been interpreted that the HHCS para- and orthogneisses mostly represent metamorphic equivalents of the Upper Proterozoic to Cambrian sediments that form the base of the Tethyan Himalaya. These units are intruded by Cambro-Ordovician granitic plutons. Beneath the MCT, the lower unit of the Himalayan crystalline core is predominantly composed of amphibolite facies augen- and paragneisses that are related to the Lesser Himalayan Crystalline Sequence (LHCS). The base of the LHCS is bounded by the Munsiari Thrust (Valdiya, 1980b; Vannay and Grasemann, 1998). $^{40}Ar/^{39}Ar$-data constrain a late Miocene to present kinematic evolution and exhumation along the Munsiari Thrust (Copeland and Harrison, 1990; Metcalfe, 1993; Vannay et al., 2004).

2.4 The Lesser Himalaya

The Lesser Himalaya is bounded by the Main Boundary Thrust at the base and by the Main Central Thrust at the top, and consists mainly of Precambrian clastic sediments and medium-grade metasedimentary rocks, granitic gneisses, and granites (Brookfield 1993). Crystalline nappes forming complex synformal klippes that have been thrusted southward over less metamorphosed Lesser Himalayan sequence rocks have been associated with erosional outliers of the High Himalayan Crystalline (Gansser, 1964; Stöcklin, 1980; Schelling, 1992) or the Lesser Himalayan Crystalline (Valdiya, 1980b). The contact to the Subhimalaya is marked by north-dipping, cataclastic faults, which are associated with the Main Boundary thrust system (DeCelles et al., 2001; Huyghe et al., 2001; Srivastava and Mitra, 1994). On the basis of sedimentation patterns in the Subhimalayan zone, Meigs et al. (1995) suggested that the MBTS may have developed as early as 11-9 Ma. Along the Sutlej Valley the Lesser Himalaya sequence mainly consists of massive quartz-arenites intruded by basalts dated at

1800 ± 13 Ma (Miller et al., 2000).

2.5 Sub-Himalayan zone

The Sub-Himalayan zone is defined as a 10- to 25-km-wide belt of Neogene and Quaternary molasse sediments exposed between the Main Boundary Thrust and the Main Frontal Thrust system (e.g.,Burbank et al., 1996a; DeCelles et al., 1998b; Yeats et al., 1992). The Subhimalaya forms the southern toe of the Himalayan orogenic wedge. In general, two stratigraphic sequences have been described: (1) the uppermost Paleocene or lower Eocene to lower Miocene siltstones and sandstones of the Rawalpindi Group, and the (2) lower Miocene to Pleistocene, upward coarsening succession of fluvial siltstones, sandstones and conglomerates of the Siwalik Group (Burbank et al., 1996a). Paleocurrent data and sediment petrographic analyses indicate that these rocks were derived from the southern front of the developing Himalayan fold-and-thrust belt and deposited within the flexural foredeep on the Himalayan foreland basin (DeCelles et al., 1998a; DeCelles et al., 1998b). The Main Frontal thrust system is interpreted to form the surface expression of a low-angle, basal thrust with no basement involvement, along which the Indian plate is subducted beneath the Himalaya and southern Tibet (Molnar, 1984; Yeats and Lillie, 1991). There is no direct geologic evidence related to the initiation age of slip on the Main Frontal thrust system, although it is usually assumed to be a Pliocene-Holocene structure (Molnar, 1984).

3. EROSION AND ROCK UPLIFT IN OROGENESIS

At the orogen-scale, erosion and rock-uplift are intimately linked. Analog and numerical models simple orogenic systems reveal the nature of this linkage (Beaumont et al., 2001; Hoth et al., revised; Whipple and Meade, 2004; Willett, 1999). These models assume that an orogen is of constant width, isostatically compensated, deformed by homogeneous pure shear deformation, and has a fixed accretionary influx rate. Without erosion, the near-surface rock uplift rate is determined by the isostatic compensation of crustal thickening (Whipple and Meade, 2004). The orogenic wedge will develop by internal shortening, where rocks in the hinterland are uplifted to an elevation at which the gravitational potential energy reaches a critical level (Dahlen, 1990; Dahlen and Suppe, 1988). To accommodate further shortening beyond this critical point, the deformation will propagate toward the foreland, and as a consequence the orogenic wedge also grows and propagates foreward.

In models where erosion increases with topographic slope angle or relief, the system evolves to a steady state when the topographic slope has increased such that erosional efflux matches the accretionary influx. Under these conditions, all accreted material is removed via the surface rather than being stored in the crustal root, and steady-state rock uplift rate increases by a factor of ~6 (Molnar and England, 1990). As a possible consequence deformation is localized on the same structures for a long duration, preventing the propagation of deformation. In this case rock uplift is primarily a response to erosion. Thus the relative efficiency of erosion on the orogen exerts a fundamental control on steady state wedge width, topographic relief, and patterns of internal deformation within the wedge. Dynamic coupling between erosional efficiency and rock-uplift rate can only occur where the intensity of spatial distribution of erosion can induce a concentration of strain, either through a narrowing of the orogen or through the development of discrete shear zones that accommodate focused erosion by thrust advection of material, as seen in some coupled thermomechanical surface process models (Beaumont et al., 1996a; Willett, 1999). Thereby the critical taper theory (Dahlen, 1990; Dahlen and Suppe, 1988; Dahlen et al., 1984; Davis et al., 1983) provides the framework for considering how erosional efficiency may influence orogen width, rock uplift rate, and deformation within the wedge, allowing an exploration of the dynamic coupling between climate-driven erosion and tectonics.

However, the role of the controlling parameters that place constraints on the distribution of erosion over geologic time scale remains controversial. For example, how strongly is the distribution of erosion influenced by the distribution of precipitation across an orogen? Most geomorphologists believe that river incision rates are constrained by the relationships of the stream-power-law (Hack, 1957; Howard, 1998; Howard et al., 1994). Thereby the average fluvial discharge is controlled both by the precipitation pattern, by the size of the catchment area, and average gradient and width of the longitudinal river profiles. However, the topography and climate can strongly influence the distribution of precipitation and potentially

cause high discharge rates to occur in comparatively small catchment areas (Barros and Lettenmaier, 1994). In addition, fluvial runoff and sediment-flux rates are positively correlated (Bookhagen et al., in review). Over geologic timescales the distribution and amount of precipitation are subjected to climatically controlled fluctuations. During phases of enhanced precipitation increased sediment flux and higher frequency of flood events are expected to create favorable conditions for deep-seated river incision and erosion. Enhanced discharge and sediment flux provides increased erosive tools, which strengthens the fluvial bedrock incision by exceeding the critical boundary threshold of the boundary shear stress (e.g., Sklar and Dietrich, 2001; Snyder et al., 2003; Tucker and Slingerland, 1997). Modeling and field studies illustrate that increased discharge and sediment flux results in lateral undercutting and oversteepening of hillslopes (e.g., Hancock and Anderson, 2002). Thus, annual to millennial climate variations can have a strong influence on variations in erosion and sediment flux rates, because enhanced precipitation increases groundwater pore pressure and therefore lowers hillslope stabilities, and may thus trigger large landslides and debris flows (Bookhagen et al., in press). These relationships indicate a direct and close link between precipitation and erosion affecting the evolution of tectonically active orogens.

Any tectonic uplift within an orogen leads to a steepening of topography and disequilibrated longitudinal river gradients (Burbank et al., 1996b; Leland et al., 1998). This forces fluvial erosive processes continually to incise by trying to adjust to a longitudinal equilibrium line, which causes massive denudation combined with high sediment flux rates. Numerous isotopic studies of river, delta and Bengal submarine fan sediments indicate that rivers draining the Himalaya contribute a significantly larger share of the dissolved and particulate loads than rivers draining the Indian shield (Galy and France-Lanord, 2001; Galy et al., 1999). A second major pattern to emerge is the dominant role of summer monsoon precipitation in controlling water discharge and sediment supply with approximately 80 - 95% of the total material being delivered in only the 4 months of the Indian summer monsoon (Barros et al., 2000). This causes a strong seasonal runoff variation of the large river systems leaving the Himalaya in which peaked flows are capable of transporting significantly more sediment than the annual mean discharge might suggest (Galy et al., 1996).

Several studies confirm that the monsoonal precipitation pattern currently affecting the southern Himalayan front was established sometime between 9 and 12 Ma (Dettman et al., 2003; Dettman et al., 2001; Prell and Kutzbach, 1992). In any case, once the Tibetan plateau had attained a threshold elevation, it caused a major reorganization of atmospheric circulation pattern at approximately 12 Ma, and a shift to a monsoonal circulation system similar to that of today (Dettman et al., 2003; Kutzbach et al., 1993; Molnar et al., 1993; Ruddiman and Kutzbach, 1989). The timing of this reorganization (12 Ma) may represent the time at which the Tibetan plateau achieved sufficient elevation to block the penetration of moisture from the Indian Ocean and from the south Pacific into western China (Dettman et al., 2003; Dettman et al., 2001; Garzione et al., 2000a). This is consistent with the recent paleo-elevation estimates for the Tibetan plateau, which indicate that the elevation of Southern Tibet has been similar to

its present elevation since 15 Ma (Spicer et al., 2003), 11 Ma (Garzione et al., 2000a), or 10 Ma (Rowley et al., 2001). Enhanced aridity in the Asian heart indicates strengthening of the Indian and East Asian monsoon at 9-8 Ma (Zhisheng et al. 2001).

Thus, highly seasonal precipitation pattern, fluvial erosion and high sediment flux rates have been sustained along the Southern Himalayan Front since the late Miocene, at approximately 12 Ma.

4. DATING METHODS

In order to examine the relationship between climatically versus tectonically dominated exhumation, I applied a number of thermochronometers with a range in closure temperatures from ~ 400°C to < 60° C. This range in closure temperatures provides the opportunity to reconstruct the distribution of cooling rates and the thermal structure which yields rock uplift and exhumation rates. By comparing the pattern of cooling ages with the location of major tectonic structures within the study region, it is possible to determine whether or not the cooling age patterns agree with the tectonic exhumation pattern. If the cooling ages are more or less homogeneous across major faults, erosional factors may dominate the cooling pattern.

4.1 $^{40}Ar/^{39}Ar$ thermochronology

The $^{40}Ar/^{39}Ar$ method is based on the natural spontaneous radioactive decay of the ^{40}K potassium mother isotope and the accumulation of the daughter isotope ^{40}Ar, produced at a constant decay rate over geologic time (Aldrich and Nier, 1948). The $^{40}Ar/^{39}Ar$ dating technique is an advancement of K-Ar method, in which potassium and argon are effectively being determined simultaneously by measurement of the relative argon isotope ratios of ^{40}Ar, ^{39}Ar, and ^{36}Ar in a mass spectrometer (Merrihue and Turner, 1966; Wänke and König, 1959). ^{36}Ar is used as in K-Ar dating to provide information about the non-radiogenic ^{40}Ar, most commonly in making a correction for the amount present in air. The ability to derive age information solely from Ar isotope ratios provides the opportunity to date samples with potential K heterogeneities, such that they are not a source of error. Because isotope ratios can be measured more precisely than concentrations of potassium and argon, not only can the method yield very precise ages, but can also be used measuring very small samples. Turner (1966) found that $^{40}Ar/^{39}Ar$ step heating experiments provide information relating to the spatial distribution of radiogenic argon in a sample, as the release of argon is controlled by diffusion. This opened an opportunity to identify samples that had been thermally disturbed subsequent to their original crystallization, as well as to determine the age of such a thermal event (Merrihue and Turner, 1966). The $^{40}Ar/^{39}Ar$ thermochronology provides the opportunity to date several mineral phases, such as muscovite, biotite, phlogopite, pengite and hornblende, in order to obtain a range of cooling ages with respect to the different isotopic closure temperatures of the respective minerals.

Determination of the neutron flux requires Ar-isotope analysis to use a standard of known age that received the same neutron dose as the unknown target sample. The accuracy of the $^{40}Ar/^{39}Ar$-method depends strongly on the accuracy of the age determination of the standard, and as such, the chosen standard should be as close to the unknown sample age as possible. However, the true ages of some standards are still controversial, because different laboratories use different individual true ages for the same standard (Renne, 2000).

Before the calculation of ages, all data have to be corrected for blank, mass discrimination,

post irradiation decay, and interfering reactions (Dalrymple et al., 1981). The analytical steps are said to be successful, if they yield reproducible apparent ages and the spectrum is concordant. Concordant age spectra are generally interpreted to reflect a homogenous internal distribution of $^{40}Ar/^{39}Ar$, and thus provide evidence against heterogeneous mobility of K and Ar. In such cases a “plateau age” is defined as the mean of the individual step ages, with each step weighted by its inverse variance. Various definitions have been proposed for an apparent age plateau (e.g., Dalrymple and Lanphere, 1974; Lanphere and Dalrymple, 1978; McDougall and Harrison, 1999 and ref. therein). Most definitions agree that a plateau comprises at least three contiguous steps, containing >50% of the total ^{39}Ar released, whose ages do not differ at the 95% confidence level when only internal errors are considered. However, discordant spectra are relatively common, and the nature of discordance varies significantly (Renne, 2000).

4.2 Apatite Fission Track (AFT)

Apatite fission-track thermochronology is commonly used to determine the magnitude of cooling, rock uplift, and exhumation through the uppermost crustal levels; see Fig. 4 (e.g., Fitzgerald et al., 1995; Wagner and Reiner, 1972). Apatite Fission Tracks (AFT) are linear damage trails (see Fig.5) in the crystal lattice that form as the result of spontaneous nuclear fission of trace ^{238}U nuclei (Wagner, 1968; Wagner and Van den Haute, 1992). New ^{238}U fission tracks form at an essentially constant rate and with a constant track length, while older tracks simultaneously anneal (and ultimately are erased) at high temperatures, but at low temperatures fission track are preserved and stable (e.g., Dumitru, 2000; Gleadow and Duddy, 1981; Green et al., 1989b; Naeser and Faul, 1969). At temperatures over ~150-110 °C, all fission tracks are totally annealed, resetting the fission track ‘clock’ to zero. The total annealing temperature (TAT) and the effective closure temperature depend on the kinetic characteristics of the apatite and the cooling rate (Ketcham et al., 1999). For F-rich apatites (95% of all apatites), significant annealing causing track length shortening occurs between 110 and 60 °C at geological cooling rates (approximately 1-10 °C/Myr (Gleadow et al., 1986; Green et al., 1986). This temperature range (110 - 60 °C) is generally referred to as the partial annealing zone (PAZ) (Gleadow and Fitzgerald, 1987). At temperatures below 60 °C AFT are effectively stable because annealing occurs at a very slow rate (e.g., Gleadow et al., 1986).

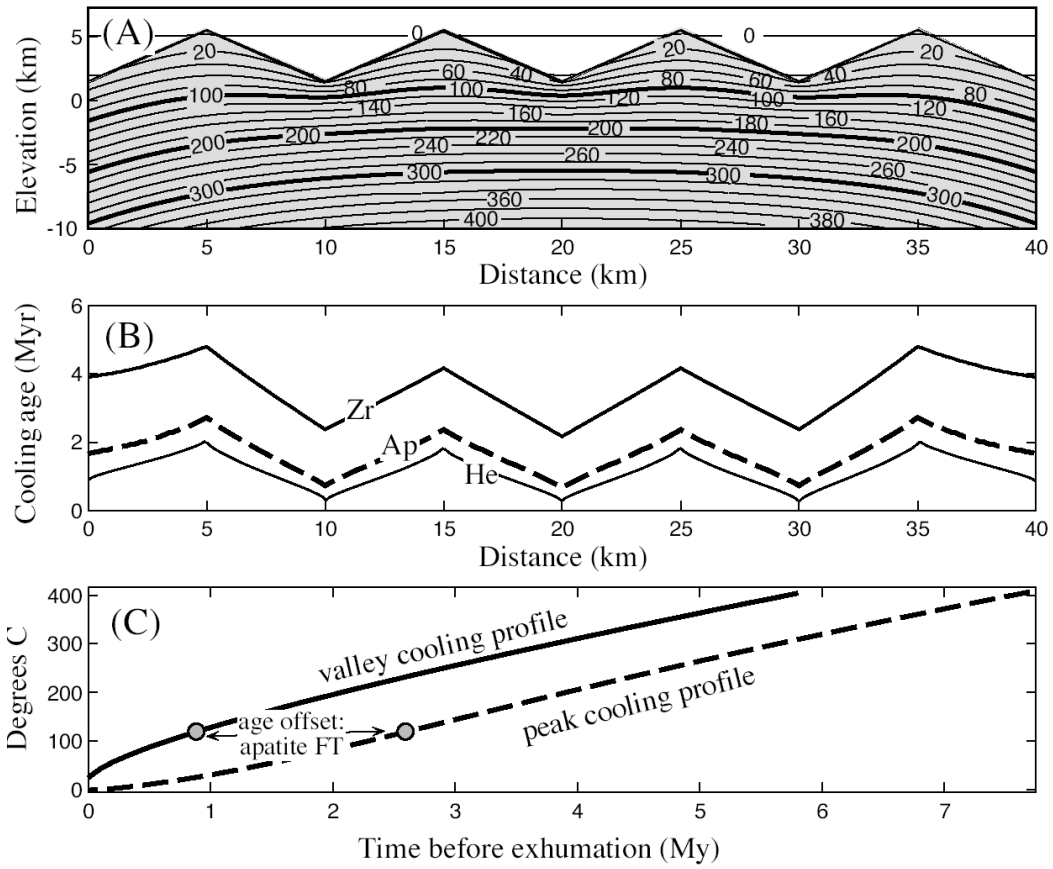

Fig. 4. Calculated cooling age pattern of the U/Th-He and apatite fission track geochronomenters exhumed to the surface for a two-dimensional, V shaped topography with 4 km relief and 10 km wavelength (after Burbank and Anderson, 2001). Model calculated with spacially uniform erosion rates at 2 mm/yr, assuming the landscape reached a steady state after several million years. For apatite fission track the total annealing temperature is ~110 ºC, for U/Th-He the closure temperature is ~60 ºC. (A) computerized thermal structure below topography. Note the warping of isotherms near the surface and the contrasts in gradients beneath the peaks and the valleys. (B) Expected spatial distribution of cooling ages for apatite fission track and U/Th-He. (C) Temperature paths taken by rocks being exhumed in the central valley (solid) and a peak (dashed) of the topography.

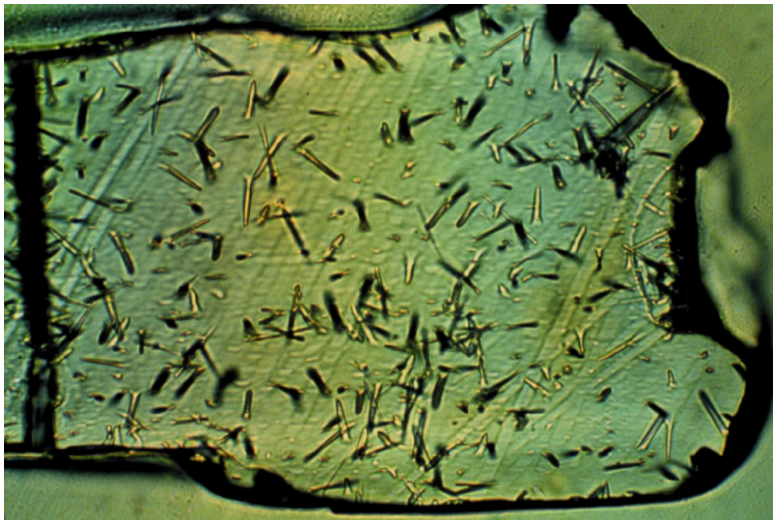

Fig. 5: Photomicrograph of etched apatite crystals showing randomly distributed fission tracks (Photo from T. Dumitru). (Scale ~200x100 µm)

The fission-track age of a sample is commonly interpreted as the time at which the sample cooled below the closure or total annealing temperature, and is determined by measuring the mean track density and U concentration of the sample. The annealing rate of fission tracks and the temperature at which all tracks are totally annealed can be correlated with the apatite chemical composition, in particular the Cl content (Green, 1989; Green et al., 1986; Green et al., 1985), or etching characteristics using the mean etch pit diameter parallel to the crystallographic c-axis, usually referred to as Dpar (Burtner et al., 1994; Carlson et al., 1999). Thereby the total annealing temperature can vary between ~110 –150 °C for chlorine-rich and ~90–110 °C for fluorine-rich apatites (Carlson et al., 1999; Corrigan, 1993; Green et al., 1989a; Ketcham et al., 1999). Accounting for this range of kinetic behaviors is crucial for analysis of samples containing apatite grains of various Cl and/or Dpar values, because samples experiencing identical thermal histories yield different fission track apparent ages and exhibit different track length distributions (Donelick et al., 1999). Thus, analyzing samples without determining the compositional variations within them can lead to erroneous interpretations. This is particularly critical in sedimentary rocks that possibly contain detrital apatites derived from a variety of provenance regions.

Track length distributions are also affected by variations in apatite composition which leads to slightly varying initial track lengths (Burtner et al., 1994), as well as misleading total track length distribution causing incorrect interpretation.

4.3 Uranium/Thorium-Helium (U/Th-He)

The potential to date minerals by measuring the ingrowth of ^{4}He as an daughter product of the U and Th decay has long been recognized (Strutt, 1905). For a certain time t, the amount of helium produced in a mineral can be expressed as:

$$^{4}He = 8^{238}U(e^{\lambda,238t}-1)+7/137.88^{238}U(e^{\lambda,235t}-1)+6^{232}Th(e^{\lambda,23et}-1).$$

Thereby the measurements of parent and daughter isotopes define the time since closure, assuming no extraneous sources of He. Apatite U/Th-He dating involves extraction of He in a vacuum by heating either in a furnace (Wolf et al., 1996; Zeitler et al., 1987) or with a laser (House et al., 2000; Reiners et al., 2002), followed by purification and analysis by mass spectrometry. After removal from the vacuum system, the apatites are dissolved and concentrations of U and Th are analyzed, usually by inductively coupled plasma mass spectrometry (ICP-MS). For apatites of typical U, Th, and He content the analytical precision of a He age is usually better than 1.5%, and accuracy better than 1% provides opportunities to date single apatites with no substantial loss in precision (Farley, 2002). However, in practice, apatite He ages do not reproduce this well. Mineral inclusions with high U and Th concentrations, especially in zircon and monazite (Fig. 6), produce erroneously high He ages in some apatites (House et al., 1997).

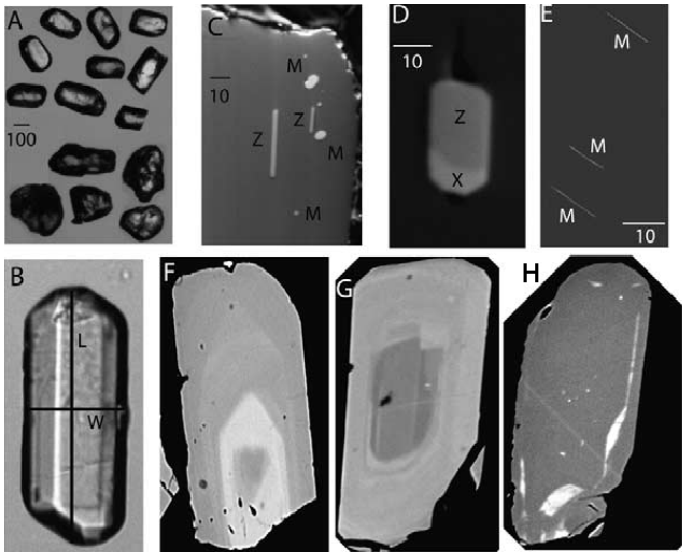

Fig. 6. Photomicrographs of apatite crystals by Ehlers and Farley (2003). (A) Euhedral grains which have typical morphology appropriate for α-ejection correction (upper), and anhedral and rounded grains with geometries to complex to apply a straightforward correction (lower). (B) An euhedral grain appropriate for α-ejection correction with the crystal length (L) and width (W). (C-E) Three SEM electron backscatter images showing common inclusions in apatite crystals which can cause erroneously high He ages such as Monazite, Zircon, and Xenotime. Note the small needles of monazite in E are not easily detected in unpolished grains under a binocular microscope. (F-H) These SEM backscatter images show zonation of major and minor elements (mostly Y, Ce, La, Si, and P). Bright regions are enriched in Y, Ce, and La, and ICP-MS analyses show that these elements correlate strongly with U and Th in these apatites. Thus these images are indicative of zonation in U and Th (Ehlers and Farley, 2003). In panels A and C-E, scale bar is in μm: in panels B and F-H the apatite grains are ~300 μm long. This figure was published by.

Microscopic examination of grains to be dated greatly reduces this problem (Farley, 2002). However, some inclusions may be too small to detect (Fig. 6). Other techniques for recognizing material compromised by inclusions have been developed (Farley, 2002). Most importantly, inclusions tend to be heterogeneously distributed from grain to grain, causing poor age reproducibility, and as such age reproducibility is an indispensable demonstration of the quality of an apatite He age.

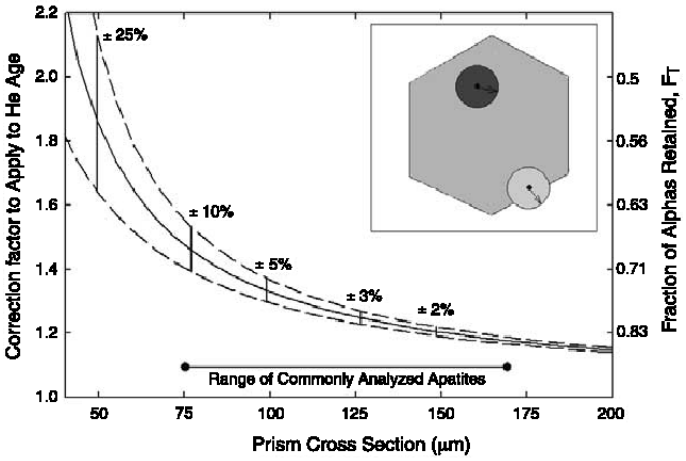

Fig. 7. The influence of α ejection on the apatite He ages after Ehlers and Farley (2003). Inset shows a conceptual model illustrating that He atoms will come to rest on the surface of a ~20 μm sphere centered by the parent nucleus. For parent nuclei more than ~20 μm from the edge of the grain (shaded hexagon), all He will be retained within the crystal lattice of the apatite (dark circle); for parent nuclei closer to the grain edge some fraction of α particle trajectories will eject the He atom from the grain (light cirle). The curve in the main figure indicates the approximate multiplication factor by which a raw He age must be multiplied to correct for this ejection, assuming a hexagonal prism with a length/cross section ration of 3 and decay in the ^{238}U series (after Farley et al., 1996). The fraction of αs retained, F_T, is shown for comparison on the right hand axis. The dashed curves indicate the 1σ uncertainty on the correction factor based on grain measurement uncertainties and a conservative estimate on how well

typical apatites approximate the idealized hexagonal prism geometry. Numbers above the curve indicate 2σ uncertainties at selected cross sections.

Because U and Th emit α particles that travel approximately 20 µm through apatite lattice, they can be ejected from crystal edges or injected from surrounding grains (Fig. 7). The α-ejection correction assumes a homogeneous spatial distribution of U and Th. Without correction for this, apatite age are underestimating the time since He closure by between 15 and 33% (Farley et al., 1996). To correct for the α-ejection the physical dimensions of a crystal to be dated are measured, from which the correction is computed (Farley, 2002). For grains >125 µm in cross section, the ±2% uncertainty is comparable to the analytical error in isotope measurements, but this source of age uncertainty grows rapidly as grain size decreases. Generally, the observed reproducibility of He ages is consistent with the combination of analytical and α-ejection uncertainties, or about ±5% (2σ) on reasonably large apatite crystals (Farley et al., 2001).

In all apatites in which He diffusion has been studied He loss is consistent with thermally activated volume diffusion (Warnock et al., 1997; Wolf et al., 1996; Zeitler et al., 1987). Simplified, the diffusivity is described as a function of temperature and the kinetic parameters in terms of closure temperature T_c. Diffusion data indicate a moderate variability in apatite He T_c: 60-75°C assuming a cooling rate of 10°C/Myr. So far no evidence has emerged to suggest that T_c varies with changing apatite composition, however it is clear that it does vary with grain size. For example, from 50 to 150 µm in grain cross section the Tc increases by ~ 10°C (Farley, 2000).

5. CLIMATIC CONTROL ON RAPID EXHUMATION ALONG THE SOUTHERN HIMALAYAN FRONT

Rasmus C. Thiede[a,*], phone: +49-331-977-2908, fax: +49-331-977-5060, thiede@geo.uni-potsdam.de
Bodo Bookhagen[a], phone: +49-331-977-2908, fax: +49-331-977-5060, bodo@geo.uni-potsdam.de
J Ramón Arrowsmith[b], phone: +1-480-965-3541, fax: +1-480-965-8102, ramon.arrowsmith@asu.edu
Edward R. Sobel[a], phone: +49-331-977-5403, fax: +49-331-977-5060, ed@geo.uni-potsdam.de
Manfred R. Strecker[a], phone: +49-331-977-5261, fax: +49-331-977-5060, strecker@geo.uni-potsdam.de

[a] Institut fuer Geowissenschaften, Universitaet Potsdam, Potsdam 14415, Germany
[b] Department of Geological Sciences, Arizona State University, Tempe, AZ 85287, USA

*corresponding author

Published 2004 in Earth and Planetary Science Letters, v. 222, p. 791-806.

5.1 ABSTRACT

Along the Southern Himalayan Front (SHF), areas with concentrated precipitation coincide with rapid exhumation, as indicated by young mineral cooling ages. Twenty new young (<1-5 Ma) apatite fission track (AFT) ages have been obtained from the Himalayan Crystalline Core along the Sutlej Valley, NW India. The AFT ages correlate with elevation, but show no spatial relationship to tectonic structures, such as the Main Central Thrust or the Southern Tibetan Fault System. Monsoonal precipitation in this region exerts a strong influence on erosional surface processes. Fluvial erosional unloading along the SHF is focused on high mountainous areas, where the orographic barrier forces out >80% of the annual precipitation. AFT cooling ages reveal a coincidence between rapid erosion and exhumation that is focused in a ~50-70-km-wide sector of the Himalaya, rather than encompassing the entire orogen. Assuming simplified constant exhumation rates, the rocks of two age-vs.-elevation transects were exhumed at ~1.4±0.2 and ~1.1±0.4 mm/a with an average cooling rate of ~50-60 °C/Ma during Plio-Pleistocene time. Following other recently published hypotheses regarding the relation between tectonics and climate in the Himalaya, we suggest that this concentrated loss of material was accommodated by motion along a back-stepping thrust to the south and a normal fault zone to the north as part of an extruding wedge. Climatically controlled erosional processes localize on this wedge and suggest that climatically controlled surface processes determine tectonic deformation in the internal part of the Himalaya.

Keywords: Himalaya, apatite fission track, geochronology, exhumation, erosion, precipitation

5.2 Introduction

High exhumation rates in orogens are driven by both, tectonic convergence and climatically controlled erosion (e.g., Koons, 1990; Whipple and Tucker, 1999; Willett, 1999). Rock uplift generates topographic relief, thereby enhancing the possibilities for orographic precipitation, which in turn focuses erosion. Enhanced precipitation (1) controls effective hillslope erosional processes such as the triggering of landslides and debris flows, and (2) increases river discharge, which in addition to channel slope, is an important parameter of determining the stream-power law (Horton, 1945; Whipple and Tucker, 1999). The fluvial incision rate, overall fluvial erosion, and sediment evacuation are thus strengthened. In those sectors affected by concentrated erosion, deformation and the rock uplift will be focused in response to the regional compression (Willett, 1999). The relationship between erosion and exhumation is primarily characterized by mass redistribution along river valleys running perpendicular to strike of a range (e.g., Vannay et al., 2004; Zeitler et al., 2001b). Thereby two requirements must be accomplished in order to keep the positive feedback between erosion and exhumation operating over geologic time: (1) For high regional erosion the river network has to provide sufficient runoff to cause high fluvial incision, erosion, and sediment flux to the foreland that exceeds local sediment flux generated by hillslope erosion. (2) Coeval mass removal must be balanced by tectonic influx of material to achieve steep channel gradients and relief, respectively. For instance, the concept of the critical taper model (e.g., Davis et al., 1983) provides the framework to consider these processes. Thus, tectonically active regions with enhanced erosion are potentially subject to increased tectonic rates and may eventually influence spatial patterns of further rock uplift. However, the nature of this interaction between the distribution of precipitation, regional erosion rates, and patterns of rock uplift is still a matter of controversy (e.g., Burbank et al., 2003; Dadson et al., 2003; Reiners et al., 2003). For example, in central Nepal Burbank et al. (2003) find no significant spatial correlation between short-term precipitation and long-term erosion rates. These authors suggest that tectonically forced advection of crustal material is the most important factor affecting erosion across a region. Dadson et al. (2003) propose for the Taiwan orogen that the patterns of erosion have changed over time in response to the migration of localized tectonic deformation. In contrast, Reiners et al. (2003) show strongly varying long-term erosion rates across the Cascade Mountains (USA) closely tracking modern mean annual precipitation. Whereas Zeitler et al. (2001b) argues that within the syntaxial bends of the Himalaya the loci of deep and fast exhumation is caused by significant fluvial erosion. However, thermo-mechanical numerical models of Beaumont et al. (2001) and Jamieson et al. (2002) demonstrate how effective surface denudation may modify the internal deformation patterns of the Himalayan orogen.

Along the central part of the Southern Himalayan Front (SHF), monsoonal precipitation controlled by topography exerts a strong control on erosional processes, as these regions coincide with sectors of massive landsliding, debris-flow activity, and effective mass removal by streams (Bookhagen et al., in review) (Fig. 8a). These sectors of concentrated precipitation

also coincide with rapid exhumation, indicated by young mineral cooling ages of different isotopic systems (e.g., Catlos et al., 2001; Catlos et al., 2002; Copeland et al., 1991; Harrison et al., 1999; Harrison et al., 1997; Jain et al., 2000; Metcalfe, 1993; Vannay et al., 2004) (see Fig. 8 and Table 1). Assuming that the climatically driven erosional processes have been sustained over geologic time, and have not shifted spatially, large quantities of material should have been removed from these regions. This resulted in a situation, where mass removal is compensated by renewed rock uplift and deformation. The similar tectonic history, structural setting, rock types, and pronounced precipitation gradients thus make the Himalayan arc a prime location to assess the complex linkages between tectonics, climate, and exhumation patterns.

In this study, we present twenty new, young (<1-5 Ma) apatite fission track (AFT) ages (Fig. 9 and Table 2) that were obtained across the crystalline core along the Sutlej Valley, NW India. The samples were collected in elevation transects across major tectonic boundaries, such as the Main Central Thrust (MCT) and Southern Tibetan Fault System (STFS). This region coincides with a sector of the orogen where precipitation is concentrated and surface processes are vigorous (Bookhagen et al., in review). Previous studies along the Sutlej Valley by Jain et al. (2000) and Vannay et al. (2004) reveal a zone of young cooling ages in the footwall of the MCT based on various geochronologic systems (AFT, <1-2 Ma, Fig. 3; zircon fission track- ZFT, 2-3 Ma; $^{40}Ar/^{39}Ar$, 4-6 Ma). We use our new AFT ages combined with published data to (1) determine the spatial distribution of exhumation in the Sutlej region, (2) map out the regional exhumation pattern in NW-India to identify zones with high exhumation rates, and (3) to evaluate the correlation between high exhumation and areas of concentrated precipitation and enhanced erosion.

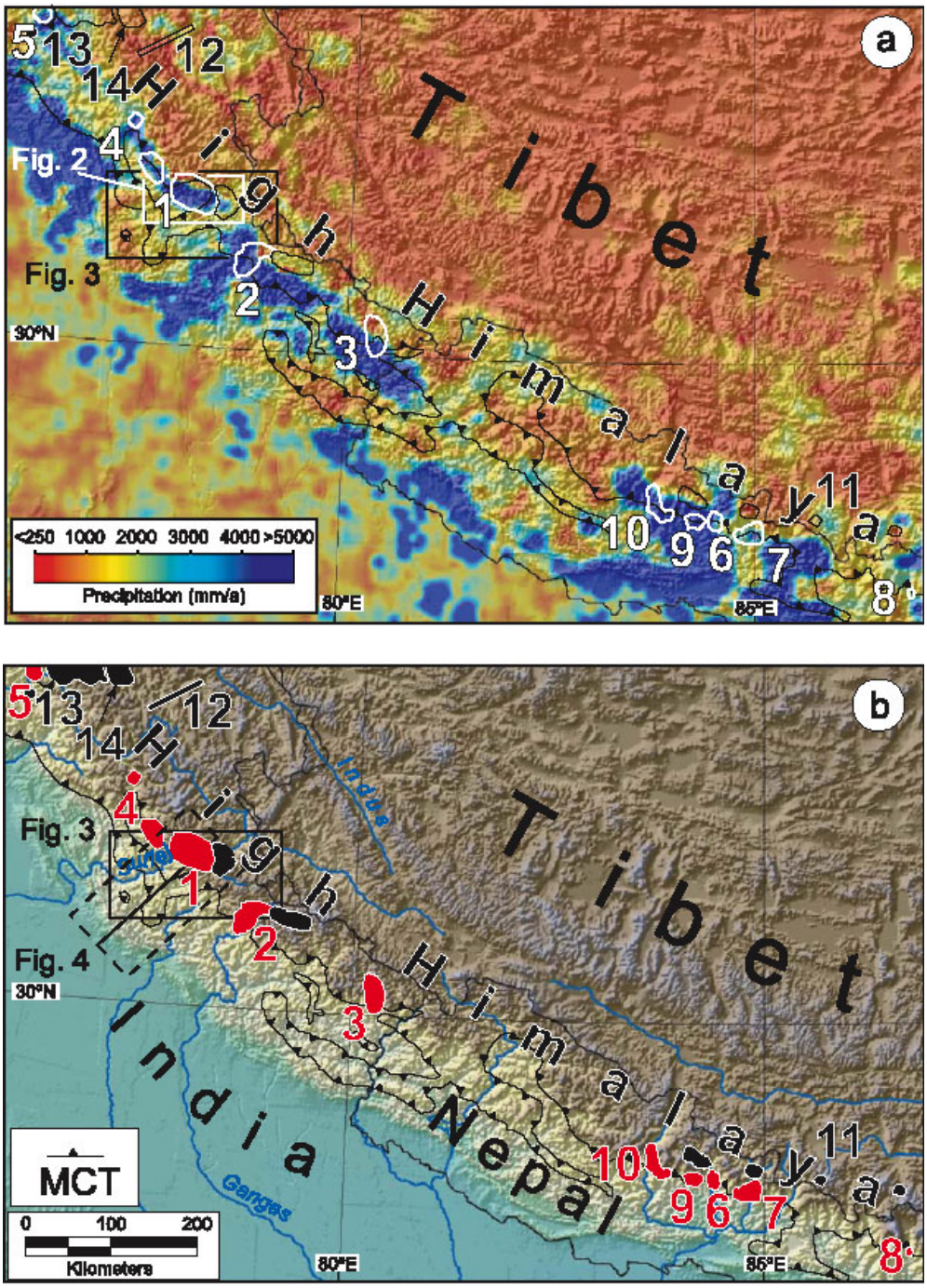

Fig. 8: GTOPO30 (USGS) map of Himalayas showing selected areas of young cooling ages (a) white polygons, b) red polygons, with no. referring to author, see table 1 over a) distribution of mean annual precipitation, and b) topography of the central Himalaya (NW-India and Nepal). Young cooling ages from different geochronologic methods are localized along the southern termination of the High Himalaya, and overlap with regions of enhanced orographic precipitation during the Indian summer monsoon. Black and white boxes denote areas of detailed study along the Sutlej Valley in Fig. 9 and 10, black line in b is the cross section in Fig. 11. Precipitation derived from calibrated SSM/I passive microwave data (Bookhagen et al., in review).

Table 1. Summary of published cooling ages from the southern Himalayan front.

No.	*Region*	*Dating method*	*Age [Ma]*	Authors
1	Sutlej Valley	FT – apatite	<1-4	Jain et al., 2000; Vanney et al., in revision; this paper
		FT – zircon	2-15	Jain et al., 2000; Vanney et al., in revision
2	Bhagirathi Valley	FT – apatite	1-4	Sorkhabi et al., 1996; Searle et al., 1999
		K/Ar – muscovite	5-22	Metcalfe, 1993
		Th-Pb – monazite	5-22	Catlos et al., 2002
3	Gori Ganga Valley	FT – apatite	<1-2	Bojar et al., 2003
		Ar/Ar - white mica	12-14	Bojar et al., 2003
4	Bandal & Rotang	FT – apatite	2- 4	Lal et al., 1999
5	Kishtwar Window	FT – apatite	1-4	Kumar et al., 1995
6	Marsyandi Valley	Ar/Ar – biotite	4-12	Edwards, 1995
		FT - apatite	<1-4	Blythe et al., 2002
		Ar/Ar - white mica	2-10	Catlos et al., 2001
		Th-Pb – monazite	3-22	Catlos et al., 2001
7	Buhri Gandaki Valley	Ar/Ar - white mica	3-10	Copeland et al., 1991
		Ar/Ar – biotite	3-14	Copeland et al., 1991
		Th-Pb – monazite	4-8	Harrision et al., 1997
8	Dudh Kosi Valley	Th-Pb – monazite	11-16	Catlos et al., 2002
9	Ampipal	FT – apatite	1-2	Gautam and Koshimizu, 1991
10	Modhi Valley/ Kali Gandaki	FT - zircon	1-2.5	Arita and Ganzawa, 1997
11	Shisha Pangma	FT – apatite	12-15	Searle et al., 1997
12	Ladakh	FT - apatite	8-40	Schlup et al., 2001
13	Bhot Nala	FT – apatite	2-8	Kumar et al., 1995
14	Padam-Zanskar	FT – apatite	6-12	Kumar et al., 1995

FT - fission track, Ar/Ar - $^{40}Ar/^{39}Ar$, K/Ar - $^{40}K/^{40}Ar$, Th-Pb - in situ Th-Pb ion microprobe dating.

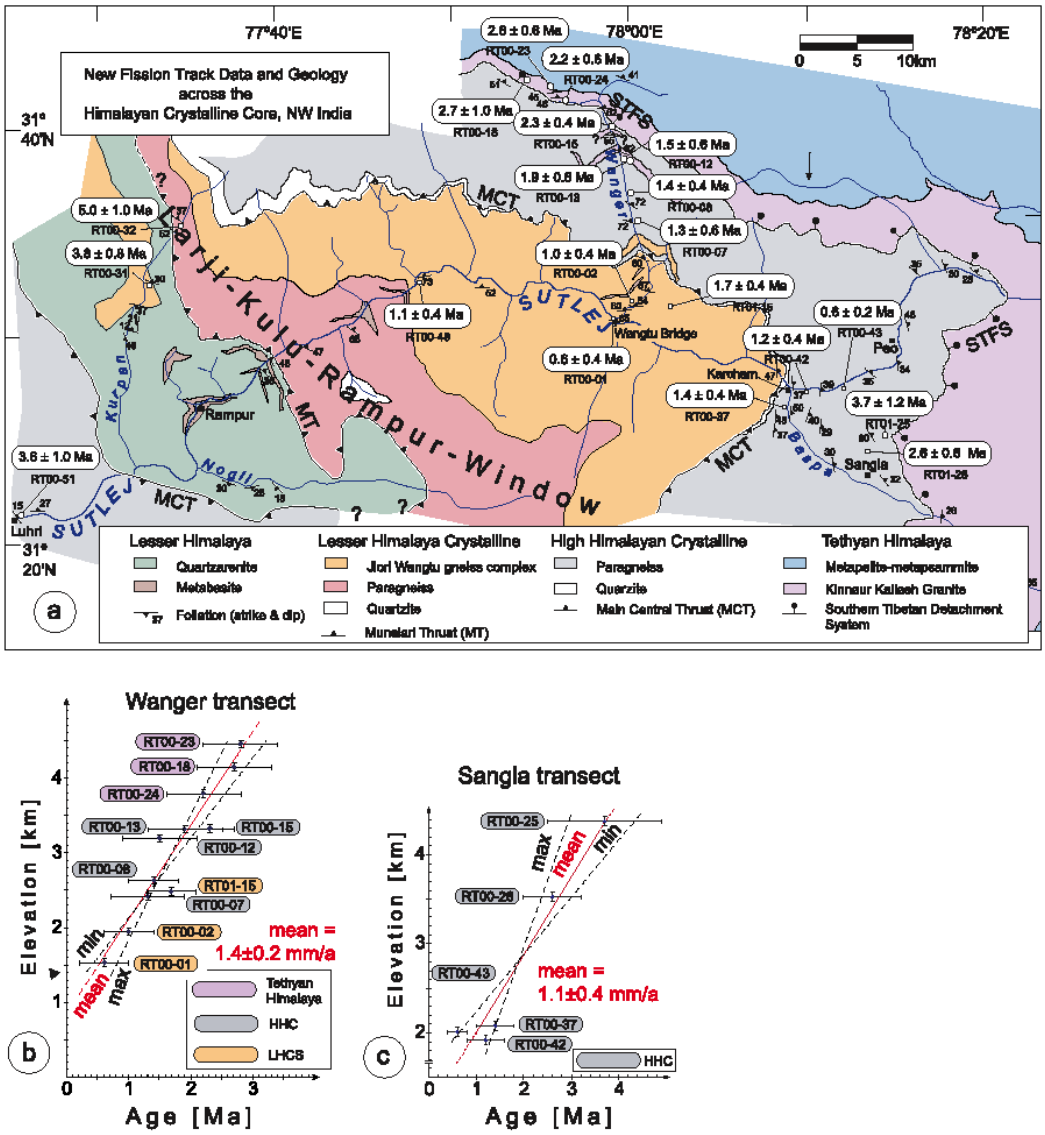

Fig. 9: a) Distribution of new apatite fission track ages (this study, errors are ±2σ) across the Himalayan Crystalline Core of Sutlej region. AFT cooling ages document young exhumation in the upper Sutlej Valley, where in a tectonic window rocks related to the Lesser Himalaya are exposed, surrounded by Higher Himalayan Crystalline rocks. Base geology modified from Vanney and Grasemann (2001a; 1998) with our observations. b) Age versus elevation transect along the Wanger Valley across the MCT and STFS. c) Age versus elevation transect from the hanging wall of the MCT in the Sangla area. Note that the transects shows no sensitivity to tectonic structures such as MCT and STFS, but rather the age correlates with elevation (see text for exhumation rate calculation/estimate.

Table 2: Apatite fission track data from the Sutlej Region, see Fig. 2 for location

Apatite fission track data from the Sutlej Region, see Fig. 2 for location

Sample number	Altitude (m)	Latitude (DM)	Longitude (DM)	Rock type	Formation	#Xls	Spontaneous		Induced		Dosimeter		χ^2 P (%)	Pooled age (Ma)	$\pm 2\sigma$	Uran. (ppm)
							Rho-S	Ns	Rho-I	Ni	Rho-D	Nd				
RT00–1	1540	N 31°32.283′	E 078°0.171′	orthogneiss	LHCS	55	0.016	7	6.925	3093	13.184	8028	82	0.6	0.4	6.6
RT00–2	1950	N 31°33.102′	E 078°1.191′	orthogneiss	LHCS	45	0.076	37	19.673	9605	13.256	8028	97	1.0	0.4	19.2
RT00–7	2420	N 31°37.950′	E 078°2.553′	orthogneiss	LHCS	54	0.034	16	6.808	3208	13.328	8028	91	1.3	0.6	6.8
RT00–8	2640	N 31°38.863′	E 078°0.938′	gneiss	HHC	42	0.223	104	40.857	19,072	13.400	8028	100	1.4	0.4	36.4
RT00–12	3200	N 31°41.806′	E 078°0.081′	orthogneiss	HHC	30	0.075	23	12.858	3925	13.472	8028	96	1.5	0.6	11.8
RT00–13	3320	N 31°41.463′	E 078°0.485′	orthogneiss	HHC	33	0.191	74	26.690	10,320	13.544	8028	100	1.9	0.6	24.4
RT00–15	3330	N 31°42.656′	E 077°59.466′	orthogneiss	HHC	30	0.585	151	67.607	17,460	13.616	8028	100	2.3	0.4	60.2
RT00–18	4150	N 31°43.548′	E 077°54.748′	orthogneiss	KKG-TH	31	0.177	39	17.352	3813	13.688	8028	91	2.7	1.0	15.4
RT00–23	4460	N 31°43.429′	E 077°56.267′	orthogneiss	KKG-TH	35	0.609	239	57.571	22,580	13.760	8028	98	2.8	0.6	51.7
RT00–24	3800	N 31°42.957′	E 077°56.779′	orthogneiss	HHC	37	0.226	90	27.209	10,844	13.832	8028	98	2.2	0.6	23.6
RT00–31	2250	N 31°32.486′	E 077°34.606′	gneiss	LHCS	29	0.603	159	43.117	11,375	13.904	8028	65	3.8	0.8	36.3
RT00–32	2200	N 31°35.099′	E 077°35.344′	gneiss	LHCS	24	0.735	157	39.853	8509	13.976	8028	96	5.0	1.0	33.9
RT00–37	2080	N 31°48.767′	E 078°10.622′	gneiss/ mylonite	HHC	45	0.228	104	44.440	20,242	14.048	8028	81	1.4	0.4	40.0
RT00–42	1920	N 31°29.539′	E 078°12.023′	paragneiss/ mylonite	HHC	56	0.096	64	22.782	15,168	14.120	8028	93	1.2	0.4	20.0
RT00–43	2010	N 31°29.799′	E 078°13.211′	paragneiss/ mylonite	HHC	46	0.048	29	21.246	12,811	14.192	8028	91	0.6	0.2	17.1
RT00–48	1625	N 31°34.019′	E 077°49.865′	orthogneiss	LHCS	42	0.106	35	21.287	7050	11.037	6644	100	1.1	0.4	24.8
RT00–51	900	N 31°20.752′	E 077°26.482′	orthogneiss/ mylonite	HHC	29	0.247	55	15.080	3352	11.095	6644	100	3.6	1.0	16.4
RT01–15	2470	N 31°33.805′	E 078°04.210′	orthogneiss	LHCS	19	0.283	67	37.480	8861	11.449	4754	66	1.7	0.4	40.5
RT01–25	4380	N 31°27.013′	E 078°15.012′	gneiss/ mylonite	HHC	44	0.099	48	5.990	2897	11.478	4754	100	3.7	1.2	7.1
RT01–26	3530	N 31°27.247′	E 078°15.775′	gneiss/ mylonite	HHC	24	0.357	138	30.834	11,904	11.508	4754	92	2.6	0.6	31.7

Abbreviations are: LHCS, Lesser Himalaya Crystalline Sequence; HHCS, High Himalayan Crystalline Sequence; KKG-TH, Kinnauer Kailash Granite-Tethyan Himalaya; #Xls, number of individual grains dated; Rho-D, induced track density in external detector adjacent to dosimetry glass ($\times 10^6$ tracks/cm^2); Nd, number of tracks counted in determining Rho-D; Rho-S, spontaneous track density ($\times 10^6$ tracks/cm^2); Ns, number of spontaneous tracks counted; Rho-I, induced track density in external detector (muscovite) ($\times 10^6$ tracks/cm^2); Ni, number of induced tracks counted; χ^2 P (%), chi-square probability [87,88]; Age is the sample pooled fission track age [90]; calculated using zeta calibration method [89]. Trackkey was used for calculating the counting results [92].

The following is a summary of key laboratory procedures. Samples were all analyzed by R. Thiede (zeta factor of 391 ± 27). Apatites were etched for 20 s in 5.5 N nitric acid at a temperature of 21 ± 0.1 °C. CN5 dosimetry glass was used as a neutron flux monitor. Samples were irradiated at Oregon State University TIRGA reactor. External detectors were etched in 40% HF. Tracks were counted with a Leica microscope with 100 × air objective, 1.25× tube factor, 10× eyepieces, using transmitted light with supplementary reflected light as needed; external detector prints were located with Kinetek computer-automated scanning stage [91].

The AFT analysis employs the external detector method following the zeta calibration approach of Hurford and Green [90]. Analytical precisions of 0.2 to 1.0 Ma ($\pm 2\sigma$) could be obtained from these young AFT ages due to the high U-content and the large number of grains counted per sample. Only grains with *c* axes parallel to slide plane were dated and zero-track grains were considered.

5.3 The Himalaya

The Himalayan orogen is the type location of an active continent-continent collision zone. It forms the southern part of the collision zone between India and Asia and results from continued convergence and crustal thickening over the last ~50 Ma (Hodges, 2000 and references therein; Klootwijk et al., 1992). Geodetic measurements, seismicity, and both steep topography (~33°) and river-profile gradients (order of magnitude change) document

ongoing convergence, deformation and uplift (Bilham et al., 1997; Duncan et al., 2003; Pandey et al., 1995; Seeber and Gornitz, 1983). The kinematic evolution of the orogen is mainly controlled by the progressive action of a series of first order crustal fault systems (STFS, MCT, Main Boundary Thrust - MBT, Main Frontal Thrust - MFT). These bound orogen-parallel tectonostratigraphic domains (Tethyan Himalaya (TH), High Himalayan Crystalline Sequence (HHCS), Lesser Himalaya (LH), and Sub-Himalaya), which have been detached along the Main Himalayan Thrust (MHT) from the underthrusting Indian plate and became incorporated into the orogen (Gansser, 1964; Hodges, 2000; Lefort, 1975; Zhao et al., 1993).

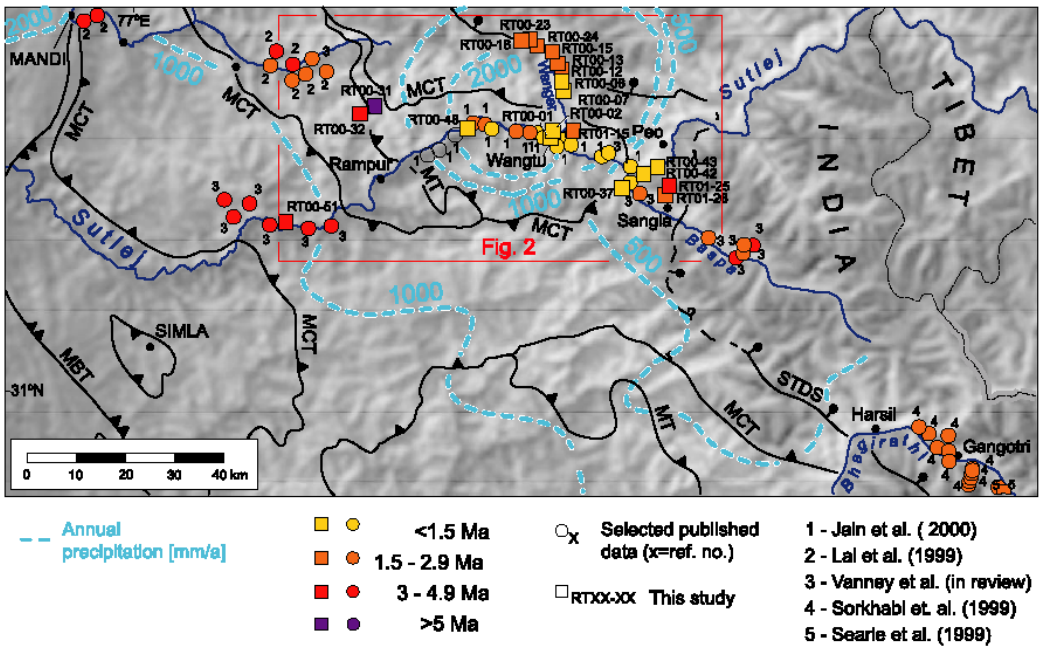

Fig. 10: Compiled AFT cooling ages across the crystalline core of the Himalaya (NW India) showing pronounced young ages in a ~50-70 km wide sector of the deformation belt. Note the strong focusing of high regional precipitation and young cooling ages across the High Himalaya. Red box denotes area of detailed study along the Sutlej Valley (Fig. 9). Precipitation derived from calibrated SSM/I passive microwave data (see Bookhagen et al., Bookhagen et al., in review), and topography based on GTOPO30 (USGS). Tectonic structures modified after Vannay and Grasemann, (2001a).

Along the Sutlej Valley in the northwestern sector of the orogen, the crystalline core of the Himalaya is exposed in two distinct gneiss units, characterized by different cooling histories (Vannay and Grasemann, 1998, see Fig. 2; Vannay et al., 2004). To the north, the HHCS, a ~10 km thick, NE-dipping sequence of highly deformed amphibolite to migmatic ortho- and para-gneisses is bounded by the Early-Mid Miocene MCT at the base (Coleman, 1998; Hubbard and Harrison, 1989), and by the probably contemporaneously active extensional STFS at the top (e.g., Burchfiel et al., 1992; Burg et al., 1984a; Dezes et al., 1999). The HHCS is interpreted to have been deformed as a southward extruding crystalline wedge (Grasemann et al., 1999; Vannay and Grasemann, 2001a). Beneath the MCT, rocks related to the Lesser Himalayan Crystalline Sequence (LHCS) or of the MCT zone (Pecher, 1989)

are exposed in the tectonic Larji-Kulu-Rampur Window (LKRW) (Frank et al., 1995) along the Sutlej. These rocks are predominantly composed of amphibolite facies augen- and paragneisses (Valdiya, 1980b; Vannay and Grasemann, 1998). Based on structural and geochronologic analysis (Vannay et al., 2004), these rock units are interpreted to be a younger southward extruding wedge bounded at the base by the Munsiari Thrust (MT, active from Mid Miocene until recent) and at the top by a passive normal fault (Karcham Normal Fault Zone (KNFZ), e.g., Hager et al., 2003). Numerous hot springs, and carbonate and sulfur-rich precipitates along cataclastic zones characterize the LHCS and the lower part of the HHCS. Toward the foreland, the MCT becomes a shallow-dipping thrust, separating the HHCS from the low- to medium-grade metamorphic sediments of the Lesser Himalaya (Vannay and Grasemann, 1998).

The central part of the Himalaya is characterized by a topographic discontinuity with a ~100-150 km wide, moderately elevated segment (<3000m asl) to the south, and the High Himalaya, a highly elevated segment with peaks of >6000m asl, high relief, and steep slopes to the north (Fig. 8b). This abrupt change in topography beneath the front of the High Himalaya might be the result of motion along a crustal ramp in the MHT and/or fault bend fold structures in the LH (e.g., Cattin and Avouac, 2000 see Fig. 4; Gansser, 1964; Pandey et al., 1995; Schelling and Arita, 1991). Alternatively, it has been interpreted to be the result of recently active thrust faulting at the base of the High Himalaya (Hodges et al., 2001; Seeber and Gornitz, 1983; Wobus et al., 2003).

The High Himalayan mountain front forms the main orographic barrier, and at elevations between ~2000 and 4000 m more than 80% of the annual precipitation (>2000 mm/a) of the Indian summer monsoon are forced out (Barros et al., 2000; Bookhagen et al., in review). This barrier forms a divide between humid areas to the south and more arid sectors (with <500 mm/a precipitation) to the north. However, where the monsoonal circulation reaches major N-S oriented valleys moisture is also channeled farther into the orogen (Bookhagen et al., in review, Fig. 1a).

5.4 Apatite Fission Track Analysis

Apatite Fission Tracks (AFT) are linear damage trails in the crystal lattice that form as the result of spontaneous nuclear fission of trace ^{238}U nuclei (Wagner and Van den Haute, 1992). New ^{238}U fission tracks form at an essentially constant rate and with a constant track length, while older tracks simultaneously anneal (and ultimately are erased) at high temperatures, making AFT an effective tool for reconstructing cooling and exhumation histories (e.g., Dumitru, 2000; Gleadow et al., 1986; Green et al., 1989b). At temperatures hotter than ~110-150 °C, all fission tracks are totally annealed, resetting the fission track clock to zero. The total annealing temperature (TAT) and the effective closure temperature depend on the kinetic characteristics of the apatite and the cooling rate (Ketcham et al., 1999). The partial annealing zone (PAZ) extends from the TAT down to ~60 °C, and within this temperature range tracks are partially annealed. Below ~60 °C, AFT are effectively stable because

annealing occurs at a very slow rate (e.g., Gleadow et al., 1986). The kinematic characteristics of apatite can be evaluated by measuring etch pits figures (Dpar, Donelick et al., 1999).

All 20 samples for AFT analysis (<1-5 Ma; table 2 and fig. 9; details of the sample preparation are listed below table 2) are bedrock samples collected across the Himalayan Crystalline Core in the Sutlej region. For very young apatites, it may be impossible to obtain sufficient Dpar data for a robust interpretation. However, several samples with older ages and/or higher U-content yielded multiple measurements for most analyzed crystals, permitting the calculation of closure temperatures (Ketcham et al., 1999). All of the single population ages in this study pass the chi-squared test, and pooled ages are reported with 2σ errors.

We collected two transects between elevations of 1.5 and 4.5 km to expand the data coverage and add more detail to sites previously sampled for AFT analysis along the Sutlej Valley (Jain et al., 2000; Vannay et al., 2004). A ~20 km long N-S transect (11 samples) extends along the Wanger Valley and crosses two major tectonic boundaries (MCT and STFS; fig. 9b). Nearly all samples were collected along the valley bottom. The Sangla transect (5 samples; fig. 9c) was sampled across the hanging wall of the MCT, from the Sutlej river to STFS over an elevation of 2.4 km and horizontal distance of ~8 km in the Baspa Valley (Fig. 9).

Samples collected in the High Himalaya near the Sutlej River have <1-2 Ma cooling ages, whereas samples at a greater distance from the river yield ages between 3 and 4 Ma (fig. 9). The lowermost sample of the Wanger Valley transect (1540 m), at the Sutlej riverbank is 0.6±0.4 Ma (RT00-1; $\pm 2\sigma$). The ages increase gradually to 2.8±0.6 Ma at 4460 m (RT00-23; Fig. 9b), the highest sample. Along the Sangla transect samples RT00-42 and -43 (between 1900-2000 m) yield ages of 1.2±0.4 and 0.6±0.2 Ma, respectively; at 4400 m sample RT01-25 yields an age of 3.7±1.2 Ma. Overall, the AFT cooling ages are young. The age trend of both transects is similar within error, with a systematic increase in age with increasing distance to the Sutlej River and rising elevation.

With the exception of one sample, the low spontaneous track density associated with the young AFT ages did not provide track-length data. However, sample RT00-23 has a high U content and an older age; it provided 20 confined tracks (Ø=14.2±1.4 μm). Modelling the age/track-length distribution with the program 'AFT solve' (Ketcham et al., 2003) confirms continues fast exhumation during Pliocene-Quaternary time, and yields an average cooling rate between ~40-50ºC for the past 3.5 Myr. This is in good agreement with results derived from the age elevation plots (below) and the results of Vannay et al. (Vannay et al., 2004)

The spatial distribution of these new AFT cooling ages are mostly consistent with recently published AFT ages from the Sutlej area (Jain et al., 2000; Lal et al., 1999; Vannay et al., 2004), and the Garwhal (Searle et al., 1999, fig. 3; Sorkhabi et al., 1996). AFT ages reported for the Nanga Parbat (Zeitler, 1985) and Nepal Himalaya (e.g., Burbank et al., 2003) are even

younger. However, because measured AFT ages by Jain et al. (Jain et al., 2000) in the lower part of LHCS are similar to $^{40}Ar/^{39}Ar$ muscovite ages of Vannay et al. (Vannay et al., 2004), they are not considered in our study.

5.5 Interpretation

AFT ages are interpreted to indicate the elapsed time since cooling below the effective closure temperature. Dpar measurements based on and corrected after Donelick et al. (Donelick et al., 1999) indicate mostly kinetically homogenous samples with a low resistance to annealing. This information suggests an effective closure temperature of 130±10 ºC for cooling rates between 10 and 100 ºC/Myr (Ketcham et al., 1999). The young (<5 Ma) AFT cooling ages imply rapid transit through the PAZ, which limits annealing (Green et al., 1989b). In addition, these young ages indicate ongoing cooling and exhumation over nearly the entire northwestern SHF (Fig. 3). Interestingly, the AFT ages show no spatial relationship (within error) to structures such as the MCT or STFS (Fig. 2). This is consistent with observations based on AFT and ZFT cooling ages from comparable structural settings as the Kishtwar-Padar-Zanskar region to the northwest (>50 AFT ages, see location #5, 13 and 14 in Fig. 1, Kumar et al., 1995), where a linear trend in age with increasing elevation is documented.

The mean of 15 AFT cooling ages from the Wanger Valley and Sangla transects is ~2 Ma, yielding an average cooling rate of ~65±5 °C/Ma during late Pliocene/Quaternary time. The age-elevation pattern of the Wanger transect shows no discernable deviations from a linear trend, considering the magnitude of uncertainties. We therefore use the simplest possible interpretation of the data: uniform exhumation over the 2.8 to 0.6 Ma interval at an average rate of ~1.4±0.2 mm/a. This is based on the inverse slope of weighted least square regression of the AFT elevation (x) vs. ages Y(x) (Fig.9). The Sangla transect has cooled within 2.8 Myr (0.9±0.3 Ma [mean of RT00-42 and -43] and 3.7±1.2 Ma), indicating exhumation rates of ~1.1±0.4 mm/a. Minor structural disruptions along transects during these intervals cannot be resolved with the available data, but large disruptions seem improbable. These rates are in good agreement with exhumation rates (1mm/a for the last 3 Myr) based on modeling results of mineral pairs for the Sutlej region (Vannay et al., 2004). Comparable exhumation rates from Garwhal (Sorkhabi et al., 1996) (~2 mm/a), Central Nepal (Burbank et al., 2003), and the Nanga Parbat (Zeitler, 1985) (~4 mm/a), respectively, are higher. However, because the shallow subsurface temperature distribution is sensitive to the effects of local topography and heat advection by rock-uplift (e.g., Mancktelow and Grasemann, 1997; Stuwe et al., 1994), these exhumation rate estimates must be interpreted with care. Assuming high long-term topographic, erosional, and geothermal steady state for the prolonged exhumation process (active since the Mid Miocene), the perturbations of the isotherms should follow topography with the amplitude, and the perturbation decaying with increasing depth. Therefore, exhumation rates derived from age vs. elevation plots could be overestimated. Modeling results by Safran (2003) using a comparable setting to the area described here indicate that our exhumation rates may yield about 60-70% of the true erosion rates. Furthermore,

predictions made by Mancktelow and Grasemann (fig. 18 in 1997) suggest that the overestimating are higher than the actual rates. However, it is therefore a possibility that transects are internally deformed in a pervasive manner and that exhumation rates decrease with increasing distance from the Sutlej River. Pervasive brittle normal faulting cutting older structures is ubiquitous and observed across both transects. Alternatively, if the exhumation phase had first started in the Late Miocene-Early Pliocene or accelerated at that time, the apparent exhumation rates could underestimate the true exhumation rates (Mancktelow and Grasemann, 1997). In fact, modeling results from that uses mineral pairs supports such higher true rates (Vannay et al., 2004).

An impact of hydrothermal activity documented by many hot springs with temperatures 35 to 70ºC near the bottom of the Sutlej Valley in the LHCS and the HHCS on AFT cooling ages must also be considered (Vannay et al., 2004). Hydrothermal activity indicates an elevated and steep near-surface geothermal gradient. However, the rather consistently young AFT cooling ages (~0.6-2 Ma) obtained by Jain et al. (2000), Vannay et al. (2004), and this study indicate smooth local thermal variations and/or that the advective heat flow by hydrothermal circulation operates in a more pervasive manner. Additional heat advection caused by hydrothermal circulation might induce an additional compression of the isotherms beneath the valley bottom and thereby decrease the amplitude of the perturbed near surface isotherms.

Our young AFT cooling ages imply that the rocks of the LHCS and the lower parts of the HHCS have experienced rapid exhumation during Late Pliocene/Quaternary time. The potential time lag between the rock uplift associated with heat advection and subsequent cooling implies that uplift detected with the AFT-ages could have commenced somewhat earlier (Late Miocene) or may only displays the young phase of continuous exhumation (ongoing since the Mid Miocene). From our data we infer steady (in time) and uniform (in space) exhumation. Before exposing rocks related to the LHCS today, ~10-15 km thick cover units of HHCS had to be removed by localized rapid erosion along the Sutlej Valley. This implies that the exhumation rates can be equated with regional erosion along the Sutlej Valley. Therefore, the young AFT cooling ages and their spatial association with high, and we assume (see below), sustained localized orographic precipitation and fluvial erosion indicate a correlation between climatically driven fluvial erosion and exhumation rates.

5.6 Discussion

The pattern of AFT cooling ages provides key constraints on Pliocene to Quaternary rock uplift and denudation across the crystalline core of the Sutlej region. All young cooling ages (Fig. 8a and 8b) are recorded along the southern termination of the Himalayan crystalline core. These areas coincide with focused orographic precipitation, steep longitudinal river profiles (Seeber and Gornitz, 1983), high relief and rapid exhumation along a 50-70 km wide sector, rather than encompassing the entire width of the orogen. This implies a coupling between the distribution of precipitation and exhumation in this region, as summarized in Figure 11. Topographic and annual precipitation swath profiles (Fig. 11a) perpendicular to the

Himalayan range show the strong control of topography over the distribution of orographic precipitation. Thereby the precipitation is focused in sectors with steep topographic gradients along the Sub-Himalaya and the southern edge of the Lesser Himalayan Thrust Systems (MBT), and between elevations of ~2000 and ~4000 m along the southern edge of the High Himalaya. The distribution of precipitation is tied to the monsoon pattern (Barros et al., 2000; Bookhagen et al., in review). About ~80% of the annual precipitation at the SHF falls during the short summer monsoon (June-August), often in intense rainfall events (Barros et al., 2000; Bookhagen et al., in review). This increased precipitation not only triggers hillslope erosion but also controls the discharge of catchment areas, and is thus an integral part of the fluvial erosion process. According to the stream-power law, river-incision rates should be highest in regions with high runoff and steep river gradients. In addition, the rivers in the Himalayan region are characterized by (1) large annual runoff variation, (2) strong correlation between discharge and sediment transport, and (3) high sediment flux during peak discharge events (e.g., Sutlej River, Bookhagen et al., in review; Ganges River, Galy and France-Lanord, 2001). This implies that the monsoonal precipitation exerts a strong control on erosional surface processes, as due to the high runoff, rivers are able to effectively incise, erode and evacuate sediments to the foreland. This is particularly the case during abnormal monsoon years, which have higher precipitation and longer lasting intensified monsoons (Bookhagen et al., in review). In order to keep long-term sustained regional erosion in such high mountainous terrains localized, the erosional effluxes have to be balanced by the tectonic influx.

The strongest argument for continuous localized erosion over geologic timescales is the complete removal of the HHCS nappes along the Sutlej valley, which correlates with approximately 10-15 km of crystalline rock. They once covered the rocks of the LHCS, which are presently exposed in the LKRW (Fig. 9). This sector correlates with the local maximum of average annual precipitation along the Sutlej Valley (Fig. 10 and 11). In addition, exhumation rates of up to 1.5 mm/a (Vannay et al., 2004 and this study) would be sufficient to remove 10-15 km rocks over a period of 10 Myr. Along the SHF several segments exist, where the HHCS nappes have been completely removed and today rocks related to the LH are exposed in tectonic windows or half windows (Fig. 1a, Gansser, 1964). This implies that efficient erosion has removed a significant volume of rock since the MCT was active (Fig. 11b).

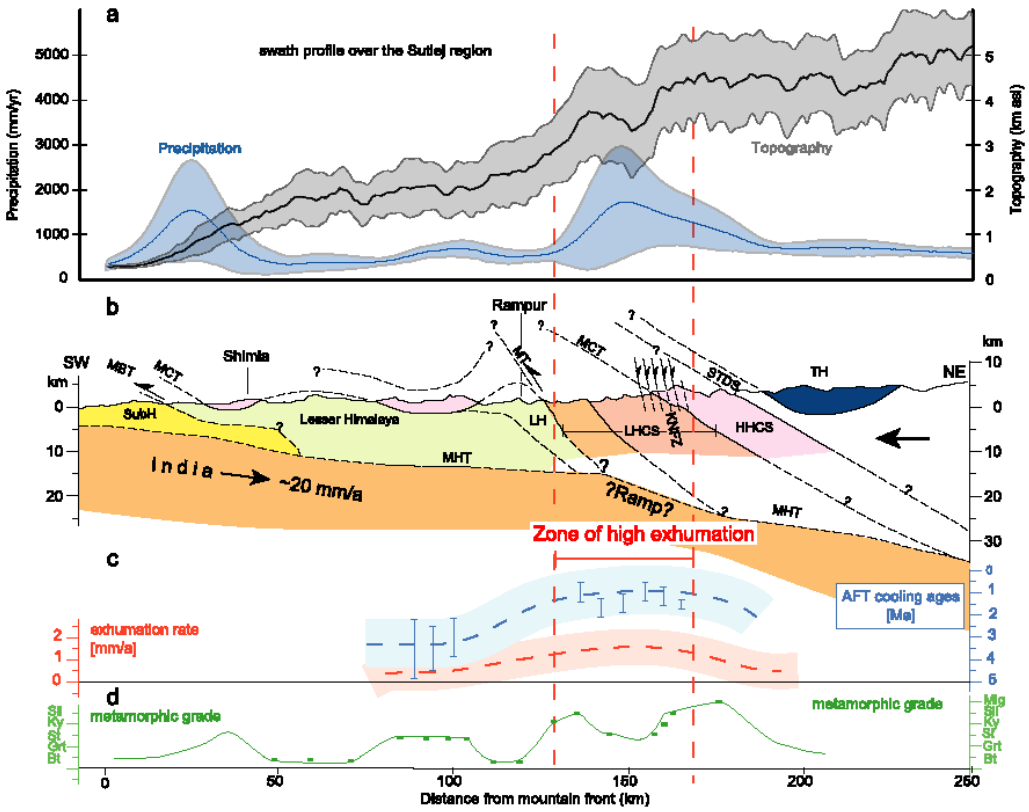

Fig. 11: a) NE-SW profiles showing the topography, precipitation, geology, exhumation, and metamorphism across the High Himalaya. Compiled data illustrate the coupling between surface processes and tectonism in the Sutlej Region. Topographic (grey) and precipitation-distribution (blue) swath profiles for the Sutlej area are oriented perpendicular to the SHF. Swath profiles centered along the rover are 250 km long and 100 km wide; thick, colored lines indicate mean values, shaded areas denote ±2σ. Topography based on GTOPO30 (USGS), mean annual precipitation is derived from SSM/I passive microwave satellite data (see Bookhagen et al. (Bookhagen et al., in review) for more details). Note the focused distribution of orographic precipitation that is focused between elevations of ~2000 to ~4000 m in a ~50-70 km wide zone. b) The simplified geologic cross section parallel to the swath profiles shows that rocks of the LHCS in the footwall of the MCT are exhumed in this sector (Geology modified from Vannay et al., (2001a) and this study). c) Parallel to the geologic cross section are AFT cooling ages along the Sutlej River shown (blue) and estimated exhumation rates (red); dashed lines indicate mean values, shaded areas denote ±2σ. In d) are metamorphic grade of the rocks units along the profile plotted (modified after Vanney et al. (1999)). Based on AFT cooling ages (c), the coincidence between rapid erosion and exhumation is focused in a ~50-70 km wide sector of the Himalayan deformation belt, rather than encompassing the entire orogen. We assume that the enhanced and focused orographic precipitation (a) has localized rapid erosion and exhumation over geologic time. To accommodate this concentrated loss of material, deeper high-grade metamorphic rocks are exhumed (d) by motion along an back stepping thrust to the south (MT) and normal fault zone (KNFZ) to the north (b) that is localized by climatically controlled erosional processes. TH, Tethyan Himalaya; HHCS, High Himalayan Crystalline Sequence; LHCS, Lesser Himalayan Crystalline Sequence; LH, Lesser Himalaya; SubH, Sub Himalaya; STFS, Southern Tibetan Fault System; MCT, Main Central Thrust; KNFZ, Karcham Normal Fault Zone; MT, Munsiari Thrust; MBT, Main Boundary Thrust; MHT, Main Himalayan Thrust.

The Indian monsoon has been active with the current patterns at least since 8 Ma (e.g., Prell and Kutzbach, 1992). However, continuously high sediment fluxes since Early-Mid

Miocene time are reported for the Himalayan foreland basin (SubH) (e.g., Burbank et al., 1996a), the Bengal, and Indus fans (e.g., Clift and Gaedicke, 2002; Copeland and Harrison, 1990; Einsele et al., 1996; Métivier et al., 1999). Rocks of the Himalayan crystalline core have dominated the provenance of Himalayan detrital sediments since that time (Derry and France-Lanord, 1997). In addition, due to the continuous unroofing, high-grade metamorphic index minerals have been deposited sequentially in the foreland basin (garnet & staurolite ~20 Ma, kynite ~12 Ma, and sillimanite ~ 8 Ma, e.g., Najman et al., 2002; Najman et al., 2003) with short lag times (~1-3 Myr) between $^{40}Ar/^{39}Ar$ white mica single-grain cooling ages and their depositional ages (Harrison et al., 1993; White et al., 2002). All these observations indicate rapid exhumation, continuous erosion, and transit of eroded materials to the sedimentary basins. We thus infer that the linked climate and erosion patterns, which we observe today along the SHF, have been sustained during Pliocene-Quaternary time, if not during the entire Late Cenozoic. This environment thus appears to record a strong feedback between monsoonal precipitation, fluvial erosion, and exhumation. Furthermore, increasing climate instability worldwide during the Pliocene-Quaternary may have accelerated the feedback system between erosion, exhumation, and tectonism (e.g., Molnar and England, 1990; Zhang et al., 2001).

To further assess the extent of high exhumation along the SHF, we compiled available AFT ages (Fig. 10) and available higher temperature thermochronology data. The AFT data show two distinguishable zones of cooling ages. Almost all ages obtained from humid and the monsoon-influenced SHF are young (<1-5 Ma) (Bojar et al., 2003, and this paper, see also Fig. 1b and 3; Burbank et al., 2003; Copeland et al., 1999; Jain et al., 2000; Kumar et al., 1995; Lal et al., 1999; Searle et al., 1999; Sorkhabi, 1993; Sorkhabi et al., 2000; Sorkhabi et al., 1996; Vannay et al., 2004). For regions where no published AFT data were available, we used young (2-3 Ma) ZFT cooling ages. Furthermore $^{40}Ar/^{39}Ar$ (4-6 Ma), and Th-Pb monazite data (3-6 Ma) from several transects in Garwhal and Nepal were available (Fig. 8 and Tab. 1 in appendix). In contrast to these young ages, AFT cooling ages obtained in arid areas north of the main orographic barrier are 12-15 Ma in southern Tibet (Searle et al., 1997, see #11 in Fig. 1), and 6-40 Ma for the internal part of the NW-Himalaya (Kumar et al., 1995; Schlup et al., 2003, see fig. 1 #12 and 14). In these areas, like the drier Padar-Zanskar region exhumation rates are low and only range between 0.1 and 0.3 mm/a for Pliocene-Quaternary time (Kumar et al., 1995; Schlup et al., 2003). These rocks of the HHCS have thus resided near the surface since the mid Miocene. Consequently, due to insufficient precipitation for effective hillslope and fluvial erosion, these sectors of the orogen have been exhumed at much lower rates than comparable rocks along the humid SHF. Due to the lack of adequate thermochronometric data no long-term exhumation rates of the southern egde of the Lesser and Sub-Hiamalaya, can be quantified.

Young cooling ages are not only obtained in areas affected by major orogen-traversing rivers like the Tsangpo, Indus, or Sutlej with large catchment areas in the hinterland (Burg et al., 1997; Vannay et al., 2004; Zeitler, 1985), but also along longitudinal rivers sourced in the

High Himalaya (e.g., Bojar et al., 2003; Burbank et al., 2003; Sorkhabi et al., 1996). Despite smaller catchment areas of river networks, these regions apparently collect enough orographic precipitation and therefore have an adequate erosional potential to exhume deeper crustal material. Thus, the distribution of enhanced orographic precipitation plays a more important role in localizing erosion and deformation than the effects of orogen-traversing rivers along the central part of the SHF.

Figures 11a and 11c document the correlation between the sector of high topographic gradients, enhanced precipitation and spatial distribution of young cooling ages and exhumation rates. Similar results have also been recently proposed for Central Nepal by Hodges et al. (2004). In the sector of reduced average annual precipitation across the HHCS in the Sutlej Valley the AFT ages are young and still indicate moderate to high exhumation, in good agreement with observation made in Central Nepal. Burbank et al. (Burbank et al., 2003) argued that due to the absence of a trend in the distribution of AFT cooling ages, no direct precipitation-exhumation linkage exists across the SHF, despite a fivefold change in precipitation. However, they neglect to discuss if (1) crustal deformation and the thermal field can be localized in the same way as the partial distribution of precipitation and (2) possible impact of phases of intensified monsoon on different timescales, where increased precipitation penetrated further into the arid sectors of the Himalaya (Bookhagen et al., in review). Recent fluctuations of precipitation and mass flux, similar to those observed during the monsoon season during 2002 and 2003 may represent analogs for more erosive climate conditions in the geologic past (Bookhagen et al., in review).

Thus, assessing the relationships between high topography, steep river gradients, orographically controlled erosion and focalized exhumation and deformation over geologic time is crucial for any feedback between erosion and rock-uplift. Several models have been proposed. Hodges et al. (2001) suggest that the distribution of gravitational potential energy acts as the driving mechanism to compensate focused erosion by southward extrusion of crustal material. The extrusion of crystalline units like the LHCS today (Vannay et al., 2004) has been inferred to explain the coeval Early-Mid Miocene extrusion of the HHCS between the MCT and STFS (Burchfiel et al., 1992; Grasemann et al., 1999; Hodges et al., 1992). Coupled thermal mechanical modelling by Beaumont et al. (2001) and Jamieson et al., (2002) emphasizes the link between ductile extrusion and focused surface denudation. These authors conclude that without erosion, the extrusion of crystalline units would not develop and that rates of exhumation and geometry of the exhuming wedge are sensitive to the erosion parameters.

Alternatively, the Critical Coulomb Wedge theory provides a simple way to explain the interaction between topography, focused erosion, and exhumation. In this context, the erosional loss of material and the geometry of a critical taper are interpreted to be maintained by back-stepping faults such as the MT (Fig. 11a-d) and other back-stepping thrust systems along the SHF (Grujic et al., 2002; Hodges et al., 2001; Seeber and Gornitz, 1983; Wobus et

al., 2003).

As a third alternative, however, critical taper could also be maintained by underplating. In such a scenario the locallity of fast uplift could be due to imbrication of slices from a decollement ramp (Fig. 11b).

Based on our results we suggest that in order to accommodate the spatially concentrated loss of material along the SHF, focused exhumation and rapid erosion must be coupled with active southward extrusion of high-grade metamorphic units, as has been previously proposed for other parts of the orogen (Grujic et al., 2002; Hodges et al., 2001). As postulated by Vannay et al. (2004), in such a setting extruding high-grade metamorphic rocks along the Sutlej Valley would be bounded to the south by the MT at their base and by the KNFZ at their top, (Fig. 11b). In Garwhal and Kumaun, to the SE (#2 and 3 on Fig. 8) the MT is recognized over a long distance along strike (Valdiya, 1980a; Valdiya, 1980b) where monsoonal precipitation affects the High Himalaya over a broad sector (Fig. 8a). Toward the NW the MT only appears in a tectonic window across Sutlej Valley (Fig. 11) and diminishes in throw. The decrease in throw is mimicked a decrease in monsoonal precipitation from east to west. Thus, a back-stepping thrust appears to have developed only in those regions affected by high rainfall, strong erosion and exhumation, which indicates a close correlation between removal of large volume of rock and the magnitude of fault offset to balance loss of material.

In summary, these observations imply that localized erosion as described here is a first order process during shortening, when a mountain belt is favorable oriented in order to intercept moisture bearing winds. This in turn determines renewed faulting in the internal part of the Himalayan orogen, and thus a more diachronous pattern of deformation pattern of deformation in the mountain belt.

5.7 Conclusions

The Himalaya is probably a unique location to improve our understanding of the couplings between surface and tectonic processes. The AFT data obtained from the Himalayan Crystalline Core along two elevation transects crossing major tectonic structures are between <1 Ma and 4 Ma. Assuming a simplified denudation with long-term steady-state erosion and exhumation, the rocks were exhumed with ~1.4 $\pm$0.2 and 1.1 $\pm$0.4 mm/a with an average cooling of ~60-70 °C/Ma during Plio-Pleistocene time. An important finding is that the sample transects correlate with distance, but show no spatial relationship (within error) to Miocene structures such as the MCT or STFS. The distribution of AFT cooling ages across the Sutlej region and the correlation between areas of focused orographic precipitation and high topography imply a strong interaction between rapid erosion, exhumation, and sediment evacuation that is concentrated in a ~50-70-km-wide sector of the Himalayan deformation belt (Fig. 4a-d). To compensate this redistribution of material, back-stepping thrusts are activated which displace the crystalline core of the high Himalaya as an extruding wedge bounded by passive normal faults at the top, also recently suggested by Vannay et al. (2004) and Wobus

et al. (2003). The denudational loss of material is balanced by tectonic uplift through a coupling between surface processes and internal deformation of the orogen at depth. Thus, surface processes control the internal deformation along the SHF.

5.8 Acknowledgements

The authors would like to thank: A.K. Jain and S. Singh for valuable discussions and logistical support; B.Grasemann, C. Janda, C. Hager, E. Draganits, and J.-C. Vannay for introducing us to the spectacular geology of the Himalaya and granting access to unpublished data; the great Indian mountain guides S. Slathia and T. Tsering for support during fieldwork; and E. Stump, G. Hilley and S. Peacock for discussion and comments on an earlier version of this manuscript. We very much appreciate the reviews by M. Brandon and K. Hodges with detailed comments and suggestions that improved the manuscript significantly. We thank the Deutsche Forschungsgemeinschaft (DFG) for financial support (Grant # STR-11/4), and the DAAD for support of R.T. while at Arizona State University (ASU).

Ref Table (Dumitru, 1993; Dunkl, 2002; Galbraith, 1981; Galbraith and Laslett, 1993; Green, 1981; Hurford and Green, 1983)

6. FROM TECTONICALLY TO EROSIONALLY CONTROLLED DEVELOPMENT OF THE HIMALAYAN FOLD-AND-THRUST BELT

Rasmus C. Thiede[a,*], phone: +49-331-977-2908, fax: +49-331-977-5060, thiede@geo.uni-potsdam.de
J Ramón Arrowsmith[b], ramon.arrowsmith@asu.edu
Bodo Bookhagen[a], bodo@geo.uni-potsdam.de
Michael McWilliams[c], mcwilliams@stanford.edu
Edward R. Sobel[a], ed@geo.uni-potsdam.de
Manfred R. Strecker[a], strecker@geo.uni-potsdam.de

a Institut fuer Geowissenschaften, Universitaet Potsdam, Postfach 601553, Potsdam 14415, Germany
b Department of Geological Sciences, Arizona State University, Tempe, AZ 85287-1404, USA
c. Geological & Environmental Sciences, Stanford University, Stanford, CA 94305-2115, USA
* corresponding author

Submitted to Geology (November 2004).

Keywords: Himalaya, exhumation, erosion, uplift, geochronology

6.1 Abstract

The role of feedback between erosion and tectonics currently or in the past in determining the development of the Himalaya remains controversial, particularly the issue of whether erosion responds purely to uniform, upward tectonic transport, controlled by subsurface structures, or whether regions of focused erosion can influence the location of deformation within the orogen. New $^{40}Ar/^{39}Ar$ muscovite and apatite fission track (AFT) thermochronologic data provide the opportunity to determine the history of rock-uplift and exhumation paths along an approximately 120-km-wide NE-SW transect spanning the greater Sutlej region of the northwest-Himalaya, India. $^{40}Ar/^{39}Ar$ data indicates that first the High Himalayan Crystalline, and subsequently the southward propagating Lesser Himalayan Crystalline nappes were rapidly exhumed during Miocene time. In contrast, AFT data delineate synchronous exhumation of an elliptically shaped, NE-SW-oriented ~80 x 40 km sector spanning both crystalline nappes during Pliocene-Quaternary time. The locus of pronounced exhumation defined by the AFT data correlates with a sector of Holocene focused precipitation, high discharge, and sediment flux rates. We therefore hypothesize that the distribution of AFT cooling ages might reflect the regional degree of effectiveness of surface processes and fluvial erosion, and thus demonstrate the influence of erosion in localizing exhumation along southern Himalayan front.

6.2 Introduction

Integrated structural, thermochronologic, sedimentologic, geomorphic and geophysical

studies demonstrate that the evolution of tectonically active mountain belts can be strongly influenced by a dynamic coupling between climate-driven erosion and tectonics (e.g., Brandon et al., 1998; Dadson et al., 2003; Koons, 1990; Reiners et al., 2003). Studies have shown that the contributions of accreted material, erosional removal of rocks, and the spatial-temporal behavior of faults during mountain building processes may control the development of fold-and-thrust orogenic belts (Dahlen and Suppe, 1988; DeCelles and DeCelles, 2001). Numerical and analog modeling of fold-and-thrust belts demonstrates that their evolution is strongly controlled by the ratio of accretionary influx and erosional removal (e.g., Beaumont et al., 1992; Hilley and Strecker, 2004; Hoth et al., revised; Whipple and Meade, 2004; Willett, 1999). Furthermore, these models indicate that asymmetric erosional removal of material causes a self-organized compensation by internal deformation within the fold-and-thrust belt (e.g., Dahlen and Suppe, 1988; Hoth et al., revised; Whipple and Meade, 2004). Consequently, erosion must have a pronounced influence on the growth and rate of propagation of the fold-and-thrust belt, as well as on the pattern of exhumation and rock-uplift within it. However, even if these theoretical models describe the general aspects of orogenic development, there are few field studies with sufficient temporal resolution and spatial coverage to test them. The Himalaya has formed through thickening and shortening under consistent convergence rates and has been affected by high monsoonal precipitation and erosional removal over myr time scales, thus providing an outstanding setting in which to test the spatial and temporal character of tectonic and erosional interactions. While Wobus at al. (2003), Hodges et al. (2004), and Thiede at al. (2004) propose a positive feedback between erosion and deep-seated exhumation along the southern front of the High Himalaya, Burbank et al. (2003) believe that erosion in this region is primarily the passive response to uniform tectonic uplift.

The vast amount of sediments in the Bengal and Indus fans and the Himalayan foreland basin imply that the Himalayan orogen has been intensely eroded over the last ca. 20 Ma (e.g., Burbank et al., 1996a; Einsele et al., 1996; Metivier et al., 1999). With new $^{40}Ar/^{39}Ar$ white mica and apatite fission track (AFT) thermochronologic data combined with published thermochronology datasets (e.g., Jain et al., 2000; Thiede et al., 2004; Vannay et al., 2004), we have reconstructed the detailed distribution of rock-uplift and exhumation paths along an ~120-km-long NE-SW oriented transect across the entire Himalaya crystalline core in the greater Sutlej region of the NW-India (Fig. 12A). We constrain the evolution of the Himalayan fold-and-thrust belt from the Miocene to the present and hypothesize that our data indicate a change from tectonically to erosionally controlled exhumation since Miocene time.

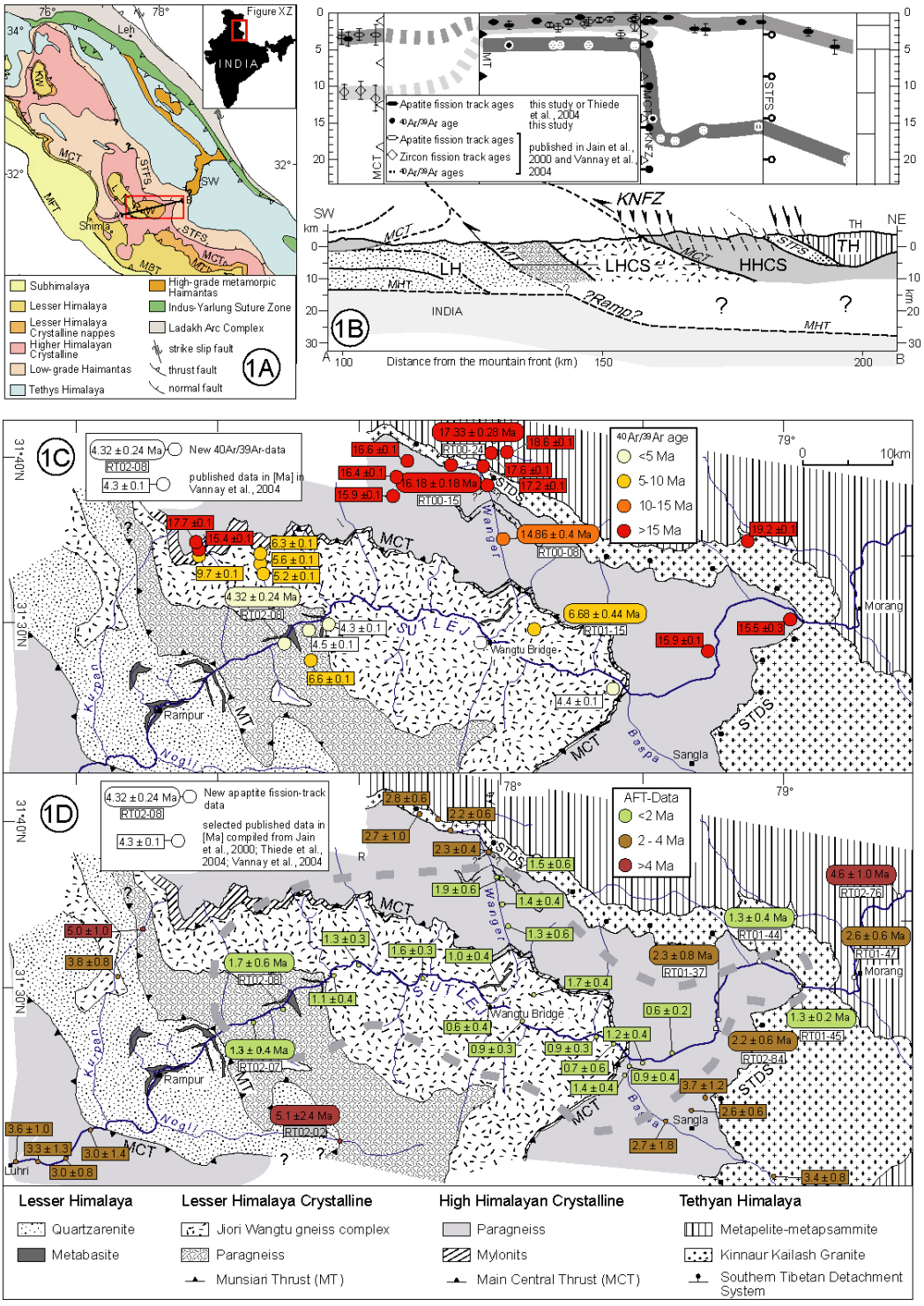

Figure 12: (12A) Generalized geologic map of the NW-Himalaya, India (after DiPietro and Pogue, 2004; Vannay and Grasemann, 1998). Red box shows the location of Figures 12C and 12D, black line denotes cross section in figure 12B. (12B) Simplified geologic cross section and distribution of cooling ages for the Sutlej valley section (after Vannay et al., 2004 and ref. therein). Cooling ages are based on new $^{40}Ar/^{39}Ar$ white mica and AFT ages and published 40Ar/39Ar, zircon, apatite fission track data (Jain et al., 2000; Vannay et al. 2004; Thiede et al., 2004). Abbreviations and geologic unit patterns as in figures 12C and 12D. (12C & 12D) Location of new samples analyzed for $^{40}Ar/^{39}Ar$ (12C) and apatite fission track (12D) geochronology marked by

rounded rectangle, whereas angular rectangle corresponds to selected published data (Jain et al., 2000; Vannay et al., 2004; Thiede et al., 2004). Dashed line define elliptic sector of rapid exhumation. HHC, High Himalayan Crystalline; KNF, Karcham Normal Fault; LH, Lesser Himalaya; LHC, Lesser Himalayan Crystalline; LKRW, Larji-Kulu-Rampur Window; MBT, Main Boundary Thrust system; MCT, Main Central Thrust system; MHT, Main Himalayan Thrust; MT, Munsiari Thrust; STFS, South Tibetan Fault System.

6.3 Geologic setting of the northwestern Himalaya

Sustained Eurasian-Indian convergence since the continental collision about 50 m.y. ago has caused persistent lateral and vertical growth of the Himalaya (e.g., Molnar and Tapponier, 1975), which has been accommodated by progressive displacement along a series of major crustal fault systems (South Tibetan fault system - STFS, Main Central thrust - MCT, Main Boundary thrust - MBT, Main Frontal thrust - MFT). These orogen-parallel fault systems bound the main Himalayan tectonostratigraphic domains (Tethyan Himalaya (TH), High Himalayan Crystalline (HHC), Lesser Himalaya (LH), and Sub-Himalaya), which are detached from the underthrusting Indian plate along the basal Main Himalayan Thrust (MHT) and incorporated into the orogen (Gansser, 1964; Molnar, 1984).

Along the Sutlej Valley in the northwest Himalaya (Fig. 12A), two crystalline nappes are exposed which are characterized by different Miocene cooling and exhumation histories (Vannay and Grasemann, 1998; Vannay et al., 2004). To the north, the HHC, a ~10 km thick, NE-dipping sequence of highly deformed amphibolite to migmatitic ortho- and para-gneisses is bounded by the MCT at the base and by the extensional STFS at the top; these faults were contemporaneously active during the early and middle Miocene (Burchfiel et al., 1992; Hubbard and Harrison, 1989). During crustal shortening, the sedimentary rocks associated with the LH were underthrust beneath the HHC nappes, which today outcroup as crystalline klippes.

In the footwall of the MCT to the south, rocks associated with Lesser Himalayan Crystalline (LHC) as part of the LH (Valdiya, 1980b) are exposed within the Larji-Kulu-Rampur Window (LKRW) (Vannay and Grasemann, 1998). These rocks are predominantly composed of amphibolite facies augen- and paragneisses. Structural and geochronologic analyses indicate that the LHC was affected by rapid cooling and exhumation during the late Miocene (Vannay et al., 2004). This sector is bounded by the Munsiari Thrust at the base and the Karcham Normal Fault Zone (KNFZ) (Hager et al., 2003) at the top. Although poorly constrained, the LH probably began thrusting onto the Sub-Himalaya along the MBT system at about the same time (Huyghe et al., 2001; Meigs et al., 1995).

6.4 Thermochronologic Data

The primary objective of our study is to constrain the regional extent and timing of rapid exhumation of rocks related to the HHC and LHC nappes. We present 5 new $^{40}Ar/^{39}Ar$ ages and 9 new AFT ages. White mica $^{40}Ar/^{39}Ar$ constrain Miocene cooling, and AFT data Pliocene-Quaternary. Analytical and sample preparation details, $^{40}Ar/^{39}Ar$ analysis release spectrums together with inverse isotope correlation diagrams in figure 13, as well as AFT data

results and analytical details listed in table 1 are documented in the data repository.

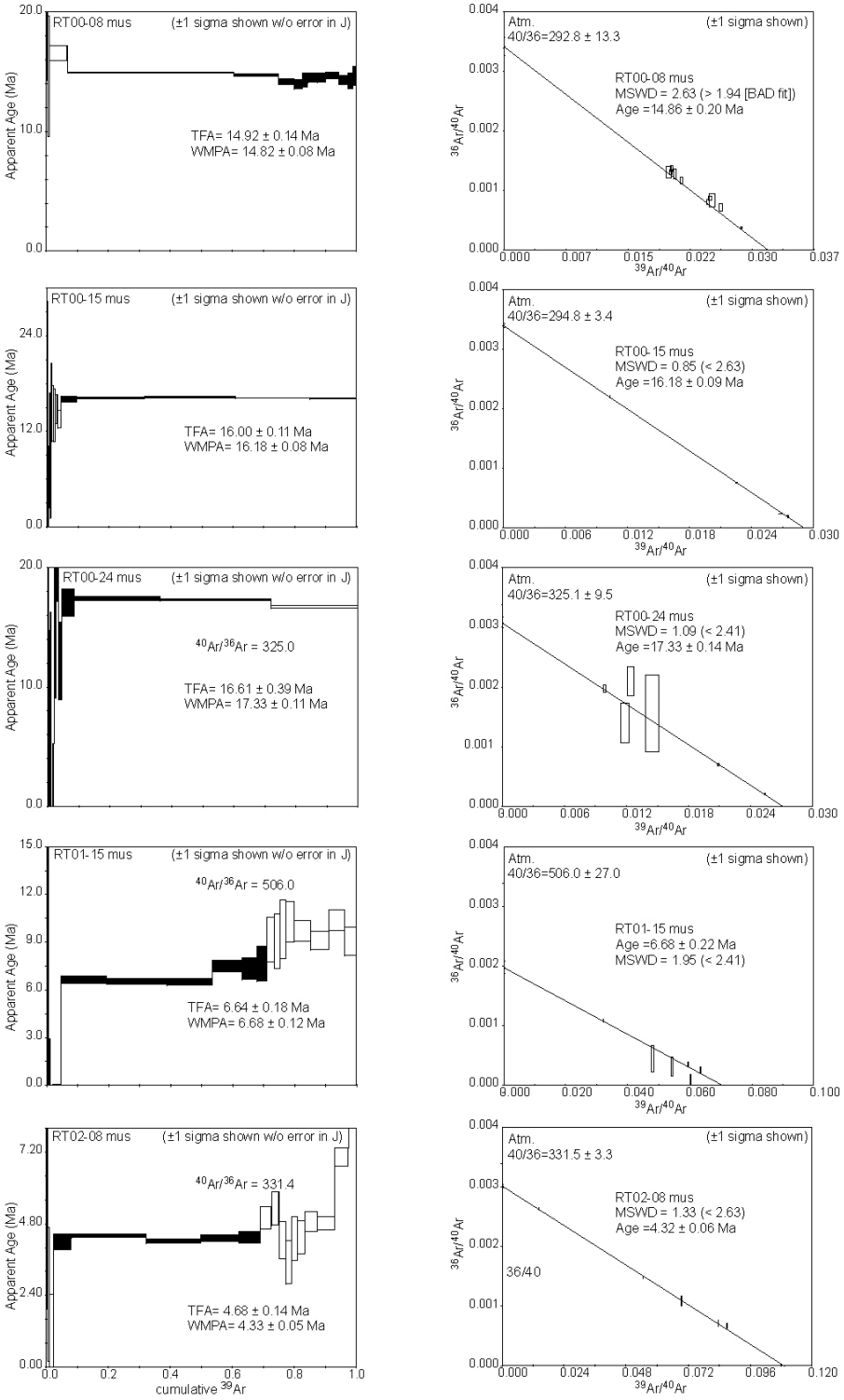

Figure 13. Spectra and inverse isochron diagrams of the $^{40}Ar/^{39}Ar$ measurements. Solid boxes show concordant steps used to compute weighted mean plateau age. One sigma uncertainties shown excluding error in irradiation parameter, J. TFA, total fusion age; WMPA, weighted mean plateau age MSWD, mean square weighted deviation (Wendt and Carl, 1991), which expresses the goodness of fit of the isochron.

We obtained $^{40}Ar/^{39}Ar$-white mica cooling ages of 4.3 ±0.2 and 6.7 ±0.4 Ma for samples of the LHC; samples from the HHC and the Tethyan Himalaya yielded ages between 14.9 ± 0.4 and 17.3 ± 0.3 Ma (Fig. 12C). The new data are consistent with published data (Vannay et al., 2004). While samples exposed in a sector between the MT and MCT yield ages between 4 and 7 Ma, those from the hanging wall yield ages between 14 and 19 Ma (Fig. 12C).

All AFT samples pass the chi-squared test, and therefore pooled ages are reported with 2σ errors (Tab. 3). Only samples with high U-content yielded a sufficient number of Dpar measurements (Tab. 3), indicating a fairly homogenous kinetic characteristic close to those of Durango apatite (Donelick et al., 1999). This observation implies a closure temperature of 140 ± 10 °C assuming a high cooling rate (~100 ºC/Ma) (Ketcham et al., 1999).

Three AFT samples were collected in the hanging wall of the MT to further constrain the southern extent of the sector of rapid exhumation. Along the bottom of the Sutlej valley two samples yield ages of 1.3 ± 0.4 and 1.7 ± 0.6 Ma, and one in the upper part of the Nogli valley 5.1 ± 2.4 Ma (Fig. 12D). An additional set of six samples were collected along the Sutlej river, covering the transition from the HHC into the Tethyan Himalaya; these help to determine the extent of the rapidly exhumed sector to the north. We obtained cooling ages between 1.3 ± 0.2 and 2.3 ± 0.8 Ma for rocks from the HHC, and 2.6 ± 0.6 and 4.6 ± 1.0 Ma for Tethyan-Himalaya rocks (Fig. 12D).

To view our new results in a regional context and to compare them to published thermochronology datasets (Jain et al., 2000; Thiede et al., 2004; Vannay et al., 2004) we plotted the data as a function of their structural position in relation to a simplified cross section (Fig. 12B). Within a transect from the MT to the STFS along the Sutlej River, cooling ages range between <1 and 2.3 Ma, whereas farther to the southwest and northeast, AFT ages increase to 2.5-5 Ma (Fig. 12B and D). In contrast, samples collected along strike of the MT to the north (RT00-32 and RT00-31) and south (RT02-02) yield ages as old as 5 Ma. Therefore, within the resolution of the method, segments of the MT situated farther away from the Sutlej valley bottom must have been inactive for the last several million years. Comparable results are obtained along the STFS, where ages of 1.3 Ma (RT01-45) were obtained from samples collected near the Sutlej valley bottom, and 3-4 Ma from samples (RT01-25) collected in the footwall of the STFS. Building on earlier interpretations (Thiede et al., 2004), this indicates the that major tectonic structures, which had accommodated displacement during the ductile deformation stage in this area, did not control brittle near-surface deformation and exhumation of the crystalline core, but rather acted as passive marker horizons during Pliocene-Quaternary time. Therefore, it is likely that tectonics is not the only control on the distribution of rock uplift in this zone during this time period.

Table 3: Apatite fission track data , see Fig. 12D for location.

Sample number	Altitude [m]	Latitude [DD]	Longitude [DD]	Rock type	Formation	# Xls	Spontaneous		Induced		Dosimeter		Chi-sq. P (%)	Pooled Age [Ma]	±2σ	Dpar [µm]/ ±σ/ n	Uran. [ppm]
							Rho-S	Ns	Rho-I	Ni	Rho-D	Nd					
RT02-02	1860	31.411	77.723	Gneiss	LHC	30	0.126	21	6.692	1111	13.86	5413	76	5.1	2.4		6.3
RT02-07	1200	31.511	77.745	Mica-shist	LHC	20	0.577	90	118	18411	13.69	5413	82	1.3	0.4		104
RT02-08	1430	31.543	77.801	Gneiss	LHC	30	0.103	28	16.47	4484	13.61	5413	64	1.7	0.6		15
RT02-76	2350	31.685	78.492	Shist	Tethyan Himalaya	19	0.647	159	32.69	8032	11.89	4721	95	4.6	1.0	2.5/0.15/76	32
RT02-84	1900	31.519	78.271	Gneiss	HHCS	30	0.361	103	38.42	10948	11.73	4721	54	2.2	0.6		39
RT01-37	2015	31.543	78.281	Gneiss	HHCS	25	0.222	44	21.61	4288	11.65	4721	45	2.3	0.8		22
RT01-44	2100	31.596	78.298	Gneiss	HHCS	25	0.305	68	51.82	11539	11.49	4721	71	1.3	0.4	2.5/0.16/100	53
RT01-45	2130	31.598	78.347	Gneiss	HHCS	22	0.517	125	91.07	22019	11.33	4721	35	1.3	0.2	2.3/0.12/84	98
RT01-47	2360	31.666	78.453	Shist	Tethyan Himalaya	20	0.424	108	35.31	8986	11.17	4721	57	2.6	0.6	2.5/0.16/80	38

Note: # Xls, number of individual grains dated;Rho-D, induced track density in external detector adjacent to dosimetry glass (x 10^6 tracks/cm^2); Nd number of tracks counted in determining Rho-D; Rho-S, spontaneous track density (x 10^6 tracks/cm^2); Ns, number of spontaneous tracks counted; Rho-I, induced track density in external detector (muscovite) (x 10^6 tracks/cm^2); Ni, number of induced tracks counted; Chi-sq. P (%), chi-sqare probability (Green, 1981; Galbraith, 1981); Age is the sample pooled fission track age (Hurford and Green, 1983); calculated using zeta calibration method (Galbraith and Laslett, 1993). Trackkey was used for calculating the counting results (Dunkl, 2002).

The following is a summary of key laboratory procedures. Samples were all analyzed by R. Thiede (zeta factor of 391 ± 27). Apatites were etched for 20 s in 5.5 N nitric acid at a temperature of 21.0 ±0.1°C. CN5 dosimetry glass was used as a neutron flux monitor. Samples were irradiated at Oregon State University TRIGA reactor. External detectors were etched in 40% HF, 21°C, 45 minutes. Tracks were counted with a Leica microscope with 100x air objective, 1.25x tube factor, 10x eyepieces, using transmitted light with supplementary reflected light as needed; external detector prints were located with kinetek computer-automated scanning stage (Dumitru, 1993).

The AFT analysis employs the external detector method following the zeta calibration approach of Hurford and Green (1983). Analytical precisions with and error of 0.2 to 0.8 Ma (±2σ) could be obtained from these young AFT ages due to the high U-content and the large number of grains counted per sample. Only grains with c axes parallel to slide plane were dated; zero-track grains were analyzed.

6.5 From diachronous to synchronous cooling of the Himalayan crystalline core

White mica samples derived from two crystalline nappes yield significant different white mica $^{40}Ar/^{39}Ar$ cooling ages, indicating diachronous thrusting and exhumation during the Miocene (Vannay et al., 2004). The MCT hanging wall cooled through the argon white mica closure temperature during early-middle Miocene time, consistent with the exhumation of the HHCS and the Tethyan Himalaya controlled by thrusting along the MCT since ~23 Ma (e.g., Hubbard and Harrison, 1989). In the MCT footwall, $^{40}Ar/^{39}Ar$ ages document late Miocene to early Pliocene cooling from which significantly younger phases of rock-uplift and exhumation can be inferred for the LHC nappe (Vannay et al., 2004). Differential uplift between HHC and LHC is accommodated by a zone of pervasive high-angle ductile to brittle-ductile normal faults, possibly related to the KNFZ (Hager et al., 2003). The diachronous exhumation could have been caused by a southward propagation of the sector of rapid rock-uplift (DeCelles et al., 2001; Vannay et al., 2004) or by underplating of a crystalline nappe detached from the Indian plate (Avouac, 2003).

In contrast, Pliocene-Quaternary AFT cooling ages reveal a marked change in the pattern of exhumation across the Himalayan crystalline core. While along the entire southern front of the High Himalaya all AFT samples yield ages of approximately 5 Ma or less indicating relatively high exhumation rates (Thiede et al., 2004 and ref. therein), certain sectors along the mountain front yield significantly younger AFT ages (0.5-2 Ma), (Thiede et al., 2004 and ref. therein). Modifying the earlier interpretation of the Sutlej region of Vannay et al. (2004) and Thiede et al. (2004), the new AFT ages indicate focused exhumation in a NE-SW oriented, elliptical sector of approximately 80 x 40 km extending from the MT to the STFS (Fig. 12D, dashed line). Concordant, young AFT ages across both the HHC and LHC nappes along the Sutlej imply that both nappes cooled synchronously and more rapid than segments toward the foreland and the hinterland. Importantly, within this sector, AFT ages are particularly young where the longitudinal profile of the Sutlej River has a steep gradient and is deeply incised where it crosses the southern front of the High Himalaya. Rather than being uniform along strike and parallel to major mountain-bounding structures of the orogen, this sector of pronounced exhumation correlates with the local maximum of focused monsoonal precipitation (Thiede et al., 2004), an area also affected by high discharge and sediment flux, indicating intense erosion (Bookhagen et al., in review; Bookhagen et al., in press)

6.6 Geodynamic Implications and Conclusions

Changes in the locus of rapid exhumation from HHCS to LHCS rocks indicates that the Himalayan fold-and-thrust belt propagated southward during early to mid Miocene time (e.g., DeCelles et al., 2001; Vannay et al., 2004). Although scarce, paleo-elevation estimates indicate that the High Himalaya and Southern Tibet had reached elevations similar to present at 10-12 m.y. ago (e.g., Garzione et al., 2000a). As a mechanical consequence, it has been suggested that the orogenic deformation front has propagated southward, activating the MBT

fault system, and causing uplift and exhumation of the LH (e.g., Huyghe et al., 2001; Meigs et al., 1995). This indicates that Himalayan fold-and-thrust belt had fully established an orographic barrier by late Miocene time (Rowley et al., 2001). This is in agreement with the creation of a monsoonal circulation pattern (Dettman et al., 2003 and ref. therein). Although the southern Himalayan front is affected by heterogeneous erosion at the myr timescale, the topography forms a nearly perfect arc (e.g., Bendick and Bilham, 2001). This suggests that the focused erosion is compensated by self-organized thrust activation resulting in heterogeneous distribution of rock-uplift and exhumation along the SHF. Rock-uplift in turn may have maintained a state of disequilibrium of longitudinal rivers, which forced these rivers to continually to incise. For example, the removal of the 10-15-km-thick HHCS nappe, which today is replaced at the surface by LHC-rocks forming the domelike Larji-Kulu-Rampur Window, indicates sustained high erosion rates of crystalline rocks in the Sutlej region (Fig. 12C and D). This assessment is consistent with the spatial distribution of $^{40}Ar/^{39}Ar$ and AFT cooling ages. Thus the distribution of AFT cooling ages may reflect the regional degree of effectiveness of the surface processes and fluvial erosion in the Sutlej region. Apparently, sustained erosion can localize tectonic processes, rather than exhumation being controlled purely by deeper crustal deformation processes. We therefore interpret that the change to synchronous exhumation of both crystalline nappe systems suggests that the orographic barrier, when a critical threshold is exceeded, plays a fundamental role in intercepting moisture, in focusing discharge, erosion and sediment transport and in controlling the distribution of exhumation within the compressive orogen.

6.7 Acknowledgment

The authors are grateful for discussions and logistical support of A.K. Jain, S. Singh, and B. Grasemann; the help of the great Indian mountain guide T. Tsering, L. Schoenbohm for reading earlier manuscript version; B. Fabian for figure drafting; the Deutsche Forschungsgemeinschaft (DFG) for financial support (Grant # STR-11/4).

6.8 Appendix

Electronic appendix and supplementary material for the manuscript: “From a tectonically to erosionally controlled development of the Himalayan fold-and-thrust belt” by Thiede, Arrowsmith, Bookhagen, McWilliams, Sobel, Strecker.

6.8.1 Thermochonology

All samples used for $^{40}Ar/^{39}Ar$ and AFT analysis are fresh, unalterated bedrock samples. The micas were saparated from five coarse-grained gneisses that also used for the AFT method. Pure Mica separates were prepared by crushing, sieving, washing in H2O and handpicking to achieve the desired purity of (>99%). The $^{40}Ar/^{39}Ar$ analyses were conducted at the Stanfrod University geochronology laboratory. The separates were rinsed in acetone and alcohol, subsequently wrapped in pure Cu foil, baked at 125ºC for 1 hour in air, and stacked in a pure SiO2 vial together with foil-packaged neutron flux monitors. Irradiated at the

TRIGA reactor at Orogon State University. Sanidine from Taylor Creek rhyolite, with an assumed age of 27.92 ± 0.17 Ma (Duffield and Dalrymple, 1990) was used as a neutron flux monitor. All analyses were conducted in a double-vacuum resistance furnace. Ages and isotopic ratios are reported at a 2σ-uncertainty level. Samples were step-heated to obtain three-isotope plots to correct for the composition of trapped Ar. Figure 2 illustrates $^{40}Ar/^{39}Ar$ release spectrum and inverse isotope correlation diagram for each sample. The solid steps within the release spectra indicate the increments used for calculating plateau ages. Further analytical details are found in Hacker et al. (1996).

Apatite Fission Tracks (AFT) are linear damage trails in the crystal lattice that form as the result of spontaneous nuclear fission of trace ^{238}U nuclei (Wagner and Van den Haute, 1992). New ^{238}U fission tracks form at an essentially constant rate and with a constant track length, while older tracks simultaneously anneal (and ultimately are erased) at high temperatures, making AFT an effective tool for reconstructing cooling and exhumation histories (e.g., Dumitru, 2000; Gleadow et al., 1986; Green et al., 1989b). At temperatures hotter than ~110-150 °C, all fission tracks are totally annealed, resetting the fission track clock to zero. The total annealing temperature (TAT) and the effective closure temperature depend on the kinetic characteristics of the apatite and the cooling rate (Ketcham et al., 1999). The partial annealing zone (PAZ) extends from the TAT down to ~60 °C, and within this temperature range tracks are partially annealed. Below ~60 °C, AFT are effectively stable because annealing occurs at a very slow rate (e.g., Gleadow et al., 1986). The kinematic characteristics of apatite can be evaluated by measuring etch pits figures (Dpar, Donelick et al., 1999). Durango apatite standarts were etched together with our samples. Length deviation between Dpar measurements derived from Donelik measurements (Donelick et al., 1999) of Durango apatites and our own measurement were corrected by linear correlation.

All samples are bedrock samples. For very young apatites, it may be impossible to obtain sufficient Dpar data for a robust interpretation and it was impossible to obtain sufficient track length data. However, several samples with older ages and/or higher U-content yielded multiple Dpar measurements for most analyzed crystals, permitting the calculation of closure temperatures (Ketcham et al., 1999). All of the single population ages in this study pass the chi-squared test, and pooled ages are reported with 2σ errors.

7. MID MIOCENE TO RECENT E-W EXTENSION IN THE TETHYAN HIMALAYA, LEO PARGIL DOME, NW-INDIA

Rasmus C. Thiede[a,*], phone: +49-331-977-2908, fax: +49-331-977-5060, thiede@geo.uni-potsdam.de
J Ramón Arrowsmith[b], ramon.arrowsmith@asu.edu
Bodo Bookhagen[a], bodo@geo.uni-potsdam.de
Michael McWilliams[c], mcwilliams@stanford.edu
Edward R. Sobel[a], ed@geo.uni-potsdam.de
Manfred R. Strecker[a], strecker@geo.uni-potsdam.de

[a] Institut fuer Geowissenschaften, Universitaet Potsdam, Postfach 601553, Potsdam 14415, Germany
[b] Department of Geological Sciences, Arizona State University, Tempe, AZ 85287-1404, USA
[c.] Geological & Environmental Sciences, Stanford University, Stanford, CA 94305-2115, USA
[*] corresponding author

Submitted to Geological Society of America Bulletin (July 2004).

7.1 ABSTRACT

Despite an overall convergent tectonic setting, synorogenic extensional processes play an important role in the extrusion of major gneiss domes during the evolution of orogenic belts. Since the Indian-Eurasian collision ~50 Ma ago several metamorphic-igneous gneiss dome complexes continuously developed in the collisionzone, though the origin of these processes is remaining controversial.

In NW-India the Leo Pargil metamorphic-igneous gneiss dome (31-34° N/77-78° E) is located in the Tethyan Himalaya. Here we present new field mapping, structural, and geochronologic data document that the western flank of the Leo Pargil dome was formed by extensional deformation along linked normal faults system. Along a Leo Pargil detachment zone (LPDZ) this has led to the juxtaposition of low-grade metamorphic, sedimentary rocks in the hangingwall and high-grade metamorphic gneisses in the footwall. However, the distributions of new $^{40}Ar/^{39}Ar$ data are less dependant by local structures but rather indicate a regional cooling during the mid Miocene. New apatite fission track (AFT) data demonstrate that much of the footwall was extruded along the LPDZ in a brittle-ductile stage between 10 and 2 Ma with a minimum displacement of ~9 km. Additionally, since ~4 Ma AFT-data indicate a regional accelerated cooling and exhumation episode.

The Leo Pargil and Gurla Mandata dome are characterized by E-W extension since the Mid Miocene whereas Eocene to mid Miocene gneiss domes by N-S extension. This is consistent with major changes in mid Miocene displacement pattern from contraction to normal and strike-slip faulting in the internal part of the Himalayan orogen.

Keywords: Himalaya, Tibet, extension, gneiss dome, geochronology, exhumation.

7.2 Introduction

Gneiss domes are tectonic culminations found in many orogens, characterized by localized extension (e.g., Eskola, 1949; Fossen, 2000; Jolivet and Goffe, 2000; Teyssier and Whitney, 2002). They play an important role in upper crustal tectonic denudation by ensuing exposure of formerly deep, and high-grade metamorphic continental crust. In collisional mountain belts, upper crust is tectonically thickened, deeply buried and heated (England and Thompson, 1984). Buoyancy forces and the ascent of hot, low-density crust may cause near-isothermal decompression that drives partial melting, leading to a positive feedback between these processes (Teyssier and Whitney, 2002). Both tectonic and surface processes may trigger this near-isothermal decompression, through the removal or thinning of upper crust by erosion and/or tectonic denudation (Burg et al., 1997; Teyssier and Whitney, 2002; Zeitler et al., 2001a). The association of these spatial and temporal patterns of exhumation with the development of large collisional orogens in the geologic past, has lead to the concept of "post-orogenic collapse" (Andersen, 1998; McClelland and Gilotti, 2003; Vanderhaeghe et al., 1999). However, the India-Eurasia collision zone illustrates that gneiss domes develop not only in post-collisional stage, but also in sectors of the orogen characterized by extension (e.g., Burg et al., 1984b; Scharer et al., 1986), during ongoing collision and shortening at the margins of the orogen (Fig. 14).

A variety of models have been proposed to explain extensional processes that may have lead to the evolution of these gneiss domes in the northern Himalaya and southern Tibet. These models include: (a) gravitational collapse due to overthickened upper crust (Molnar and Lyon-Caen, 1988; Molnar and Tapponnier, 1978); (b) extension due to regional conjugate strike-slip faulting associated with eastward extrusion of Tibetan crust (Armijo et al., 1986; Armijo et al., 1989; Taylor et al., 2003); (c) oblique convergence between India and Asia (Dubey and Bhakuni, 2004; McCaffrey and Nabelek, 1998; Ni and Barazangi, 1985); (d) arc-parallel extension by oroclinal bending (Klootwijk et al., 1985; Ratschbacher et al., 1994; Seeber and Pecher, 1998); (e) the isostatic response of mantle lithosphere due to erosion under Tibet (England and Houseman, 1989); (f) slab breakoff (Maheo et al., 2002); or (g) the effects of lower crustal partial melting and flow (Nelson et al., 1996; Royden et al., 1997). However, in order to validate these models, field and geochronologic data are necessary to precisely determine the time relations between shortening and extension or, to constrain the kinematics of deformation, and to quantify the amount of displacement.

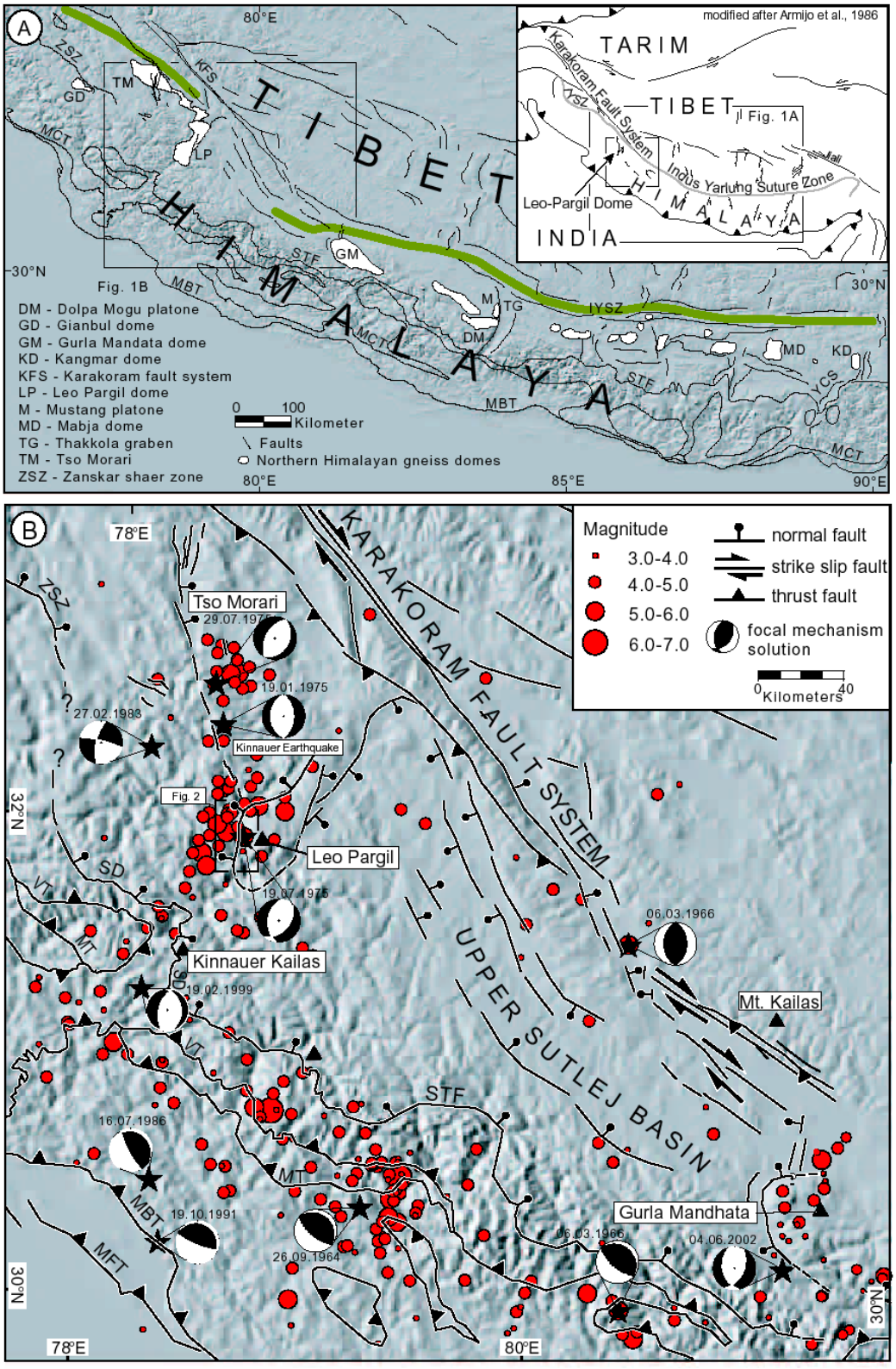

Fig. 14: Distibution of Northern Himalaya gneiss domes and major faultsystems of the Himalaya and Southern Tibet superposed on shaded relief (GTOPO 30 USGS). B shows major faults and seismicity of the NW-Himalaya and Southern Tibet (NEIC 1977-2004, ISC, Molnar and Lyon-Caen, 1989). Lower hemisphere diagrams of focal spheres show fault plane solution, open quadrants include compressional P-wave first

motion, black quadrants include dilatational first motion. Inset indicates location, modified after Armijo et al. (1986). VT, Vaikrita Thrust = MCT, Main Central Thrust; MT, Munsiari Thrust; MBT, Main Boundary Thrust; MFT, Main Frontal Thrust; SD, Sangla Detachment; STF, Southern Tibetan Fault system, ZSZ, Zanskar Shear Zone. Faults modified after Gansser (1964), Armijo et al. (1986), Hodges (2000), and Vannay et al. (2004).

Deformation at the lithospheric-plate scale, and crustal shortening and thickening in southern and central Asia record the ongoing continent-continent collision between India and Eurasia since the Early Cenozoic and have caused uplift of the Himalaya, the Tibetan Plateau, and adjacent mountain ranges (e.g., Allegre et al., 1984; Gansser, 1964; Molnar and Tapponier, 1975; Tapponnier and Molnar, 1977; Yin and Harrison, 2000). The southern Eurasian plate margin is separated from the sedimentary strata of the former Indian shelf by the Indus-Yarlung-Suture zone (IYSZ) and has undergone repeated north-south directed contraction since collision began in Paleocene time (Ratschbacher et al., 1994; Yin et al., 1999; Yin et al., 1994). Coeval, a discontinuous belt of metamorphic culminations, referred to as the North Himalayan gneiss domes (Fig. 14A), began to form (Burg et al., 1984b; Scharer et al., 1986). These domes are often associated with mid to late Miocene granite intrusions that can be traced across southern Tibet and were exhumed between Eocene and late Miocene time. The most prominent examples are the 55-30 Ma Tso-Morari (e.g., Berthelsen, 1953; Fuchs and Linner, 1996; Steck et al., 1998), the 15-10 Ma Kangmar dome (Burg et al., 1984b; Chen et al., 1990; Lee et al., 2000), the Gianbul dome (Robyr et al., 2002) and the dome exposed in the Suru valley (Ladakh, Gapais et al., 1992) both presumably exhumed in the early-mid Miocene time, and the <12 Ma Gurla Mandhata dome (Murphy et al., 2002)

While the Indian craton continues to collide with Eurasia, deformation in the northern Himalaya and southern Tibetan Plateau have changed since the Mid Miocene from approximately N-S shortening to mainly E-W extension, manifested by a complex and pervasive pattern of strike-slip and normal faulting (see Figure 14, Armijo et al., 1986; Coleman and Hodges, 1995; Molnar and Tapponnier, 1978; Ni and Barazangi, 1985; Ni and York, 1978; Taylor et al., 2003). The change in kinematic style has caused: (1) significant tectonic denudation of the Tethyan sedimentary sequence and the further formation of high-grade metamorphic gneiss domes (Gansser, 1964; Murphy et al., 2002); (2) the propagation of several N-S striking graben systems through the southern Tibetan Plateau, and into the High Himalaya (Armijo et al., 1986; Coleman and Hodges, 1995); (3) the formation of intramontane basins such as the Upper Sutlej basin (Gansser, 1964; Ni and Barazangi, 1985) or the Pulan basin (Gansser, 1964; Murphy et al., 2002; Ni and Barazangi, 1985) as well as several subbasins along the Karakoram Fault system. Overall structural character, tectonic landforms, and earthquake focal mechanisms demonstrate that this pattern of deformation is still active (e.g., Molnar and Lyon-Caen, 1989; Ni and Barazangi, 1984, Fig. 14).

In this study we address the evolution of ongoing east-west extension of the Leo Pargil dome complex in the NW-Himalaya at the Indian-Tibetan border. We present new quantitative data on the timing of strain and stress states. Detailed mapping of ductile and brittle structurs, as well as thermochronologic data are used to characterize the deformation kinematics of this

intramontane extensional environment. We present new apatite fission track and $^{40}Ar/^{39}Ar$ analyses to reconstruct the history of normal faulting and upper-crustal cooling through a temperature range of c. 450-100°C, and demonstrate sustained regional E-W to ESE-WNW extension since late Miocene time. We show that the Leo Pargil dome and the neighboring Gurla-Mandhata dome (Murphy et al., 2002) are young structures that extruded in an E-W direction, whereas older domes, such as the Kangmar dome, extruded in N-S direction, which is consistent with the major change in mid Miocene displacement patterns.

7.2.1 The Himalayan-Tibetan orogen

The Tibetan plateau comprises a complex tectonic collage that developed by sequential accretion of several microcontinents and terranes between the early Paleozoic and Cretaceous (e.g., Allegre et al., 1984; Yin and Harrison, 2000 and references therein). The Himalaya forms as a consequence of Cenozoic deformation between the Indian shield and the IYSZ (Fig. 14A). It consists of four major tectono-stratigraphic units including the Tethyan Himalaya, the High Himalayan Crystalline, the Lesser Himalaya, and the foreland basin (e.g., Lefort, 1975). These sectors of the orogen are bounded by north dipping crustal-scale fault systems (e.g., Burchfiel et al., 1992; Burg and Chen, 1984; Gansser, 1964; Lefort, 1975): the Main Frontal thrust (MFT); the Main Boundary thrust (MBT); the Main Central thrust (MCT); and the South Tibetan fault system (STFS). Between the STFS to the south and the IYSZ to the north, the Tethyan Himalaya (TH) comprises of two sedimentary successions, the lower Proterozoic to Cambrian sediments of the Haimanta Group (Frank et al., 1995), and the Paleozoic-Eocene Tethyan Sedimentary Sequence (TSS) (e.g., Gaetani and Garzanti, 1991; Gansser, 1964; Steck, 2003).

Until approximately mid Miocene time the IYSZ was strongly modified, first by the north-dipping Gangdese thrust to the north between 30 and 24 Ma (Copeland et al., 1995; Yin et al., 1999; Yin et al., 1994), and then by the south-dipping Great Counter thrust to the south (Heim and Gansser, 1939; Ratschbacher et al., 1994). The timing of this last thrust is still largely debated. Quidelleur et al. (1997) propose an age between 19 and 10 Ma in southeastern Tibet while Yuan et al. (2002) suggest 20 and 14 Ma and Yin et al. (1999) 13 and 10 Ma, respectively, in the Mount Kailas region.

Within the Tethyan Himalayan fold and thrust belt early crustal shortening during the India-Asia collision was accommodated by thin-skinned crustal thickening within the TSS and in general only caused moderate burial with low metamorphic overprint. This crustal shortening is expressed by SW-verging folds, NE-dipping axial-surfaces schistosity with a NE-dipping stretching lineation and related top-to-the-SW sense of shear (Ratschbacher et al., 1994; Steck et al., 1993; Wiesmayr and Grasemann, 2002). This deformation phase has been associated with the Eo-Himalayan deformation phase between 60 and 33 Ma (Hodges and Silverberg, 1988; Steck, 2003 and references therein; Wiesmayr and Grasemann, 2002). However, in several sectors of the orogen the mean NE-direction of underthrusting of the Indian passive margin below Asia was accommodated along a basal detachment at the

contact between the TSS and the Haimanta group (Herren, 1987; Wiesmayr and Grasemann, 2002), resulting in deeper burial, stronger metamorphic overprinting, and partial melting of the Haimanta group rocks during the Eo-Himalayan deformation phase. During early to mid Miocene the southwestern termination of the TSS the STFS was reactivated as an extensional structure due to rapid extrution of the HHCS to the south in relation to the TSS to the north (Burchfiel et al., 1992; Burg and Chen, 1984). Coeval, N-S shortening was accommodated along the Great Counter thrust system along the northern termination of the TSS (Gansser, 1964; Quidelleur et al., 1997; Ratschbacher et al., 1994; Yin et al., 1999).

7.2.2 Karakorum Fault system

The 1000-km-long dextral Karakoram fault system (KFS) is the most active NW-SE-striking tectonic feature in the region extending from the Pamir mountains in the northwest to the Gurla Mandata in the southeast (Fig. 14). The trace of the Karakoram fault cuts obliquely across the Tibetan terranes and the IYSZ, but strikes approximately parallel to the western sector of the Himalayan arc. Onset, total displacement, and rates of motion of the active KFS are still being debated (Avouac and Tapponnier, 1993; Brown et al., 2002; Lacassin et al., 2004 and references therein; Murphy et al., 2002; Peltzer and Tapponnier, 1988; Ratschbacher et al., 1994; Searle, 1996). Although the degree of seismicity along the southern section of the Karakorum fault is low, fault scarps cutting Quaternary alluvial fans, moraines and fluvial terraces suggest considerable recent activity (Armijo et al., 1989; Avouac and Tapponnier, 1993; Brown et al., 2002). Along strike of the KFS, several pull-apart sub-basins opened and have been filled with Late Miocene to Quaternary sediments (Armijo et al., 1986). The most prominent basin is the Upper Sutlej basin, containing thick Neogene-Quaternary lacustrine and fluvial deposits, which were inferred to cover the TSS (Gansser, 1964). To the NW the Sutlej basin terminates at normal-fault scarps bounding the Leo Pargil dome, whereas the SE-margin is delimeted by the Gurla Mandata dome (Murphy et al., 2002).

7.2.3 Mid to late Miocene normal and strike-slip-faulting

Similar to other regions in the Himalaya, two systems of high angle, brittle normal faults cross-cut older low angle ductile deformation structures in the greater Leo Pargil region. The first set is parallel to the Himalayan arc, and is characterized by NW-SE striking faults with top-to-the-NE normal displacement, such as the hanging wall of the Zanskar Shear zone (Dezes et al., 1999), the Sarchu Fault (Spring and Crespoblanc, 1992) or the Dutung-Thaktote fault zone (Steck et al., 1998). In contrast, the second set of faults, including the Tso Morari normal fault (Berthelsen, 1953; Steck et al., 1998), and normal faults west of lake Tso Kar (Fuchs and Linner, 1996) strikes N-S and overprints all other structures. Similar strikes and structural relations are observed in the graben systems of Southern Tibet (e.g., Armijo et al., 1986; Coleman and Hodges, 1995).

Major E-W extensional, low-angle detachment faults bounding the western termination of the Gurla Mandata have caused significant tectonic denudation of the TH (Murphy et al.,

2002), which is consistent with observations along the flanks of the Leo Pargil dome. The uplifted Leo Pargil dome is a NE-SW trending, metamorphic-igneous gneiss dome, with peaks reaching ~6500 m. The dome is bounded by normal faults on its northwestern and southeastern flanks (Fig. 14, Hayden, 1904; Ni and Barazangi, 1985). The extension and orientation of faults along the dome has been explained by an oblique thrust ramp (Dubey and Bhakuni, 2004).

Seismic activity is heterogeneously distributed across the Himalaya and Southern Tibet (see Fig. 14, Chen and Molnar, 1983; Ni and Barazangi, 1984; Pandey et al., 1995). The earthquakes in the TH and Southern Tibet are shallow intraplate events restricted to the overriding Himlayan plate, where focal mechanisms indicate strike-slip and normal motion (Molnar and Chen, 1983).

7.3 Methods

Apatite fission track (AFT) and $^{40}Ar/^{39}Ar$ thermochronology are effective tools for characterizing the exhumation history and cooling of footwall rocks accompanying major normal fault slip in the brittle crust (Armstrong et al., 2003; Ehlers et al., 2001; e.g., John and Foster, 1993).

We investigated the western flank of the Leo Pargil dome along a N-S traverse from Sumdo to the Spiti-Sutlej river confluence (Fig. 15). In addition, we conducted two E-W transects, one close to the Chango village (A-A'), and a second to the west of Sumdo village (B-B'). A total of 14 AFT-samples and 4 $^{40}Ar/^{39}Ar$-mica samples were collected along the valley bottoms. The transect A-A' was investigated in order to assess the deformation of the footwall (Fig. 16 and 17), and transect B-B' that of the hanging wall (Fig. 20). Both transects are oriented parallel to the mylonitic and mineral stretching lineation, thus parallel to the dominant displacement direction. In addition, the N-S oriented traverse was sampled to constrain fault displacement along strike. Therefore, if fault slip was rapid and of sufficient displacement, $^{40}Ar/^{39}Ar$ and apatite fission track thermochronology would constrain the time of cooling and exhumation.

7.3.1 Low-Temperature Thermochronology

Apatite Fission Tracks (AFT) are linear damage trails in the crystal lattice that form as the result of spontaneous nuclear fission of trace ^{238}U nuclei (Wagner and Van den Haute, 1992). New tracks form at an essentially constant rate and track length, while older tracks simultaneously anneal (and ultimately are erased) at high temperatures. The annealing process causes measurable reduction in both track lengths and apparent fission track ages (e.g., Gleadow et al., 1986; Green et al., 1989a; Green et al., 1989b). At temperatures higher than the total annealing temperature (T_a) between ~150 and 110 °C all fission tracks are completely annealed, resetting the fission track clock to zero. The T_a depends on the kinetic characteristics of apatite and the cooling rate (Ketcham et al., 1999). The partial annealing zone (PAZ) extends from the T_a down to ~60 °C, and within this temperature range tracks are partially annealed. Below ~60 °C annealing occurs at a very slow rate, therefore AFT are

effectively stable (e.g., Gleadow et al., 1986). The kinematic characteristics of apatite can be evaluated by measuring etch pit figures called Dpar (Donelick et al., 1999). Analytical procedures for AFT analyses and details of the sample preparation are listed with Table 4.

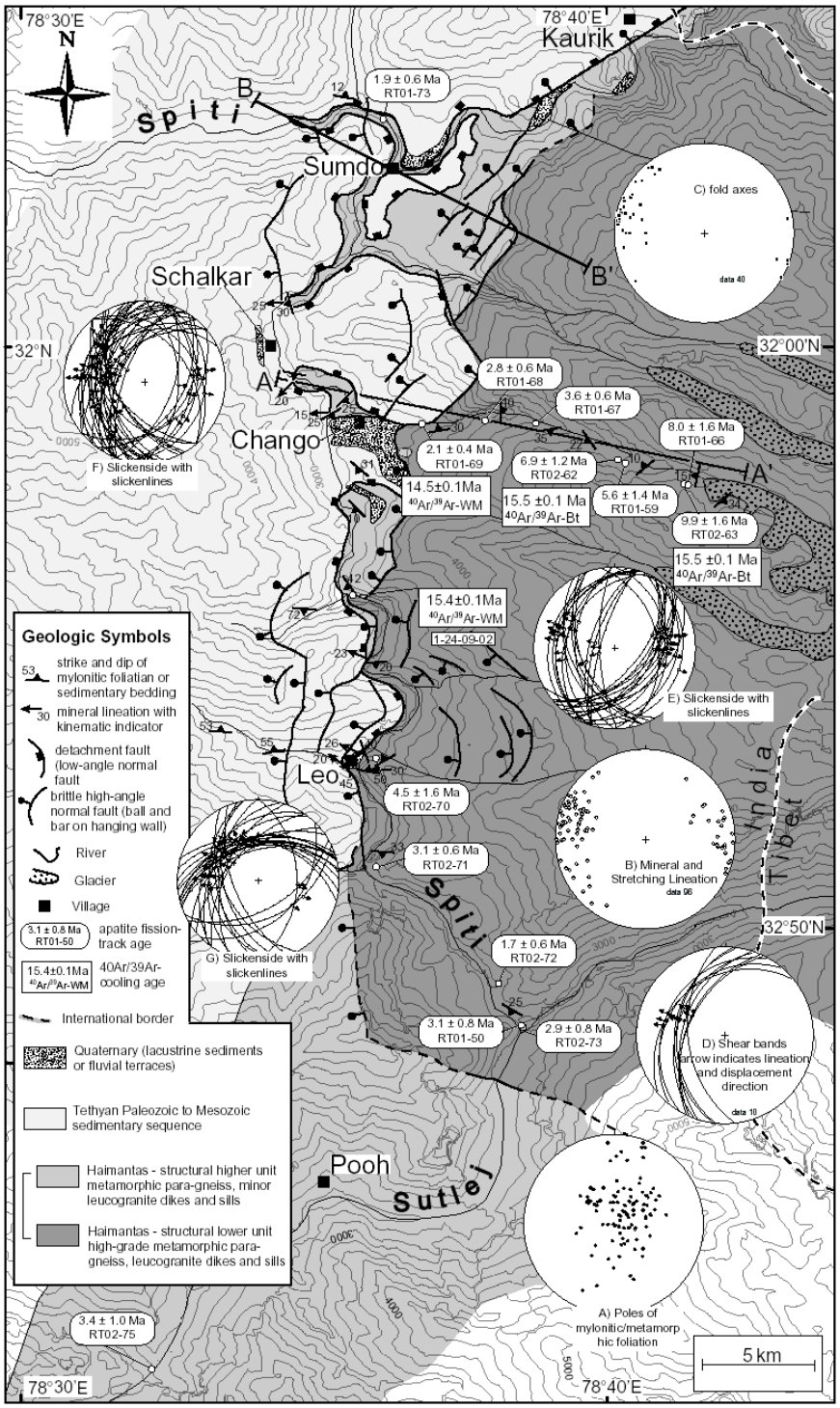

Fig. 15: Geologic map of the western flank of the Leo-Pargil dome derived from field mapping and extraction of TM-Landsat images (1:100,000). Steroplots (lower hemisphere) of a) poles of mylonitic foliation, b) orientation of mineral and stretching lineation, C) fold axes, D) shear bands (great circle fault surface, arrow

indicating displacement direction, E-G) Great circles are slickensides, arrows indicate displacement direction.

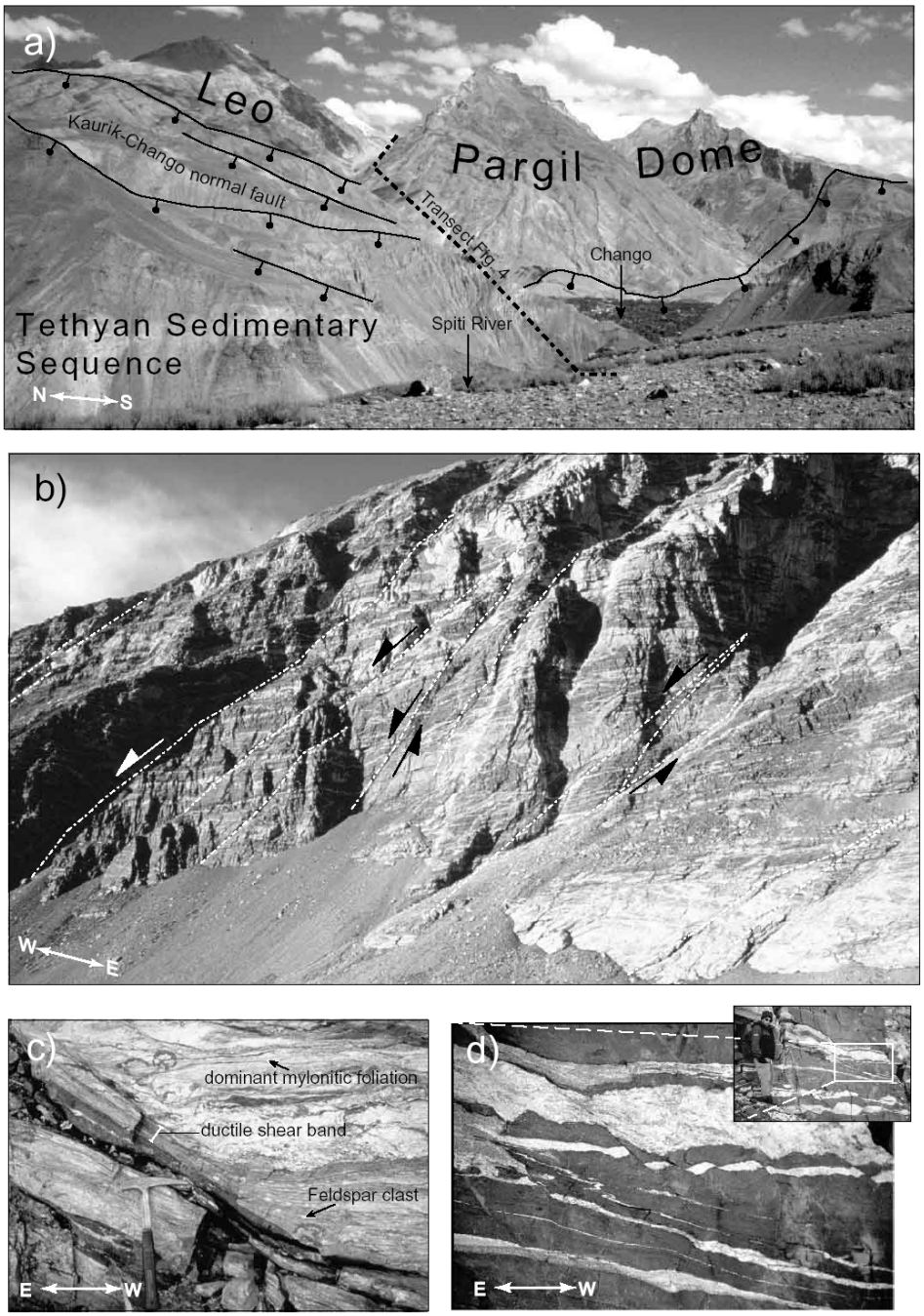

Fig. 16: a) View of the Leo Pargil dome to the E of the Kaurik-Chango normal fault zone. b) Dark colored high-grade metamorohic paragneiss of the Leo Pargil dome intruded by leucocratic dikes and sills. Note the pervasive, w-dipping faults are interpreted as forming Riedel shears of the brittle-ductile stage of LPDZ. c) Ductile shear band from high grade metamorphic paragneiss cross-cutting the mylonitic foliation and metamorphic layering incicates top-to-the-W normal displacement. d) The metamorphic layering is offset by brittle-ductile faults and/or backrotated by boudinage. Note feldspar enriched layers react in a more brittle manner, whereas quartzrich deform ductile.

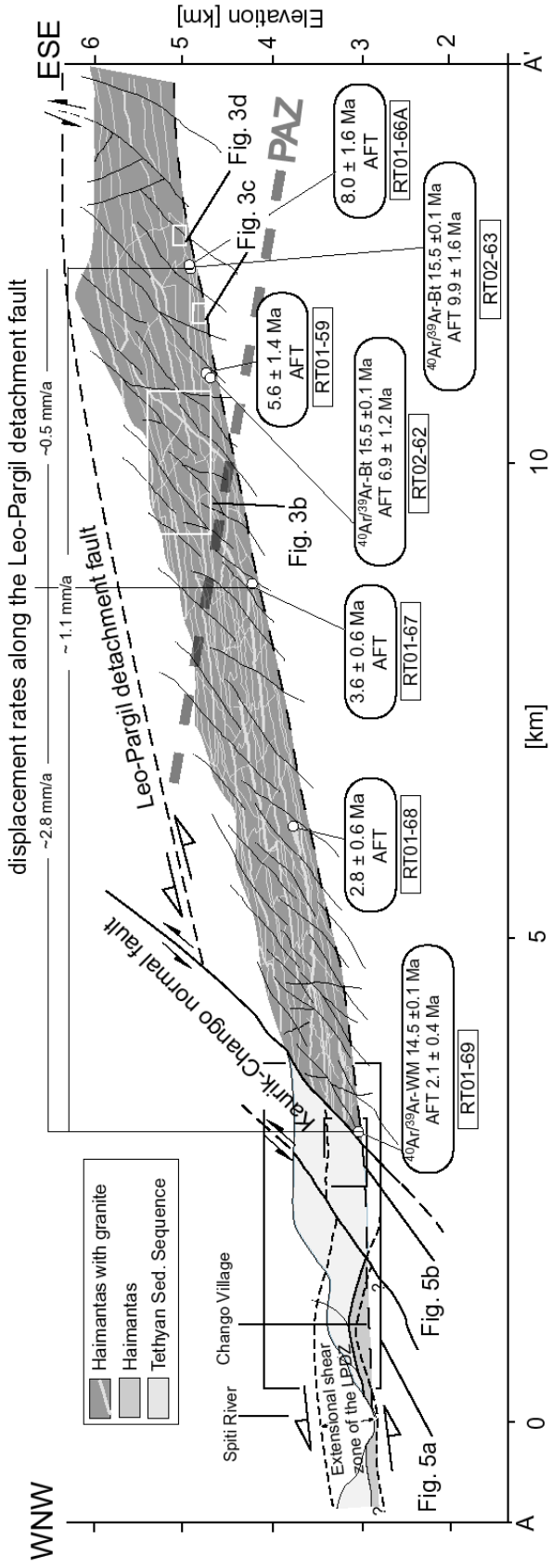

Fig. 17: E-W transect across the western flank of the Leo Pargil dome at the latitude of Chango village. Apatite fission track ages along the transect reveal continuous cooling and extrusion of the high-grade metamorphic footwall rocks of the Leo Pargil detachment fault between 10 and 2 Ma. 40Ar/39Ar data indicate a regional cooling between 16-14 Ma. The extensional shear zone of the LPDZ is only exposed in the western sector of the transect, to the east the LPDZ has been offset by the Kaurik-Chango normal fault zone (KCnf). In the footwall of the KCnf the LPDZ is removed by erosion and only structural deep section of the LPDZ footwall is exposed.

Fig. 17. E-W transect across the western flank of the Leo Pargil dome.

Table 4: Apatite fission track data from the Leopargil Region, see fig. 15 for location.

Sample number	Altitude [m]	Latitude [DM]	Longitude [DM]	Rock type	Formation	# Xls	Spontaneous		Induced		Dosimeter		Chi-sq. P (%)	Pooled Age [Ma]	±2σ	Dpar [µm]/ ±σ/ n	Uran. [ppm]
							Rho-S	Ns	Rho-I	Ni	Rho-D	Nd					
RT01-50	2600	N 31° 48.290'	E 078° 38.538'	granite	Haimantas	25	0.422	72	29.628	5055	11.015	4721	94	3.1	0.8	2.51/ 0.17/ 100	35
RT01-59	4670	N 31° 57.934'	E 078° 40.321'	granitic dike	Haimantas	8	2.038	120	81.616	4806	11.537	4754	96	5.6	1.4		84
RT01-66	4950	N 31° 57.616'	E 078° 41.345'	granitic dike	Haimantas	9	2.243	178	63.017	5001	11.566	4754	1	8.0	1.6		64
RT01-67	4160	N 31° 59.008'	E 078° 38.817'	granitic dike	Haimantas	25	1.220	266	76.360	16646	11.625	4754	71	3.6	0.6	2.33/ 0.10/ 100	81
RT01-68	3770	N 31° 58.658'	E 078° 37.900'	granitic dike	Haimantas	20	0.897	251	73.712	20625	11.654	4754	52	2.8	0.6	2.34/ 0.08/ 84	75
RT01-69	3200	N 31° 58.640'	E 078° 36.810'	granitic dike	Haimantas	23	0.524	114	57.764	12564	11.713	4754	21	2.1	0.4	2.33/ 0.10/ 92	60
RT01-73	3150	N 32° 03.840'	E 078° 36.207'	paragneiss	Tethyan Himalaya	20	0.305	62	37.493	7614	11.742	4754	68	1.9	0.6		39
RT02-62	4590	N31° 58.003'	E078° 40.207'	coarse paragneiss	Haimantas	30	1.802	512	67.124	19076	13.262	5413	57	6.9	1.2	2.64/ 0.14/ 100	62
RT02-63	4930	N31° 21.113'	E078° 41.363'	coarse paragneiss	Haimantas	30	1.770	491	45.139	12520	13.005	5413	15	9.9	1.6	2.45/ 0.10/ 100	43
RT02-70	2870	N31° 52.921'	E078° 36.046'	mylonite	Haimantas	30	0.180	40	9.969	2213	12.834	5413	100	4.5	1.6		10
RT02-71	2980	N31° 51.078'	E078° 36.085'	mica schist	Haimantas	25	0.498	162	39.356	12804	12.748	5413	90	3.1	0.6	2.72/ 0.13/ 100	37
RT02-72	2680	N31° 49.054'	E078° 38.139'	paragneiss	Haimantas	18	0.274	43	39.442	6191	12.663	5413	58	1.7	0.6	2.49/ 0.19/ 72	38
RT02-73	2560	N31° 48.227'	E078° 38.519'	paragneiss	Haimantas	24	0.342	66	27.573	5328	12.123	4721	83	2.9	0.8	2.75/ 0.21/ 96	34
RT02-75	2380	N31° 42.509'	E078° 32.212'	paragneiss	Haimantas	20	0.591	75	40.469	5137	12.044	4721	74	3.4	1.0	2.40/ 0.17/ 76	41

Note: # Xls, number of individual grains dated;Rho-D, induced track density in external detector adjacent to dosimetry glass (x 10^6 tracks/cm^2); Nd number of tracks counted in determining Rho-D; Rho-S, spontaneous track density (x 10^6 tracks/cm^2); Ns, number of spontaneous tracks counted; Rho-I, induced track density in external detector (muscovite) (x 10^6 tracks/cm^2); Ni, number of induced tracks counted; Chi-sq. P (%), chi-square probability (Green, 1981; Galbraith, 1981); Age is the sample pooled fission track age (Hurford and Green, 1983); calculated using zeta calibration method (Galbraith and Laslett, 1993). Trackkey was used for calculating the counting results (Dunkl, 2002).

The following is a summary of key laboratory procedures. Samples were all analyzed by R. Thiede (zeta factor of 391 ± 27). Apatites were etched for 20 s in 5.5 N nitric acid at a temperature of 21.0 ±0.1°C. CN5 dosimetry glass was used as a neutron flux monitor. Samples were irradiated at Oregon State University TRIGA reactor. External detectors were etched in 40% HF, 21°C, 45 minutes. Tracks were counted with a Leica microscope with 100x air objective, 1.25x tube factor, 10x eyepieces, using transmitted light with supplementary reflected light as needed; external detector prints were located with kinetek computer-automated scanning stage (Dumitru, 1993).

The AFT analysis employs the external detector method following the zeta calibration approach of Hurford and Green (1983). Analytical precisions with and error of 0.2 to 0.8 Ma (±2σ) could be obtained from these young AFT ages due to the high U-content and the large number of grains counted per sample. Only grains with c axes parallel to slide plane were dated; zero-track grains were analyzed.

All analyzed samples (Table 4 and Fig. 15) were collected in fresh bedrock outcrops. For very young apatites, it may be impossible to obtain sufficient Dpar data for a robust interpretation. However, several samples with older ages and/or higher U-content yielded multiple measurements for most analyzed crystals, permitting the calculation of closure temperatures (Ketcham et al., 1999). With exception of sample RT01-66, all of the single population ages in this study pass the chi-squared test, and pooled ages are reported with 2σ errors. Three partially annealed AFT ages with a sufficient track-length population along the Chango transect were modeled with the 'AFT solve' program (Ketcham et al., 2003) in order to constrain of the time-temperature pathway during cooling of the Leo Pargil dome.

In addition, $^{40}Ar/^{39}Ar$-analyes on mica were conducted to characterize the time of high temperatures cooling and exhumation within the footwall rocks of the LPDZ. All ages and isotopic ratios are reported at a 2σ-uncertainty level. Samples were step-heated to obtain three-isotope plots to correct for the composition of trapped Ar. Estimated isotopic closure temperatures for Ar are ~300º-350ºC for biotite and ~330º-430ºC for muscovite (McDougall and Harrison, 1999).

7.4 The Leo Pargil Dome

The geologic setting of the western flank of the Leo Pargil dome comprises the TSS to the west and high-grade metamorphic gneisses to the east, probably associated with the Haimanta Group or the HHCS (Fig. 15 and 16). The Leo Pargil dome is defined by the spatial extent of the high-grade metamorphic rocks. The leucocratic sills and dikes are limited to the high-grade metamorphic gneisses and constitute between 10 and 50% of the host rocks (Fig 16b-d). Several granite types exist including white mica granite, white mica and tourmaline-bearing granite, two-mica granite, and granite rich in biotite.

The western flank of the Leo Pargil dome is bounded by west-dipping low angle (<45°) normal faults (Fig. 17 and 18a) that form a detachment fault zone, which we have termed the Leo Pargil detachment zone (LPDZ). The LPDZ is a ductile shear zone separating high-grade metamorphic mylonitic schists, paragneisses, and variably deformed granite dikes and sills, in the footwall, and low-grade to non-metamorphic marbles to limestones, quarzites and sandstone of the TSS in the hanging wall. The footwall rocks have been exhumed from substantial depths as indicated by metamorphic index minerals such as garnet, staurolite and kyanite. The fault zone is a mylonitic shear zone, several tens of meters thick. Preferred shear horizons are quartz and limestone-rich layers (Fig. 19).

The continuation of the fault trace to the NE and SW is unclear and can only be inferred from satellite imagery. In the vicinity of Chango the tectonic contact is exposed between dark paragneiss and a dominantly layered section associated with the Paleozoic sequence of the TSS (Fig. 18a). In only a few locations do thin leucocratic dykes intrud into this high level of the paragneiss. Highly deformed phyllites, marbles, and quarzites form the covering base of TSS. The trace of the detachment fault undulates with a kilometer wavelength and fold axes

are oriented subparallel to the stretching lineation. Additionally, wide, open folding is found with subhorizontal, N-S oriented fold axes, perpendicular to the stretching lineation. The LPDZ and hangingwall rocks are cross-cut by brittle-ductile, listric normal faults (Fig. 20a and b). All structures are cross-cut by N-Sstriking, high angle, brittle normal faults, which are associated with the Kaurik-Chango normal fault zone (KCnf, Hayden, 1904). The KCnf juxtaposes two different structural levels of the LPDZ-footwall rocks (Fig. 17). In the hangingwall the LPDZ is preserved, whereas deeper levels of the LPDZ-footwall rocks form the footwall.

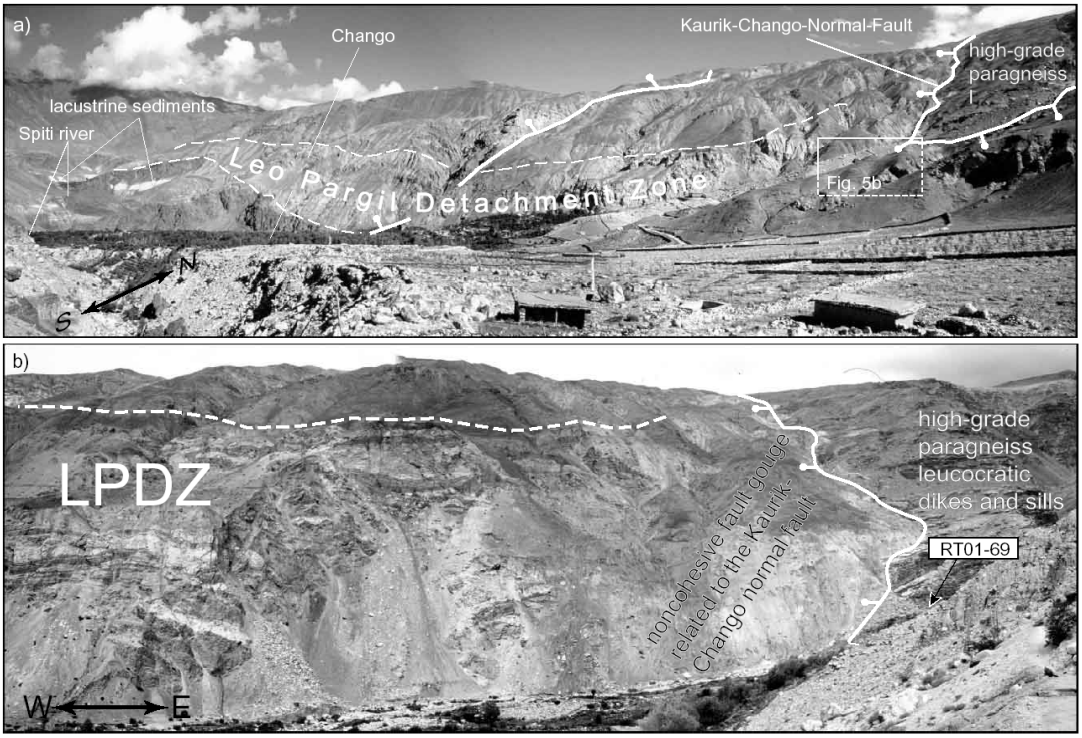

Fig. 18: a) View of the Leo Pargil detachment zone at the contact between the Haimantas unit (dark colored rocks) and the base of the Paleozoic section of the Tethyan Sedimentary Sequence. Brittle, high-angle normal faults associated with the Kaurik-Chango normal fault zone crosscut the detachment zone. The footwall rocks are interpreted to correspond to deeper segments of the Haimantas, which are pervasively intruded by leucocratic dikes and sills, as seen in figure 16b. White rectangle delineates Fig. 18b. b) Eoroded non-cohesive fault gouge zone of the Kaurick-Chango normal fault zone illustrates the brittle character.

7.4.1 Rock types and structures of the LPDZ-footwall

The upper section of transect A-A' (Fig. 17) is dominated by dark colored quartz-feldspathic mica-garnet gneisses and mica schists, inferred to be of sedimentary protolith. The paragneisses are characterized by a dominant, penetrative schistosity with a mainly sub-horizontal and preferentially west dipping orientation (Fig. 15, stereonet plot A). Well-aligned E-W to WNW-ESE oriented micas, feldspar, and quartzite grains define a closely spaced mineral lineation (Fig. 15, plot B). Occasionally, mylonitic shear zones parallel to the metamorphic fabric are observed. The mylonitic schistosity is folded at micro and macro scales. Axes of tight to isoclinal folds are oriented sub-parallel to the dominant mineral

lineation (Fig. 15, plot C). S-C and S-C' foliations are defined by aligned micas (biotite and white mica) and recrystallized quartz, and indicate a top-to-the-W sense of shear.

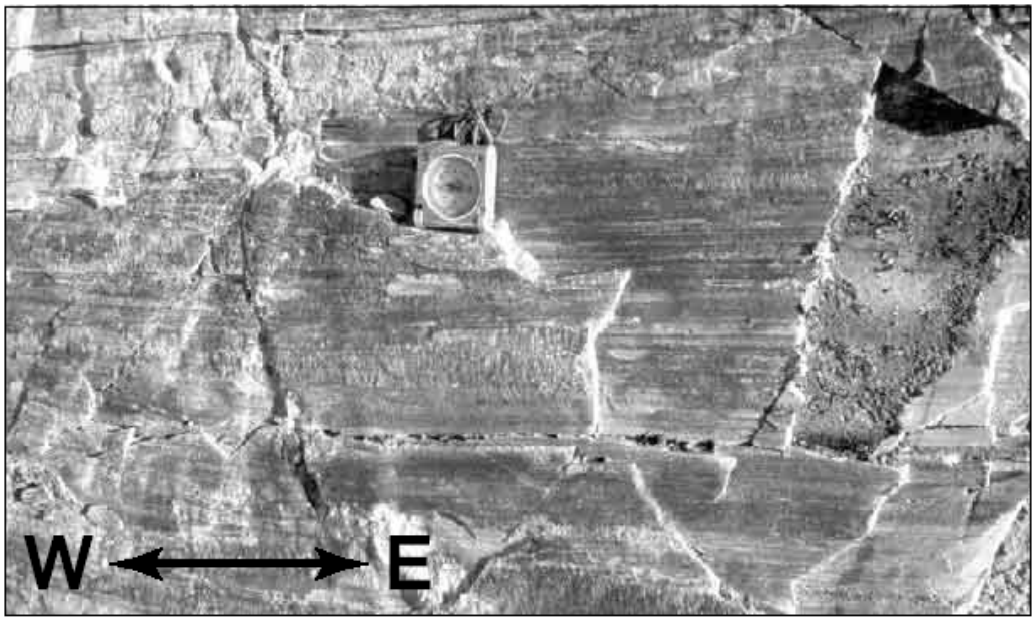

Fig. 19: Quartzitic mylonite at the base of the LPDZ hanging wall . Mylonitic stretching lineation is oriented E-W.

Based on cross-cutting relationships, several generations of granitic intrusions and varying intensites of ductile deformation are observed. The majority of the sills are parallel to the penetrative gneissic foliation as well as the mylonitic shear-zone foliation of the LPDZ (Fig. 16b). Late-stage, virtually undeformed granitic to pegmatitic dykes consisting of coarse feldspar and centimeter-scale white mica packages cross-cut the metamorphic fabrics. We interpret this relationship to be representative of different intrusion generations, which were implaced syntectonically.

The footwall rocks are deformed by ubiquitous shear bands from millimeters to several meters in scale cross-cutting the main paragneiss foliation (See Fig. 15 plot D and Fig. 16c). The shear bands are equally distributed in the upper 2 km of the exposed footwall rocks and indicate a pervasive ductile to brittle-ductile deformation of the footwall units. In most cases the paragneisses form low-strain lenses at centimeter to kilometer-scales and are surrounded by anastomosing leucogranites. Typically, the quartz-rich layers appear to have behaved in a ductile manner during deformation, while feldspars mainly deformed by brittle fracturing, or flowed within a quartz-rich matrix (Fig. 16c). This indicates temperatures of around 300ºC during deformation (Linker et al., 1984; Tullis and Yund, 1987). Most shear bands are synthetic, with a penetrative E-W stretching lineation, and reveal normal top-to-the-W sense of shear (Fig. 15, plot D).

Furthermore, the high-grade metamorphic rocks in transect A-A' (Fig. 17) are, characterized by penetrative, west-dipping brittle-ductile (Fig. 16d) to brittle faults. However,

using the granitic sills as offset markers, only minor offset can be documented (Fig. 16b). Thus, these faults may represent Riedel shears associated with the brittle-ductile stage of the main fault zone of the LPDZ. In addition, conjugate sets of high angled faults, W and E dipping slickensides with steep slickenlines, quartzitic fibers, and bent mylonitic schistosity clearly indicate E-W extension (Fig. 15, plot E).

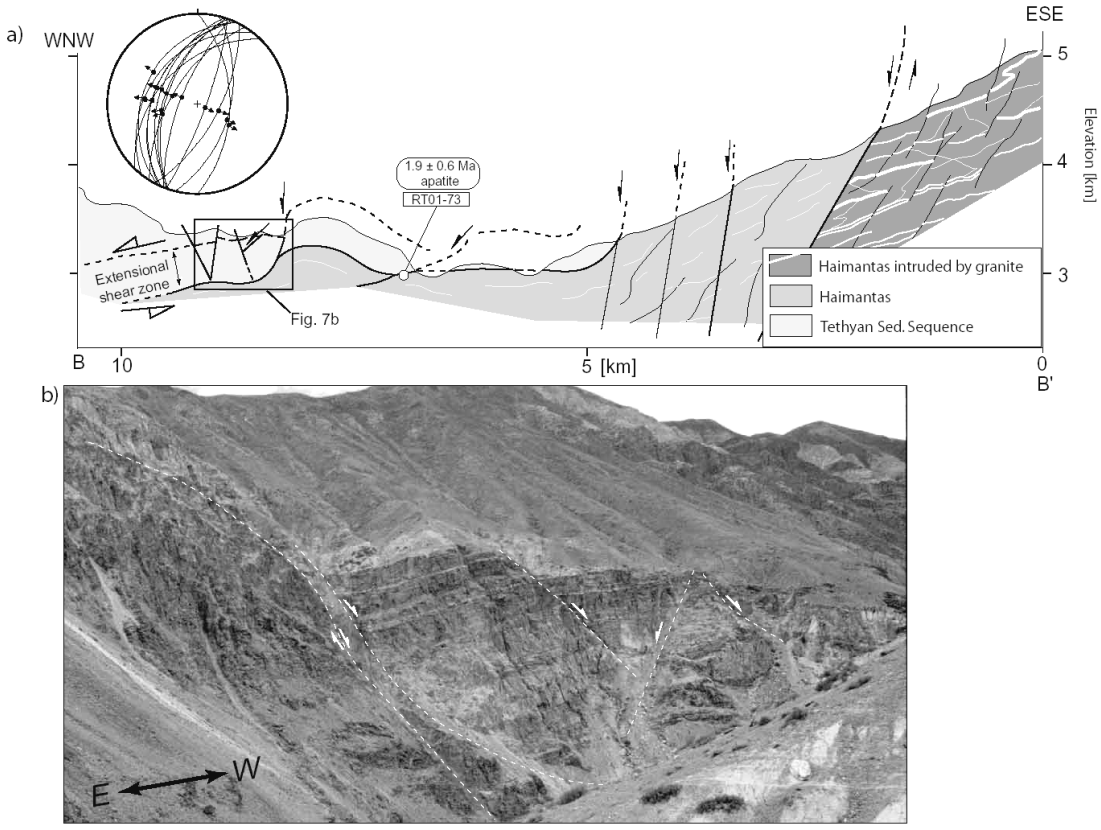

Fig. 20: WNW-ESE geologic cross section near Sumdo. Listric normal faults cut the LPDZ and sole into the base of the extensional shear zone (see figure b). Stereonet plot (lower hemisphere) showing slickensides (great circles) with corresponding slickenlines (arrows indicate sense of shear). Note that figure a and b show opposite orientation.

7.4.2 Hanging wall rocks of the Leo Pargil detachment fault

The hangingwall rocks consist of phyllites, marbles in transition to limestones, as well as quarzites and sandstones. Only the basal few hundred meters has a strong mylonitic and metamorphic overprint indicated by the synkinematic growth of micas (Fig. 18). In particular layers rich in quartz and limestone are completely recrystallized, highly deformed, thinned and characterized by a mylonitic fabric (Fig. 19). Therefore, it is difficult to associate these layers with their corresponding stratigraphic unit, but the appearance of the exposed succession clearly implies a sedimentary origin.

In transect B-B' west-dipping listric normal faults (Fig. 20a) cut hanging wall rocks of the LPDF at a high angle, seal out into the footwall rocks, subparallel to the mylonitic fabric in deeper structural levels (Fig. 20b), and display a kilometer-scale open folding perpendicular to

the stretching lineation. In addition, these rocks are overprinted by conjugated sets of brittle, N-S striking, high-angle normal faults (Fig. 20a), with well developed slickenfibers and striations, indicating down-to-the-W and E normal displacements, respectively.

At the base of the TSS forming the LPDZ-hanging wall a rapid decline of metamorphic overprint is observed, which indicates that the TSS rocks were neither deeply buried nor subjected to strong regional metamorphism. Thus, we interpret this thin, metamorphosed, and highly deformed layer of rocks as being formed syntectonically by contact with hot, high-grade metamorphic rocks of the LPDV footwall during exhumation.

In summary, the juxtaposition of high and low-grade metamorphic rocks along the LPDZ is the result of major tectonic displacements. Both hanging and footwall rocks of the LPDZ have a structural inventory of common origin, such as equal oriented mylonitic mineral and stretching lineation, sense of shear, and fold-axis that record a coeval E-W to WNW-ESE directed tectonic evolution with ductile normal displacement. In this context, parallel orientation of isoclinal fold axes and mylonitic lineation with axial fold planes parallel to mylonitic foliation may be related to coaxial thinning during extensional faulting (e.g., Mancktelow and Pavlis, 1994). In addition, ductile shear bands, and SC and SC' fabrics confirm protracted top-to-the-W normal displacement.

7.4.3 Kaurik-Chango normal fault zone

The Kaurik-Chango normal fault zone (KCnf) strikes north-northeast, dips up to 80º to the west (Fig. 16 and 18b), and comprises a cataclastic fault zone along the western flank of the Leo Pargil dome (Bhargava et al., 1978; Gupta and Kumar, 1975; Hayden, 1904). The faults cut both the hanging and footwall rocks of the LPDZ, and thus offset the youngest structures in the area. The most prominent fault zone has created a pronounced break in topography that separates moderately inclined hillslopes in the footwall from steep hillslope sectors in the hanging wall (Fig. 16a). Fault kinematic data collected in this normal fault zone document WNW-ESE dipping fault planes (Fig. 15, plot E and F) with steep slickenlines and striations indicating dip-slip normal faulting and E-W extension. Recent tectonic activity along this structure is underscored by faulted lacustrine and fluvial units, which are 26 to 90 ka old and contain seismite horizons (Banerjee et al., 1997; Mohindra and Bagati, 1996; Singh et al., 1975).

Furthermore, recent earthquakes and aftershock sequences provide insight into the modern kinematics of faulting in the Leo Pargil region (Fig. 14). For example, earthquake focal-mechanisms and aftershock studies of the 1975, Mb = 5.8, Kinnauer Earthquake (Singh et al., 1975), indicate dominant normal dip slip displacement (Molnar and Chen, 1983). The earthquake epicenter (N 31.94º, E 078.53º, ISC) was located about 30 km north of the Leo Pargil dome (Figure 14). The clustering of earthquakes shown in Figure 1 is mainly a result of the Kinnaur earthquake aftershocks, and defines a NNE-trending seismic zone along the western flank of the dome. The zone of seismicity is thus subparallel to the strike of major crustal faults (Ni and Barazangi, 1985). No epicenters, however, were recorded along the

eastern flank of the Leo Pargil dome.

7.5 Age constraints

Figure 17 summarizes apatite fission track and $^{40}Ar/^{39}Ar$ ages from the transect A-A' across the western flank of the Leo Pargil dome. We obtained AFT ages between ~10 and 2 Ma (Fig. 17). The apparent ages and track lengths plotted versus structural level exhibit a characteristic pattern, with systematically older AFT ages with increasing distance from the KCnf. Based on the observation that the main metamorphic fabric is sub-horizontal or dips slightly W, we infer that all samples were collected at approximately the same structural level, below but somewhat parallel to the LPDZ. AFT ages of 8-10 Ma of samples RT01-66 and RT02-63 are consistent with a minimum age for cooling and exhumation, and sample RT01-69, collected approximately 100 m E of the KCnf with an AFT age of 2.1 ±0.4 (±2σ) Ma, is consistent with continues exhumation. No alteration, which might indicate hydrothermal circulation, was observed.

Three samples with high U-content and older cooling ages yield representative track-length population. Samples RT02-62 and 63 have a moderately shortened track-length distribution of 13.9 ±0.2 and 13.1 ±0.3 µm (mean track length, Fig. 21), respectively; whereas sample RT01-67 is characterized by long mean track lengths of 14.3 ± 0.2 µm. The unimodal track-length distributions are characterized by progressively shorter mean track lengths with increasing distance from the KCnf, indicative of increasing degrees of annealing. This indicates that samples RT02-62 and 63 may have resided within the paleo-PAZ prior to exhumation or moved slowly through the PAZ during exhumation. Instead, sample RT01-67 has only a few moderately annealed track lengths, indicating that it stayed below the base of the paleo-PAZ prior to exhumation. Therefore, the base of the paleo-PAZ has to be placed somewhere between the positions of samples RT01-67 and RT02-62. Thus, all samples collected below the paleo-PAZ with young cooling ages (< 4 Ma) indicate that these rocks cooled more rapidly from >150 to <60 ºC between 4 and 2 Ma.

This interpretation is consistent with thermal modeling using 'AFT-Solve' of samples RT02-62, 63 and RT01-67, which suggest relatively slow cooling between 5 and 19 ºC/Myr during the late Miocene, followed by relatively rapid cooling between 20 and 35 ºC/Myr during Pliocene-Quaternary time (Fig. 21). Due to the fact that only samples obtained from the Leo Pargil yield this pattern, we interpret this in terms of moderate cooling and exhumation to be associated with localized tectonic extrusion along the LPDZ during mid-late Miocene time. In contrast, the Pliocene-Quaternary periods are characterized by faster cooling patterns.

The lack of unambiguous geologic offset markers makes it difficult to assess the fault-normal displacement rates across the LPDZ fault zone. However, a first order estimate of LPDZ slip rates can be derived from the change in time and space of the AFT results, assuming that the samples were exposed about in the same structural level. The displacement estimate is based on the ages of samples RT02-62 and –63. The footwall block

of the LPDZ accommodated ~9 km of displacement in a brittle-ductile to brittle stage between 10 and 2 Ma with an average displacement rate of ~1.1 ± 0.3 mm/a (Fig. 17). However, the data also indicate accelerated displacement through time with lower rates of ~0.5 ±0.2 mm/a between 10 and 4 Ma obtained from the upper three samples (RT02-63, -62, RT01-67) and displacement rates as high as ~2.8 ±0.5 mm/a of faster cooling between 4 and 2 Ma of the lower three samples (RT01-67, -68, -69).

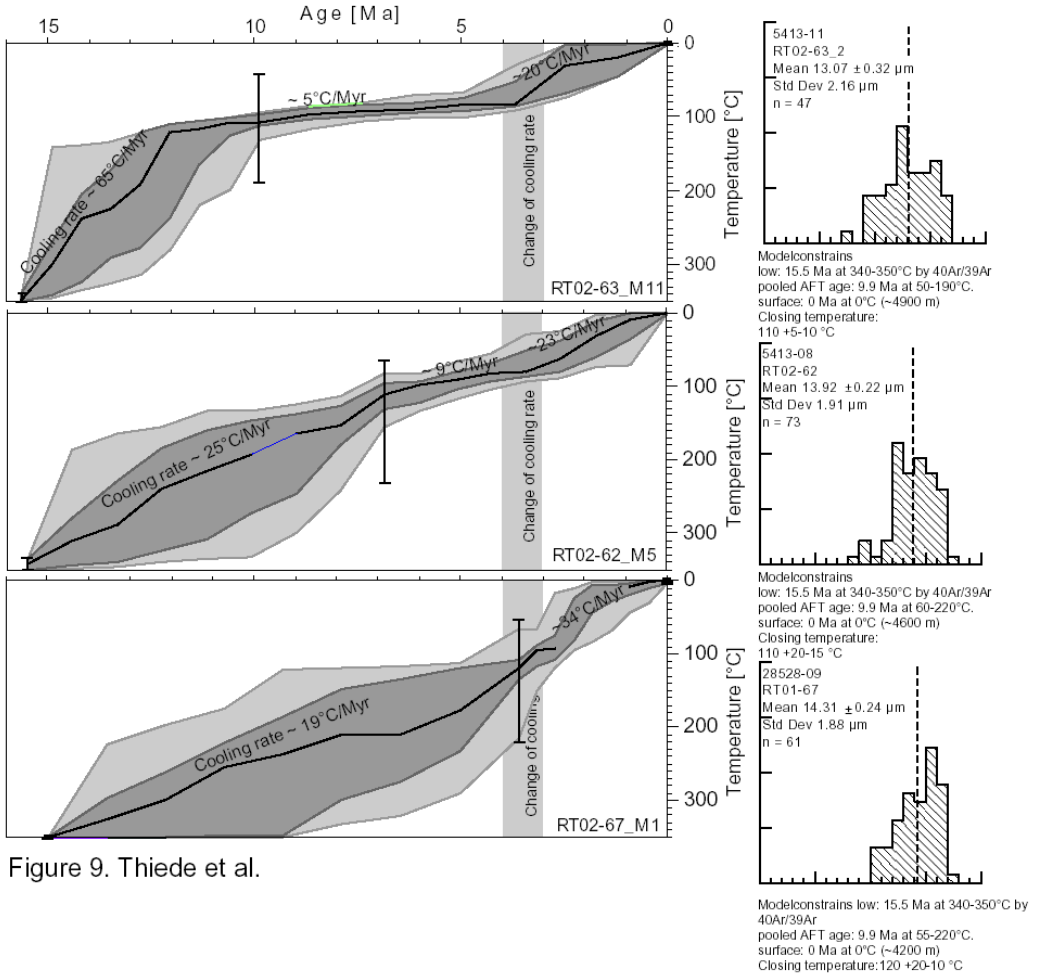

Figure 9. Thiede et al.

Fig. 21. Time-temperature modeling results obtained with AFT-Solve and track-length population, right plot. The black line indicates the best fit time-temperature path, the dark gray envelope bounds all nods with good fit and light gray area with acceptable fit. Note consistent increase in cooling rate between 4 and 3 Ma for all three samples. Cooling path for temperatures higher that the Ta are only constrained by Ar-ages. Modeling parameter: The 'inverse modeling constrained random search' with 10,000 calculated paths was used. Individual model constrains are given in text.

7.5.1 Lower Spiti valley traverse

Along the NS segment of the lower Spiti River, seven samples were collected from hanging and footwall rocks of the KCnf. The samples yield concordant AFT ages between 4.5 and 1.7 Ma (Fig. 15 and Table 4). The hanging wall samples (RT01-73 and RT02-75) have ages of 3.4 ±1 and 1.9 ±0.6 Ma; the footwall samples (RT02-70, -71, -72, -73, and RT01-50)

are 4.5 ±1.6 and 1.7 ±0.6 Ma. Due to the young AFT-ages only insufficient confined fission tracks length populations were obtained.

Due to the fact that the data provide neither a correlation between age and distance to the KCnf (Fig. 21A) nor between age and elevation (Fig. 22B), they indicate coeval cooling of the hanging and footwalls of the KCnf during late Miocene-Pliocene time. The fault offset, therefore, can only be moderate and was not significant enough to have displaced the isotherms. Thus, between ~ 4 and 2 Ma the age distribution was characterized by regional cooling, rather than displacement along the KCnf (Fig. 22A). For this reason, the inception of faulting along KCnf has been first established post 2 Ma and consequently, the majority of the tectonic denudation along the western flank of the Leo Pargil dome was accommodated by the LPDZ.

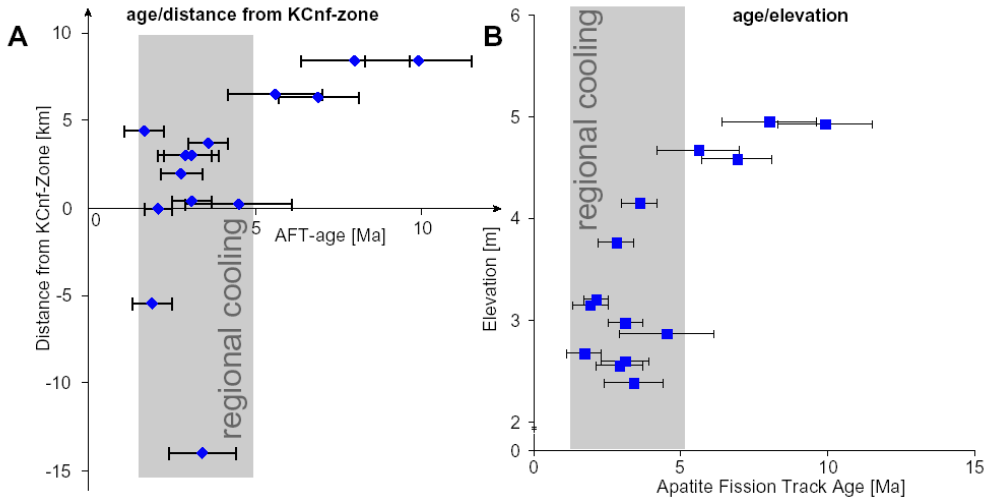

Fig. 22. Apatite fission track ages plotted versus horizontal distance perpendicular to the Kaurik-Chango normal fault (A) and versus elevation (B). AFT-ages within the grey sector yield ages between 5 and 2 Ma indepented of the distance to the KCnf-zone and elevation, respectively, indicating regional cooling rather then cooling related to tectonic denudation.

7.5.2 $^{40}Ar/^{39}Ar$-Thermochronology

The two white mica samples 1-24-09-02 and RT01-69 yield flat release spectra with plateau ages ranging from 14.5 ± 0.2 to 15.4 ± 0.2 Ma (Fig. 23). Both inverse isochron ages fall within the error of the plateau ages. Sample 1-24-09-02 has a well-constrained, near modern day atmospheric $^{40}Ar/^{36}Ar$ ratio of 339 ± 11 defined through regression analysis (modern atmosphere = 296), with a MSWD of 1.32. Although only 4 of 17 increments are considered, they show a wide spread on the inverse isochron plot. The low temperature increments indicate some excess Ar, however, the plateau age with >90% of the total released ^{39}Ar is well constrained. Sample RT01-69 has a slightly less precise isochron age because most data cluster closer to the $^{39}Ar/^{40}Ar$ axis, resulting in less well-constrained initial $^{40}Ar/^{36}Ar$ ratios. Even if the low temperatures step indicate some Ar loss, the plateau age with a total of ~70% ^{39}Ar released is still well constrained.

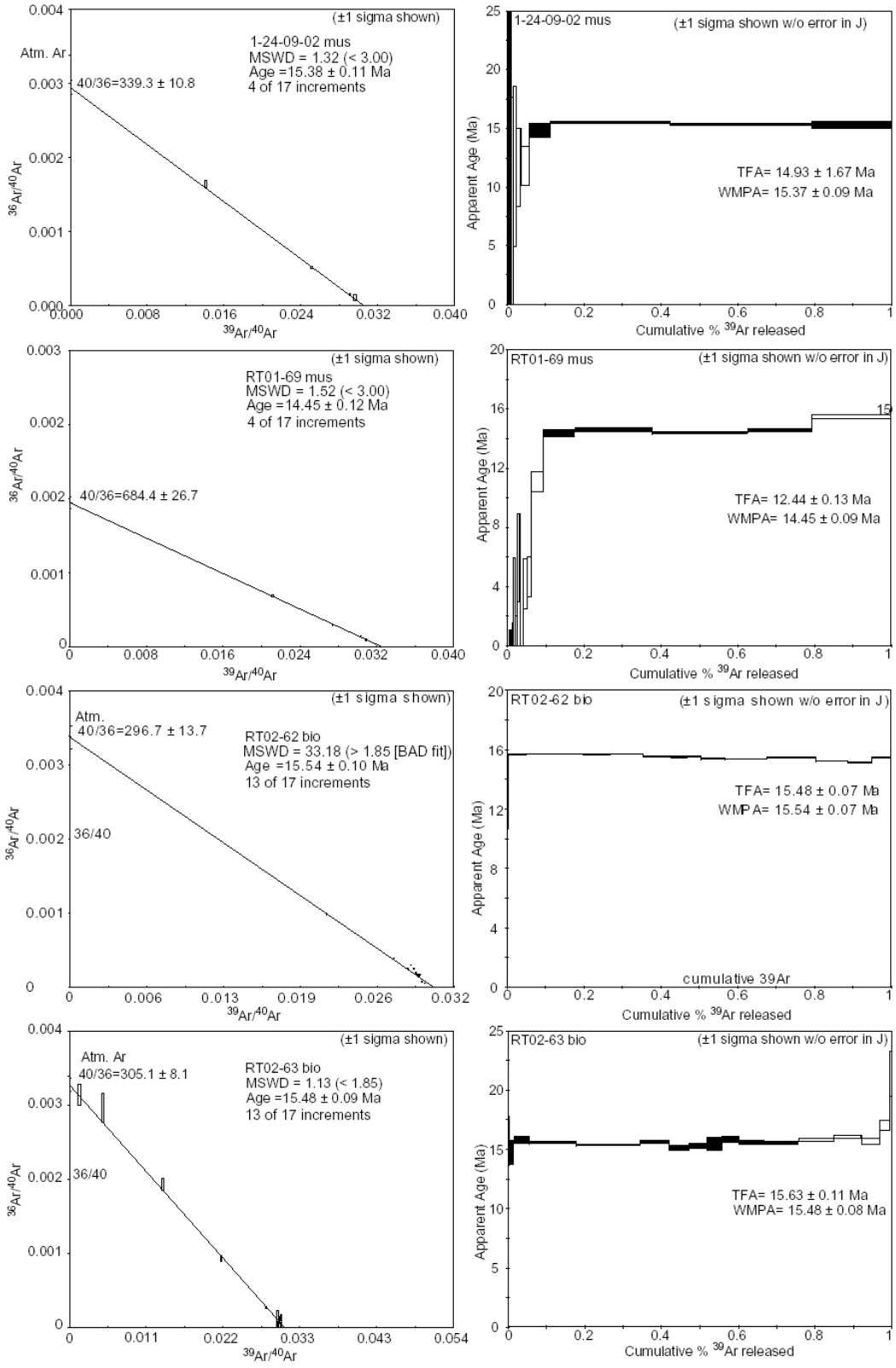

Figure 23. $^{40}Ar/^{39}Ar$ age isochron and spectra diagrams for muscovite and biotite from rocks in the footwall of the Leo-Pargil detachment system.

The two biotite samples (RT02-62 and RT02-63) both yield well defined flat plateau ages of 15.5 ±0.2 Ma with >75% of the total ^{39}Ar released (Fig. 23). The isochron ages give the same age using 13 of 17 increments in the regression calculation. In both samples the initial atmospheric $^{40}Ar/^{39}Ar$ ratio is well constrained and is close to present-day atmosphere (~300).

The ages show no systematic correlation between mica cooling ages and structural position within the footwall of the LPDZ, indicating that the entire metamorphic core of the Leo Pargil cooled homogeneously and rapidly below 300 – 450 ºC between 16 and 14 Ma (McDougall and Harrison, 1999). We infer the rapid cooling event to have been associated with the emplacement of hot high-grade metamorphic rocks close to the surface after near-isothermal decompression during exhumation. The samples therefore represent a minimum age constraint for the onset of extrusion.

7.6 Discussion

The LPDZ and KCnf are interpreted as a continuously evolving fault system accommodating E-W extension and exhumation within an overall contractional tectonic setting since late Mid Miocene time. Structural data document the evolution along the LPDZ from ductile displacement at deeper crustal levels to younger brittle structures formed at successively higher structural levels while maintaining the E-W extension direction. The thermochronologic data, modeling, and slip rate estimates suggest that rocks cooled slowly through the paleo-PAZ during early Late Miocene time and subsequently accelerated during the Pliocene and sustained during the Quaternary, indicating ongoing extrusion of the Leo Pargil dome. The distribution of AFT ages and modeling results of the track length population indicates a more regional signature of accelerated cooling rather than cooling associated with accelerated localized displacement along the LPDZ. Therefore, we suggest that the normal-fault displacement rates along the LPDZ may have been uniform during the entire interval between 10-2 Ma with rates of ~0.5 ± 0.2 mm/a (Fig. 17). This rate, however, only considers extension along the western flank of the Leo Pargil. Even if displacement rates along the KFS are still controversial, rates of approximately 5-10 mm/a are likely (Brown et al., 2002; Murphy et al., 2000; Searle, 1996). Thus the western flank of the Leo Pargil dome accommodates only a fraction of the total E-W extension of the termination of the KFS.

Pre-collisional palinspastic reconstruction of the Indian passive margin in the NW Himalaya reveals that a basal detachment for the TSS probably formed along the rheologic interface between the TSS and the Early Proterozoic-Cambrian Haimanta Group sediments (Wiesmayr and Grasemann, 2002). This contact is exposed along the Leo Pargil dome and might indicate that the LPDZ forms the basal detachment of the Eohimalayan crustal shortening. Chen et al. (1990) and Murphy et al. (2002) suggested that this detachment is an expression of the basal detachment of the STFS that was exhumed by a doming process. This would mean that the LPDZ may have developed as a contractional SW vergent structure during Eohimalayan crustal shortening and was reactivated during Early Miocene amphibolite facies NE-displacement, associated with the extrusion of HHCS along the STFS (Grujic et al.,

1996; Nelson et al., 1996; Neumayer et al., in press). Thus, the LPDZ may not only be related to the extrusion of the gneiss dome, but may rather represent a long-lasting evolution with several phases of ductile reactivation. This assessment is consistent with observation along the Zanskar shear zone or the STFS in the NW-Himalaya (Dezes et al., 1999; Herren, 1987; Steck, 2003, and ref. therein; Wiesmayr and Grasemann, 2002).

To date, only a very limited number of low-temperature thermochronologic studies are available from comparable structural settings in the NW-Himalaya and southern Tibet. Along the Sutlej Valley about 50 to 100 km SW of the Leo Pargil dome, several studies have been carried out and yield very young AFT cooling ages (0.5-5 Ma) (Jain et al., 2000; Thiede et al., 2004; Vannay et al., 2004). These data reveal fast exhumation along the Southern Himalayan Front. Approximately 100 to 150 km to the NW of the Leo Pargil dome, a ~100-km-long N-S transect adjacent to the Tso Morari lake has yielded predominately old AFT ages between 15-40 Ma across the TH and Tso Morari gneiss dome (Schlup et al., 2003). Only in the north across the Indus Suture zone and the Ladakh Batholith to moderately young ages of 5 to 8 Ma indicate somewhat faster exhumation during Late Miocene time. Across the Zanskar Shear Zone as associated as part of the STFS, which was active in early Miocene time (Dezes et al., 1999), AFT ages between 6 and 11 Ma (Kumar et al., 1995) indicate moderate to slow regional exhumation since the Mid Miocene.

It is interesting that there is a general dichotomy of AFT ages in the Himalaya and in southern Tibet. While young AFT ages (<~5Ma) have been recorded along the southern Himalayan front, where high exhumation rates coincides with high precipitation and erosion (Hodges et al., 2004; Thiede et al., 2004), Tibet and the high arid portions of the Himalaya appear to be characterized by relatively old AFT ages, indicating moderate exhumation (e.g., Kumar et al., 1995; Schlup et al., 2003). However, localized late Miocene to recent ages record fast exhumation along extensional structures such as Leo Pargil, Gurla Mandhata dome (Murphy et al., 2002), and the N-S striking graben in south Tibet such as theYangbajain graben close to Lhasa (Pan et al., 1993) and document striking similarities regarding the tectonic setting, structural evolution, and timing.

The timing of accelerated exhumation is intriguing in the context of global climate change and concomitant changes in erosion rates and the resulting impact on orogenic systems beginning at about 4 Ma (e.g., Zhang et al., 2001). Thus, an increase in orogen-wide erosion and/or the effects of the establishment of a new, more effective river network with increased river-incision rates could have caused the regional accelerated cooling pattern, which may also have been coupled with an increase in relief.

In any case, results presented here support a growing body of evidence that an important change in the strain field occurred in southern Tibet and the northern Himalaya. This changeover occurred approximately at the transition between mid to late Miocene time, when dominant N-S to NW-SE crustal shortening was superseded by E-W oriented upper crustal extension. (Coleman and Hodges, 1995; Ratschbacher et al., 1994; Searle et al., 1998; Yin et

al., 1999; Yin et al., 1994). Approximately at the same time exhumation and extensional E-W faulting were initiated along the Leo Pargil dome. Thereby the rather pervasive and regional character of E-W extension makes it unlikely that extension along the Leo Pargil is related to oblique thrust ramp, as suggested by Dubey and Bhakuni (2004).

There are several young structures observed in the northwest Himalaya that are compatible with active E-W extension or dextral strike-slip along the IYSZ and KFS. These include (1) the NNE-SSW striking and WNW-dipping Yurda normal fault between the Kashmir basin to the west and the Zanskar crystalline and Kishtwar dome, respectively, to the east, (Fuchs, 1975); (2) the E-dipping Tso Morari normal fault, the NNE-SSW striking conjugate Kiagor Tso normal faults, (Steck et al., 1998); and (3) the E-dipping normal fault at the western border of the Tso Kar (Fuchs and Linner, 1996).

The change of the internal strain field may have been caused by a regional reorientation of the tectonic stress field in which σ_1 became vertical and σ_3 horizontal, and E-W directed. Interestingly, this reorientation is also consistent with displacement patterns of the extruding gneiss domes and major fault systems such as the KFS of the Northern Himalaya. Older domes are characterized by dominantly N-S oriented extension (Burg et al., 1984b; Lee et al., 2000), whereas the younger structures such as the Leo Pargil and Gurla-Mandhata document east-west extension. Searle et al. (1998) documented two periods of rapid cooling along the central portions of the KFS, with transpressional fault motion at 18 Ma to 11.3 Ma, and a sustained transtensional character from 11.3 Ma to the present. This is consistent with new Ar/Ar K-feldspar thermochronology data revealing accelerated cooling between 14 and 10 Ma from the KFS caused by normal faulting (Lacassin et al., 2004).

A common model invoked to explain regional extension is related to gravitational instability of the Tibetan Plateau during the mid Miocene (Coleman and Hodges, 1995; Molnar and Chen, 1983; Molnar and Tapponnier, 1978). Alternatively, normal faulting may be caused by processes associated with slab break-off (Chemenda et al., 2000; Maheo et al., 2002) or right lateral oblique convergence (McCaffrey and Nabelek, 1998). In another model differential eastward extrusion of central and northern Tibet relative to southern Tibet is accommodated by right-lateral motion of the Karakorum-Jiali fault zone and normal faulting (Armijo et al., 1986). Within the sector of the NW-Himalaya studied here, however, extension is E-W to WNW-ESE rather than arc-parallel, NW-SE with structures perpendicular to the arc. This observations indicating that models involving oroclinal bending (Klootwijk et al., 1985; Ratschbacher et al., 1994) may be insufficient to explain the kinematics of ongoing extension.

In summary, the sustained E-W extension in the Leo Pargil is the expression of localized extensional tectonics in an overall contractional setting. The onset is related to regional stress-field reorganistation during the Mid Miocene, which also control the displacement direction of extruding domes and major faults systems such as the KFS (Lacassin et al., 2004; Searle et al., 1998). In addition, there appears to have been an impuls of accelerated regional cooling since the Pliocene, which may reflect more pronounced climaticalley driven

exhumation related to increased climatic instability.

7.7 Acknowledgments

The authors would like to thank: A.K. Jain and S. Singh for valuable discussions and logistical support; the great Indian mountain guides S. Slathia and T. Tsering for support during fieldwork; and Barbara Carrapa, Estelle Mortimer, and Lindsey Schoenbohm for discussion and comments on an earlier version of this manuscript. We thank the Deutsche Forschungsgemeinschaft (DFG) for financial support (Grant # STR-11/4), and the DAAD for support of R.T. while at Arizona State University (ASU).

(Ref. Table 1: (Dumitru, 1993; Dunkl, 2002; Galbraith, 1981; Galbraith and Laslett, 1993; Green, 1981; Hurford and Green, 1983).

8. CONCLUSIONS

The Himalayan crystalline core underwent several phases of rapid rock uplift and exhumation since the early Miocene (e.g., Catlos et al., 2001; Coleman, 1998; Hubbard and Harrison, 1989; Vannay et al., 2004; Vannay and Hodges, 1996). First, the rocks related to the High Himalayan Crystalline (HHC) and Tethyan Himalaya (TH) had cooled below the closure temperature for Ar-diffusion in white mica between 17 and 15 ± 0.4 Ma. This is consistent with combined thrusting along the Main Central Thrust and normal faulting along the Southern Tibetan Fault System (STFS) that involved rapid exhumation and cooling of HHC-related rocks from approximately 23 Ma onward(Coleman, 1998; Hubbard and Harrison, 1989). For rocks associated with the Lesser Himalayan Crystalline (LHC), we obtained significantly younger white mica $^{40}Ar/^{39}Ar$ ages, ranging between 7 and 4 ±0.4 Ma. These ages are consistent with sustained shortening within the Himalayan fold-and-thrust belt that resulted in southward propagation, of both rapid rock-uplift and the deformation front of the Himalayan fold-and-thrust belt. These space time patterns are conform with contemporaneous exhumation of the LHC nappes (DeCelles et al., 2001; Vannay et al., 2004) and activity on the Main Boundary Thrust (MBT) system during the late Miocene (Huyghe et al., 2001; Meigs et al., 1995).

In contrast, concordant apatite fission track data from both the HHC and LHC nappes in the Sutlej valley region (from the Munsiari thrust to the STFS), indicate synchronous cooling and exhumation during Pliocene to Quaternary time (between 2 and 0.5 Ma) indicating rapid cooling below ~140 ± 10 ºC. With increasing distance from the Sutlej river in any geographic direction, the ages increase to between 3 and 5 Ma. This indicates lower cooling rates since the Pliocene. Thus, by integrating my own and published fission track data (Jain et al., 2000; Vannay et al., 2004), within the resolution of the method, I was able to identify an elongated, E-W-oriented, approximately 80 x 40 km region of intensified and concordant cooling of both crystalline nappes during the Pliocene-Quaternary. Assuming a simplified denudation model with long-term steady-state erosion and exhumation, the rocks were exhumed with ~1.4±0.2 and 1.1±0.4 mm/a with an average cooling of ~50-60 °C/Ma during Plio-Pleistocene time. In the absence of evidence for any tectonic reactivation at this time, my preferred interpretation of this cooling age pattern is that this change to synchronous and reactivated exhumation of both the HHC and LHC crystalline may indicate a change from tectonically to erosionally controlled exhumation processes.

Our favored scenario is as follows: Localized rapid exhumation of deep crustal rocks which is limited to the elongated sector along the Sutlej river correlates with a steep longitudinal river gradient, high relief and high precipitation during the Indian summer monsoon. Consequently, based on the assumptions of the stream power law (Howard and Kerby, 1983) the combination of high river discharge, steep riverbed gradient, and narrow channels provide

conditions of high erosional potential. This in turn enables pervasive erosional surface processes. During the Holocene, the Sutlej region in the High Himalaya is characterized by high fluvial erosion and sediment flux rates (Bookhagen et al., in review; Bookhagen et al., in press). Thus, this elongated sector is characterized by a close spatial correlation between high Holocene erosion rates and Pliocene-Quaternary rapid exhumation. In addition, thermal-mechanical numerical modeling by Koons et al. (2002) indicates that rapid fluvial-incision at the scale of large river gorges can result in a localization of strain in topographic gaps, where localized exhumation of high metamorphic rocks can occur as a consequence of efficient erosional sediment removal.

Since the early Miocene, vast sediment accumulation within the Himalayan foreland basin, the Indus and Bengal fans implies sustained high fluvial erosion and sediment flux rates derived from the southern Himalayan front (Burbank et al., 1996a; Einsele et al., 1996; Metivier et al., 1999). Paleoelevation estimates indicate that approximately 11 Ma ago the uplift of the High Himalaya and Southern Tibet had reached elevations similar to present (e.g., Garzione et al., 2000b), which would imply that the Himalayan fold-and-thrust belt had been fully established as an orographic barrier by that time. This inference agrees with a widely held view that monsoonal circulation pattern had also been fully operational by that time (Dettman et al., 2003; Dettman et al., 2001).

Thus compensating focused erosion imposed by monsoonal rainfall and effective sediment removal is driven by heterogeneous distribution of rock-uplift and exhumation along the SHF since the late Miocene. This rock uplift has maintained a state of disequilibrium in the longitudinal river profile, which forces fluvial erosive processes continually to incise and adjust to an equilibrium profile. This is consistent with observations that longitudinal river profiles show knick points and are steep across the High Himalaya (Seeber and Gornitz, 1983). Thus, the denudational loss of material is balanced by tectonic uplift through a coupling between surface processes and internal deformation of the orogen at greater depth. These relationships lead me conclude that the distribution of AFT cooling ages may reflect the regional degree of effectiveness of the surface processes and fluvial erosion in the Sutlej region. For the High Himalaya, I argue that sustained erosion localizes the tectonic processes, rather than exhumation being controlled by deep crustal deformation processes. Therefore, the change to synchronous and concordant exhumation of both crystalline nappe systems suggests that the orographic barrier, after reaching a critical threshold plays a fundamental role in intercepting moisture. This, in turn leads to enhanced discharge, erosion and sediment transport and possibly controls the distribution of exhumation within an orogen, affected by active compression.

In contrast, the Leo Pargil dome is located in the arid, internal parts of the Himalayan range where plateau internal forces primarily control deformation within the northern Himalaya and Southern Tibetan Plateau and erosion plays a marginal role (Armijo et al., 1986; Coleman and Hodges, 1995; England and Houseman, 1989; Molnar and Chen, 1983; Molnar and

Lyon-Caen, 1989; Molnar and Tapponier, 1975; Nelson et al., 1996; Tapponnier et al., 2001; Yin and Harrison, 2000). The Leo Pargil ridge forms a metamorphic igneous dome complex, which is bounded by major fault zones. I observed ductile to brittle structures indicating sustained E-W extension along the western flank of the Leo Pargil in an overall contractional setting. Mica-$^{40}Ar/^{39}Ar$ and apatite fission track ages reveal two phases of cooling, one from mid to late Miocene and subsequently a second during the Plio-Quaternary. The onset of extension may be related to regional stress-field reorganization during middle Miocene time, which also controls the displacement direction of the extruding domes such as the Gurla Mandhata and major faults systems such as the Karakoram Fault System (Lacassin et al., 2004; Murphy et al., 2000; Murphy et al., 2002; Ratschbacher et al., 1994; Searle et al., 1998 and ref. therein). In addition, the impulse of accelerated regional cooling since the Pliocene may reflect more pronounced erosion driven exhumation related to increased global climatic instability (e.g., Zhang et al., 2001). These studies illustrate that tectonic processes affect the development of the entire orogenic system, while potential feedbacks between erosion and tectonics appears to be restricted to the windward sides of an orogenic system.

9. REFERENCES

Ahmad, T., Harris, N., Bickle, M., Chapman, H., Bunbury, J., and Prince, C., 2000, Isotopic constraints on the structural relationships between the Lesser Himalayan Series and the High Himalayan Crystalline Series, Garhwal Himalaya: Geological Society of America Bulletin, v. 112, p. 467-477.

Aldrich, L.T., and Nier, A.O., 1948, Argon 40 in potassium minerals: Physical Review, v. 74, p. 876-877.

Allegre, C.J., Courtillot, V., Tapponnier, P., Hirn, A., Mattauer, M., Coulon, C., Jaeger, J.J., Achache, J., Scharer, U., Marcoux, J., Burg, J.P., Girardeau, J., Armijo, R., Gariepy, C., Gopel, C., Li, T.D., Xiao, X.C., Chang, C.F., Li, G.Q., Lin, B.Y., Teng, J.W., Wang, N.W., Chen, G.M., Han, T.L., Wang, X.B., Den, W.M., Sheng, H.B., Cao, Y.G., Zhou, J., Qiu, H.R., Bao, P.S., Wang, S.C., Wang, B.X., Zhou, Y.X., and Ronghua, X., 1984, Structure and evolution of the Himalaya-Tibet Orogenic Belt: Nature, v. 307, p. 17-22.

Andersen, T.B., 1998, Extensional tectonics in the caledonides of southern Norway, an overview: Tectonophysics, v. 285, p. 333-351.

Armijo, R., Tapponnier, P., Mercier, J.L., and Han, T.L., 1986, Quaternary extension in Southern Tibet - Field observations and tectonic implications: Journal of Geophysical Research, v. 91, p. 13803-13872.

Armijo, R., Tapponnier, P., and Tonglin, H., 1989, Late Cenozoic right-lateral strike-slip faulting in Southern Tibet: Journal of Geophysical Research, v. 94, p. 2787-2838.

Armstrong, P.A., Ehlers, T.A., Chapman, D.S., Farley, K.A., and Kamp, P.J.J., 2003, Exhumation of the central Wasatch Mountains, Utah: 1. Patterns and timing of exhumation deduced from low-temperature thermochronology data: Journal of Geophysical Research-Solid Earth, v. 108.

Avouac, J.P., 2003, Mountain building, erosion, and the seismic cycle in the Nepal Himalaya, Advances in Geophysics, Vol 46, Volume 46: Advances in Geophysics: San Diego, ACADEMIC PRESS INC, p. 1-80.

Avouac, J.P., and Tapponnier, P., 1993, Kinematic model of active deformation in Central Asia: Geophys. Res. Lett., v. 20, p. 895-898.

Banerjee, D., Singhvi, A.K., Bagati, T.N., and Mohindra, R., 1997, Luminescence chronology of seismites at Sumdo (Spiti valley) near Kaurik-Chango Fault, Northwestern Himalaya: Current Science, v. 73, p. 276-281.

Barros, A.P., Joshi, M., Putkonen, J., and Burbank, D.W., 2000, A study of the 1999 monsoon rainfall in a mountainous region in central Nepal using TRMM products and rain gauge observations: Geophysical Research Letters, v. 27, p. 3683-3686.

Barros, A.P., and Lettenmaier, D.P., 1993, Dynamic Modeling of the Spatial Distribution of Precipitation in Remote Mountainous Areas: Monthly Weather Review, v. 121, p. 1195-1214.

Barros, A.P., and Lettenmaier, D.P., 1994, Dynamic Modeling of Orographically- Induced Precipitation: Reviews of Geophysics, v. 32, p. 265-284.

Beaumont, C., Ellis, S., Hamilton, J., and Fullsack, P., 1996a, Mechanical model for subduction-collision tectonics of Alpine-type compressional orogens: Geology, v. 24, p. 675-678.

Beaumont, C., Fullsack, P., and Hamilton, J., 1992, Erosional control of active compressional orogens, *in* McClay, K.R., ed., Thrust Tectonics: London, Chapman and Hall, p. 1-18.

Beaumont, C., Jamieson, R.A., Nguyen, M.H., and Lee, B., 2001, Himalayan tectonics explained by extrusion of a low-viscosity crustal channel coupled to focused surface denudation: Nature, v. 414, p. 738-742.

Beaumont, C., Kamp, P.J.J., Hamilton, J., and Fullsack, P., 1996b, The continental collision zone, South Island, New Zealand: comparison of geodynamical models and observations: Journal of Geophysical Research, v. 101, p. 3333-3359.

Bendick, R., and Bilham, R., 2001, How perfect is the Himalayan arc?: Geology, v. 29, p. 791-794.

Berthelsen, A., 1953, On the geology of the Rupshu district, N.W. Himalaya.: Medd. Dansk geol. Foren. (Copenhagen), v. 12, p. 351-414.

Bhargava, O.N., Ameta, S.S., Gaur, R.K., Kumar, S., Agarwal, A.N., Jalote, P.M., and Sadhu, M.L., 1978, The Kinnaur (H.P., India) earthquake of 19 January, 1975: summary of geoseismological observations: Bulletin of the Indian Geological Association, v. 11, p. 39-53.

Bilham, R., Larson, K., Freymuller, J., and members, P.I., 1997, GPS measurements of present-day convergence across the Nepal Himalaya: Nature, v. 386, p. 61-64.

Bojar, A.V., Fritz, H., Bregar, M., Nicolescu, S., Reiners, P., Neubauer, F., and Handler, R., 2003, Quarternary exhumation and cooling of the central Himalayas by reactivation of Miocene faults: evidence from structures, $^{40}Ar/^{39}Ar$, fission-track, and U-Th/He data: Geophysical Research Abstracts, European Geophysical Society, Nice, v. 5.

Bookhagen, B., Thiede, R., and Strecker, M.R., in review, Extreme Monsoon events and their control on erosion and sediment flux in the high, arid NW Himalayas: Earth and Planetary Science Letters.

Bookhagen, B., Thiede, R.C., and Strecker, M.R., in press, Late Quaternary Intensified Monsoon Phases Control Landscape Evolution in the NW Himalaya: Geology.

Brandon, M.T., Roden-Tice, M.K., and Garver, J.I., 1998, Late Cenozoic exhumation of the Cascadia accretionary wedge in the Olympic Mountains, northwest Washington State: Geological Society of America Bulletin, v. 110, p. 985-1009.

Brookfield, M.E., 1993, The Himalayan passive margin from Precambrian to Cretaceous times: Sedimentary Geology, v. 84, p. 1-35.

Brown, E.T., Bendick, R., Bourles, D.L., Gaur, V.K., Molnar, P., and Raisbeck, G.M., 2002, Slip rates of the Karakorum fault, Ladakh, India, determined using cosmic ray exposure dating of debris flows and moraines: Journal of Geophysical Research, v. 107, p. ESE7-1-ESE7-13.

Brunel, M., 1986, Ductile thrusting in the Himalayas: shear sense criteria and stretching lineations: Tectonics, v. 5, p. 247-265.

Burbank, D.W., and Anderson, R.S., 2001, Tectonic Geomorphology: Malden, MA, Blackwell Science, 273 p.

Burbank, D.W., Beck, R.A., and Mulder, T., 1996a, The Himalayan Foreland, *in* An, Y., and Harrison, T.M., eds., Asian Tectonics: Cambridge, Cambridge University Press, p. 149-188.

Burbank, D.W., Blythe, A.E., Putkonen, J., Pratt-Sitaula, B., Gabet, E., Oskin, M., Barros, A., and Ojha, T.P., 2003, Decoupling of erosion and precipitation in the Himalayas: Nature, v. 426, p. 652-655.

Burbank, D.W., Leland, J., Fielding, E., Anderson, R.S., Brozovic, N., Reid, M.R., and Duncan, C., 1996b, Bedrock incision, rock uplift and threshold hillslopes in the northwestern Himalayas: Nature, v. 379, p. 505-510.

Burchfiel, B.D., Zhileng, C., Hodges, K.V., Yuping, L., Royden, L.H., Changrong, D., and Jiene, X., 1992, The South Tibetan detachment system, Himalayan orogen: Extension contemporaneous with and parallel to shortening in a collisional mountain belt: Geological Society of America Special Paper, v. 269, p. 1-41.

Burg, J.P., Brunel, M., Gapais, D., Chen, G.M., and Liu, G.H., 1984a, Deformation of Leucogranites of the Crystalline Main Central Sheet in Southern Tibet (China): Journal of Structural Geology, v. 6, p. 535-&.

Burg, J.P., and Chen, G.M., 1984, Tectonics and structural zonation of southern Tibet: Nature, v. 311, p. 219-223.

Burg, J.P., Davy, P., Nievergelt, P., Oberli, F., Seward, D., Diao, Z., and Meier, M., 1997, Exhumation during crustal folding in the Namche-Barwa syntaxis: Terra Nova, v. 9, p. 53-56.

Burg, J.P., Guiraud, M., Chen, G.M., and Li, G.C., 1984b, Himalayan metamorphism and deformations in the North Himalayan helt (Southern Tibet, China): Earth and Planetary Science Letters, v. 69, p. 391-400.

Burtner, R.L., Nigrini, A., and Donelick, R.A., 1994, Thermochronology of the Lower Cretaceous source rocks in the Idaho-Wyoming thrust belt: AAPG Bulletin, v. 78, p. 1613-1636.

Carlson, W.D., Donelick, R.A., and Ketcham, R.A., 1999, Variability of apatite fission-track annealing kinetics I: Experimental results: American Minerologist, v. 84, p. 1213-1223.

Catlos, E.J., Harrison, T.M., Kohn, M.J., Grove, M., Ryerson, F.J., Manning, C.E., and Upreti, B.N., 2001, Geochronologic and thermobarometric constraints on the evolution of the Main Central Thrust, central Nepal Himalaya: Journal of Geophysical Research-Solid Earth, v. 106, p. 16177-16204.

Catlos, E.J., Harrison, T.M., Manning, C.E., Grove, M., Rai, S.M., Hubbard, M.S., and Upreti, B.N., 2002, Records of the evolution of the Himalayan orogen from in situ Th-Pb ion microprobe dating of monazite: Eastern Nepal and western Garhwal: JOURNAL OF ASIAN EARTH SCIENCES, v. 20, p. 459-479.

Cattin, R., and Avouac, J.P., 2000, Modeling mountain building and the seismic cycle in the Himalaya of Nepal: Journal of Geophysical Research-Solid Earth, v. 105, p. 13389-13407.

Chemenda, A.I., Burg, J.P., and Mattauer, M., 2000, Evolutionary model of the Himalaya-Tibet system: geopoem based on new modelling, geological and geophysical data: Earth and Planetary Science Letters, v. 174, p. 397-409.

Chen, W.P., and Molnar, P., 1983, Focal depths of intracontinental and intraplate earthquakes and their implications for the thermal and mechanical properties of the lithosphere: Journal of Geophysical Research, v. 88, p. 4183-4214.

Chen, Z., Liu, Y., Hodges, K.V., Burchfiel, B.C., Royden, L.H., and Deng, C., 1990, The Kangmar Dome - a Metamorphic Core Complex in Southern Xizang (Tibet): Science, v. 250, p. 1552-1556.

Clift, P., and Gaedicke, C., 2002, Accelerated mass flux to the Arabian Sea during the middle to late Miocene: Geology, v. 30, p. 207-210.

Clift, P., Gaedicke, C., Edwards, R., Lee, J.I., Hildebrand, P., Amjad, S., White, R.S., and Schluter, H.U., 2002, The stratigraphic evolution of the Indus Fan and the history of sedimentation in the Arabian Sea: Marine Geophysical Researches, v. 23, p. 223-245.

Coleman, M., and Hodges, K., 1995, Evidence for Tibetan Plateau uplift before 14-Myr Ago from a new minimum age for east-west extension: Nature, v. 374, p. 49-52.

Coleman, M.E., 1998, U-Pb constraints on Oligocene-Miocene deformation and anatexis within the central Himalaya, Marsyandi valley, Nepal: American Journal of Science, v. 298, p. 553-571.

Copeland, P., and Harrison, M.T., 1990, Episodic rapid uplift in the Himalaya revealed by 40Ar/39Ar analysis of detrital K-felspar and muscovite, Bengal fan: Geology, v. 18, p. 354-359.

Copeland, P., Harrison, T.M., Hodges, K.V., Maruejol, P., Le Fort, P., and Pecher, A., 1991, An early Pliocene thermal disturbance of the Main Central Thrust, central Nepal: Implications for Himalayan tectonics: Journal of Geophysical Research, v. 96, p. 8475-8500.

Copeland, P., Harrison, T.M., Yun, P., Kidd, W.S.F., Roden, M., and Zhang, Y.Q., 1995, Thermal Evolution of the Gangdese Batholith, Southern Tibet - a History of Episodic Unroofing: Tectonics, v. 14, p. 223-236.

Copeland, P., Le Fort, P., Henry, P., Rai, S.M., Foster, D.A., Parrish, R.R., Pecher, A., Stuwe, K., and Upreti, B.N., 1999, Twenty million years of thrusting near Kathmandu: Everything in order here: Eos Trans. AGU, 80 , Fall Meet. Suppl., 1999, v. T31E-04.

Corrigan, J.D., 1993, Apatite fission-track analysis of Oligocene strata in south Texas, U.S.A.: Testing annealing models: Chemical Geology, v. 104, p. 227-249.

Dadson, S.J., Hovius, N., Chen, H.G., Dade, W.B., Hsieh, M.L., Willett, S.D., Hu, J.C., Horng, M.J., Chen, M.C., Stark, C.P., Lague, D., and Lin, J.C., 2003, Links between erosion, runoff variability and seismicity in the Taiwan orogen: Nature, v. 426, p. 648-651.

Dahlen, F.A., 1990, Critical taper model of fold-and-thrust belts and accretionary wedges: Annual Review of Earth and Planetary Sciences, v. 18, p. 55-99.

Dahlen, F.A., and Suppe, J., 1988, Mechanics, Growth, and Erosion of Mountain Belts, *in* Clark, S.P., Clark Burchfiel, J.B., and Suppe, J., eds., Processes in Continental Lithospheric Deformation: Boulder, Colorado, The Geological Society of America, p. 161-178.

Dahlen, F.A., Suppe, J., and Davis, D., 1984, Mechanics of fold-and-thrust belts and accretionary wedges: cohesive Coulomb wedge theory: Journal of Geophysical Research, v. 89, p. 10087-10101.

Dalrymple, G.B., Alexander, E.C.J., Lanphere, M.A., and Kraker, G.P., 1981, Irradiation of samples for 40Ar/39Ar dating using the Geological Survey TRIGA reactor: U. S. Geological Survey Professional Paper, p. 55 pp.

Dalrymple, G.B., and Lanphere, M.A., 1974, 40Ar/39Ar age spectra of some undisturbed terrestrial samples: Geochimica et Cosmochemica Acta, v. 38, p. 715-738.

Davis, D., Suppe, J., and Dahlen, F.A., 1983, Mechanics of fold-and-thrust belts and accretionary wedges: Journal of Geophysical Research, v. 88, p. 1153 - 1172.

DeCelles, P.G., and DeCelles, P.C., 2001, Rates of shortening, propagation, underthrusting, and flexural wave migration in continental orogenic systems: Geology, v. 29, p. 135-138.

DeCelles, P.G., Gehrels, G.E., Quade, J., and Ojha, T.P., 1998a, Eocene-early Miocene foreland basin development and the history of Himalyan thrusting, western and central Nepal: Tectonics, v. 17, p. 741-765.

DeCelles, P.G., Gehrels, G.E., Quade, J., Ojha, T.P., Kapp, P.A., and Upreti, B.N., 1998b, Neogene foreland basin deposits, erosional unroofing, and the kinematic history of the Himalayan fold-thrust belt, western Nepal: Geological Society of America Bulletin, v. 110, p. 2-21.

DeCelles, P.G., Robinson, D.M., Quade, J., Ojha, T.P., Garzione, C.N., Copeland, P., and Upreti, B.N., 2001, Stratigraphy, structure, and tectonic evolution of the Himalayan fold-thrust belt in western Nepal: Tectonics, v. 20, p. 487-509.

Derry, L.A., and France-Lanord, C., 1997, Himalayan weathering and erosion fluxes: climate and tectonic controls, *in* Ruddiman, W.F., ed., Tectonic uplift and climate change: New York, Plenum, p. 290-312.

Dettman, D.L., Fang, X.M., Garzione, C.N., and Li, J.J., 2003, Uplift-driven climate change at 12 Ma: a long delta O-18 record from the NE margin of the Tibetan plateau: Earth and Planetary Science Letters, v. 214, p. 267-277.

Dettman, D.L., Kohn, M.J., Quade, J., Ryerson, F.J., Ojha, T.P., and Hamidullah, S., 2001, Seasonal stable isotope evidence for a strong Asian monsoon throughout the past 10.7 m.y: Geology, v. 29, p. 31-34.

Dezes, P.J., Vannay, J.C., Steck, A., Bussy, F., and Cosca, M., 1999, Synorogenic extension: Quantitative constraints on the age and displacement of the Zanskar shear zone (northwest Himalaya): Geological Society of America Bulletin, v. 111, p. 364-374.

DiPietro, J.A., and Pogue, K.R., 2004, Tectonostratigraphic subvisions of the Himalaya: A view from the west: Tectonics, v. 23, p. 1-20.

Dodson, M.H., 1973, Closure Temperature in Cooling Geochronological and Petrological Systems: Contributions to Mineralogy and Petrology, v. 40, p. 259-274.

Donelick, R.A., Ketcham, R.A., and Carlson, W.D., 1999, Variability of apatite fission-track annealing kinetics: II. Crystallographic orientation effects: American Mineralogist, v. 84, p. 1224-1234.

Dubey, A.K., and Bhakuni, S.S., 2004, Development of extension faults on the oblique thrust ramp hanging wall: example from the Tethys Himalaya: Journal of Asian Earth Sciences, v. 23, p. 427-434.

Duffield, W.A., and Dalrymple, G.B., 1990, The Taylor Creek Rhyolite of New Mexico; a rapidly emplaced field of lava domes and flows: Bull. Volcanol., v. 52, p. 475-487.

Dumitru, T.A., 1993, A New Computer-Automated Microscope Stage System for Fission- Track Analysis: Nuclear Tracks and Radiation Measurements, v. 21, p. 575-580.

Dumitru, T.A., 2000, Fission-track geochronology, *in* Noller, J.S., Sowers, J.M., and Lettis, W.R., eds., Quaternary geochronology; methods and applications: Washigton, DC, American Geophysical Union, p. 131-155.

Duncan, C., Masek, J., and Fielding, E., 2003, How steep are the Himalaya? Characteristics and implications of along-strike topographic variations: Geology, v. 31, p. 75-78.

Dunkl, I., 2002, Trackkey: a Windows program for calculation and graphical presentation of fission track data: Computers & Geosciences, v. 28, p. 3-12.

Ehlers, T.A., Armstrong, P.A., and Chapman, D.S., 2001, Normal fault thermal regimes and the interpretation of low-temperature thermochronometers: Physics of the Earth and Planetary Interiors, v. 126, p. 179-194.

Ehlers, T.A., and Farley, K.A., 2003, Apatite (U-Th)/He thermochronometry: methods and applications to problems in tectonic and surface processes: Earth and Planetary Science Letters, v. 206, p. 1-14.

Einsele, G., Ratschbacher, L., and Wetzel, A., 1996, The Himalaya-Bengal Fan Denudation-Accumulation System during the Past 20 Ma: Journal of Geology, v. 104, p. 163-184.

England, P., and Houseman, G., 1989, Extension during continental convergence, with application to the Tibetan Plateau: Journal of Geophysical Research-Solid Earth and Planets, v. 94, p. 17561-17579.

England, P.C., and Thompson, A.B., 1984, Pressure temperature time paths of regional metamorphism .1. Heat-transfer during the evolution of regions of thickened continental-crust: Journal of Petrology, v. 25, p. 894-928.

Eskola, P.E., 1949, The problem of mantled gneiss domes: Geological Society of London Quarterly Journal, v. 104, p. 461-476.

Farley, K.A., 2000, Helium diffusion from apatite; general behavior as illustrated by Durango fluorapatite: Journal of Geophysical Research, v. 105, p. 2903-2914.

Farley, K.A., 2002, (U-Th)/He dating: Techniques, calibrations, and applications, Noble Gases in Geochemistry and Cosmochemistry, Volume 47: Reviews in Mineralogy & Geochemistry: Washington, MINERALOGICAL SOC AMERICA, p. 819-844.

Farley, K.A., Rusmore, M.E., and Bogue, S.W., 2001, Post-10 Ma uplift and exhumation of the northern coast mountains, British Columbia: Geology, v. 29, p. 99-102.

Farley, K.A., Wolf, R.A., and Silver, L.T., 1996, The effects of long alpha-stopping distances on (U-Th)/He ages: Chemical Geology, v. 60, p. 4223-4229.

Fitzgerald, P.G., Sorkhabi, R.B., Redfield, T.F., and Stump, E., 1995, Uplift and Denudation of the Central Alaska Range - a Case- Study in the Use of Apatite Fission-Track Thermochronology to Determine Absolute Uplift Parameters: Journal of Geophysical Research-Solid Earth, v. 100, p. 20175-20191.

Fossen, H., 2000, Extensional tectonics in the Caledonides: Synorogenic or postorogenic?: Tectonics, v. 19, p. 213-224.

Frank, W., Grasemann, B., Guntli, P., and Miller, C., 1995, Geological map of the Kishtwar-Chamba-Kulu region (NW Himalayas, India): Jahrbuch der Geologischen Bundesanstalt, Vienna/A, v. 138, p. 299-208.

Fuchs, G., 1975, Contributions to the geology of the North-Western Himalayas: Abhandlungen der Geologische Bundesanstalt, Vienna/A, v. 32, p. 59.

Fuchs, G., and Linner, M., 1996, On the Geology of the Suture Zone and Tso Morari Dome in Easthern Ladakh (Himalaya). Jahrbuch der Geologischen Bundesanstalt, Vienna/A, v. 139, p. 191-207.

Gaetani, M., and Garzanti, E., 1991, Multicyclic history of the northern India continental margin (Northwestern Himalaya): American Association of Petroleum Geologists Bulletin, v. 75, p. 1427-1446.

Galbraith, R.F., 1981, On Statistical-Models for Fission-Track Counts: Journal of the International Association for Mathematical Geology, v. 13, p. 471-478.

Galbraith, R.F., and Laslett, G.M., 1993, Statistical models for mixed fission-track ages: Nuclear Tracks and Radiation Measurements, v. 21, p. 459-470.

Galy, A., and France-Lanord, C., 2001, Higher erosion rates in the Himalaya: Geochemical constraints on riverine fluxes: Geology, v. 29, p. 23-26.

Galy, A., France-Lanord, C., and Derry, L.A., 1999, The strontium isotopic budget of Himalayan Rivers in Nepal and Bangladesh: Geochimica et Cosmochimica Acta, v. 63, p. 1905-1925.

Galy, A., France-Lanord, C., Hutrez, J.E., and Lucazeau, F., 1996, Mass transfer during Himalayan erosion during the monsoon: mineralogical and geochemical constraints: EOS (Transactions of the American Geophysical Union), v. 77, p. 236.

Gansser, A., 1964, Geology of the Himalayas: London, Interscience, 289 p.

Gapais, D., Pecher, A., Gilbert, E., and Ballevre, M., 1992, Synconvergence Spreading of the Higher Himalaya Crystalline in Ladakh: Tectonics, v. 11, p. 1045-1056.

Garzione, C.N., Dettman, D.L., Quade, J., DeCelles, P.G., and Butler, R.F., 2000a, High times on the Tibetan Plateau: paleoelevation of the Thakkhola graben, Nepal: Geology, v. 28, p. 339-342.

Garzione, C.N., Quade, J., DeCelles, P.G., and English, N.B., 2000b, Predicting paleoelevation of Tibet and the Himalaya from delta O-18 vs. altitude gradients in meteoric water across the Nepal Himalaya: Earth and Planetary Science Letters, v. 183, p. 215-229.

Gleadow, A.J.W., and Duddy, I.R., 1981, A natural long-term track annealing experiment for apatite: Nuclear Tracks, v. 5, p. 169-174.

Gleadow, A.J.W., Duddy, I.R., Green, P.F., and Lovering, J.F., 1986, Confined fission track lengths in apatite: a diagnostic tool for thermal history analysis: Contributions to Mineralogy and Petrology, v. 94, p. 405-415.

Gleadow, A.J.W., and Fitzgerald, P.G., 1987, Uplift history and structure of the Trans-Antarctic Mountains: New evidence from fission track dating of basement apatites in the Dry Valleys area, Southern Victoria Land: Earth and Planetary Science Letters, v. 82, p. 1-14.

Grasemann, B., Fritz, H., and Vannay, J.C., 1999, Quantitative kinematic flow analysis from the Main Central Thrust Zone (NW-Himalaya, India): implications for a decelerating strain path and the extrusion of orogenic wedges: Journal of Structural Geology, v. 21, p. 837-853.

Green, P.F., 1981, A new look at statistics in fission-track dating: Nucl. Tracks Radiat. Meas., v. 5, p. 77-86.

Green, P.F., 1989, Thermal and tectonic history of East Midlands shelf (onshore UK) and surrounding regions assessed by apatite fission track analysis: Journal of the Geological Society of London, v. 146, p. 755-773.

Green, P.F., Duddy, I.R., Gleadow, A.J.W., and Lovering, J.F., 1989a, Apatite fission track analysis as a paleotemperature indicator for hydrocarbon exploration, *in* Naeser, N.D., and McCulloh, T.H., eds., Thermal History of Sedimentary Basins: Methods and Case Histories: New York, Springer-Verlag, p. 181-195.

Green, P.F., Duddy, I.R., Gleadow, A.J.W., Tingate, P.R., and Laslett, G.M., 1986, Thermal annealing of fission tracks in apatite: 1 - a qualitative description: Chemical Geology, v. 59, p. 237-253.

Green, P.F., Duddy, I.R., Laslett, G.M., Hegarty, K.A., Gleadow, A.J.F., Tingate, P.R., and Laslett, G.M., 1985, Fission track annealing in apatite: track length measurements and the form of the Arrhenius plot: Nuclear Tracks, v. 10, p. 233-253.

Green, P.F., Duddy, I.R., Laslett, G.M., Hegarty, K.A., Gleadow, A.J.W., and Lovering, J.F., 1989b, Thermal annealing of fission tracks in apatite, 4, Quantitative modelling techniques and extension to geological timescales: Chemical Geology and Isotope Geoscience Section, v. 79, p. 155-182.

Grujic, D., Casey, M., Davidson, C., Hollister, L.S., Kundig, R., Pavlis, T., and Schmid, S., 1996, Ductile extrusion of the Higher Himalayan Crystalline in Bhutan: Evidence from quartz microfabrics: Tectonophysics, v. 260, p. 21-43.

Grujic, D., Hollister, L.S., and Parrish, R.R., 2002, Himalayan metamorphic sequence as an orogenic channel: insight from Bhutan: Earth and Planetary Science Letters, v. 198, p. 177-191.

Gupta, V.J., and Kumar, S., 1975, Geology of Ladakh, Lahaul and Spiti regions of the Himalaya, with special reference to the stratigraphical position of the flysch deposits: Geologische Rundschau (International Journal of Earth Sciences), v. 64, p. 1.

Hack, J.T., 1957, Studies of longitudinal stream profiles in Virginia and Maryland: U. S. Geological Survey Professional Paper, v. 294-B, p. 42-97.

Hacker, B.R., Mosenfelder, J.L., and Gnos, E., 1996, Rapid emplacement of the Oman ophiolite: Thermal and geochronologic constraints: Tectonics, v. 15, p. 1230-1247.

Hager, C., Janda, C., Grasemann, B., Draganits, E., and Vannay, J.C., 2003, Active extrusion in the Sutlej Valley (NW-Himalaya): Geophysical Research Abstracts, European Geophysical Society, Nice, v. 5.

Hancock, G.S., and Anderson, R.S., 2002, Numerical modeling of fluvial strath-terrace formation in response to oscillating climate: Geological Society of America Bulletin, v. 114, p. 1131-1142.

Hancock, G.S., Anderson, R.S., Whipple, K.X., and Wohl, E.E., 1998, Beyond power; bedrock river incision process and form: Rivers over rock; fluvial processes in bedrock channels, Geophysical Monograph, v. 107, p. 35-60.

Harrison, T.M., Copeland, P., Hall, S.A., Quade, J., Burner, S., Ojha, T.P., and Kidd, W.S.F., 1993, Isotopic preservation of Himalayan/Tibetan uplift, denudation, and climatic histories in the molasse deposits: Journal of Geology, v. 101, p. 157-175.

Harrison, T.M., Copeland, P., Kidd, W.S.F., and Yin, A., 1992, Raising Tibet: Science, v. 255, p. 1663-1670.

Harrison, T.M., Grove, M., Lovera, O.M., Catlos, E.J., and D'Andrea, J., 1999, The origin of Himalayan anatexis and inverted metamorphism: Models and constraints: Journal of Asian Earth Sciences, v. 17, p. 755-772.

Harrison, T.M., Ryerson, F.J., Le Fort, P., Yin, A., Lovera, O.M., and Catlos, E.J., 1997, A late Miocene-Pliocene origin for the central Himalayan inverted metamorphism: Earth and Planetary Science Letters, v. 146, p. E1-E7.

Hayden, H.H., 1904, The geology of Spiti with parts of Bushahr and Rupshu.: Memoir Geological Survay India, v. 6, p. 1-121.

Heim, A., and Gansser, A., 1939, Central Himalaya: Denkschr. Schweiz. Naturforsch. Ges., v. 73, p. 1-245.

Herren, E., 1987, Zanskar Shear Zone - northeast-southwest extension within the Higher Himalayas (Ladakh, India): Geology, v. 15, p. 409-413.

Hilley, G.E., and Strecker, M.R., 2004, Steady state erosion of critical Coulomb wedges with applications to Taiwan and the Himalaya: Journal of Geophysical Research-Solid Earth, v. 109.

Hodges, K.V., 2000, Tectonics of the Himalaya and southern Tibet from two perspectives: Geological Society of America Bulletin, v. 112, p. 324-350.

Hodges, K.V., Hurtado, J.M., and Whipple, K.X., 2001, Southward extrusion of Tibetan crust and its effect on Himalayan tectonics: Tectonics, v. 20, p. 799-809.

Hodges, K.V., Parrish, R.R., Housh, T.B., Lux, D.R., Burchfiel, B.C., Royden, L.H., and Chen, Z., 1992, Simultaneous Miocene Extension and Shortening in the Himalayan Orogen: Science, v. 258, p. 1466-1470.

Hodges, K.V., and Silverberg, D.S., 1988, Thermal evolution of the Greater-Himalaya, Garhwal, India: Tectonics, v. 7, p. 583-600.

Hodges, K.V., Wobus, C., Ruhl, K., Schildgen, T., and Whipple, K., 2004, Quaternary deformation, river steepening, and heavy precipitation at the front of the Higher Himalayan ranges: Earth and Planetary Science Letters, v. 220, p. 379-389.

Hoffman, P.F., and Grotzinger, J.P., 1993, Orographic precipitation, erosional unloading, and tectonic style: Geology, v. 21, p. 195-198.

Horton, B.K., 1999, Erosional control on the geometry and kinematics of thrust belt development in the central Andes: Tectonics, v. 18, p. 1292-1304.

Horton, R.E., 1945, Erosional development of streams and their drainage basins, hydrophysical approach to quantitative morphology: Geological Society of America Bulletin, v. 56, p. 275-370.

Hoth, S., Adam, J., Kukowski, N., and Oncken, O., revised, Influence of erosion on the kinematics of bivergent orogens. Results from scaled sandbox-simulations.: GSA special volume.

House, M.A., Farley, K.A., and Stockli, D., 2000, Helium chronometry of apatite and titanite using Nd-YAG laser heating: Earth and Planetary Science Letters, v. 183, p. 365-368.

House, M.A., Wernicke, B.P., Farley, K.A., and Dumitru, T.A., 1997, Cenozoic thermal evolution of the central Sierra Nevada, California, from (U-Th)/He thermochronometry: Earth and Planetary Science Letters, v. 151, p. 167-179.

Howard, A.D., 1998, Long profile development of bedrock channels: Interaction of weathering, mass wasting, bed erosion, and sediment transport, *in* Tinkler, K.J., and Wohl, E.E., eds., Rivers over rock: Fluvial processes in bedrock channels, Volume Geophysical Monograph 107, American Geophysical Union, p. 297-320.

Howard, A.D., Dietrich, W.E., and Seidl, M.A., 1994, Modeling fluvial erosion on regional to continental scales: Journal of Geophysical Research, v. 99, p. 13,971-13,986.

Howard, A.D., and Kerby, G., 1983, Channel changes in badlands: Geological Scoiety of Americ Bulletin, v. 94, p. 739-752.

Hubbard, M.S., and Harrison, T.M., 1989, Ar-40/Ar-39 Age Constraints on Deformation and Metamorphism in the Main Central Thrust Zone and Tibetan Slab, Eastern Nepal Himalaya: Tectonics, v. 8, p. 865-880.

Hurford, A.J., and Green, P.F., 1983, The zeta-age calibration of fission-track dating: Isotope Geoscience, v. 1, p. 285-317.

Huyghe, P., Galy, A., Mugnier, J.L., and France-Lanord, C., 2001, Propagation of the thrust system and erosion in the Lesser Himalaya: Geochemical and sedimentological evidence: Geology, v. 29, p. 1007-1010.

ISC, International Seismological Centre, On-line Bulletin, http://www.isc.ac.uk/Bull, Internatl. Seis. Cent., Thatcham, United Kingdom, 2004.

Jain, A.K., Kumar, D., Singh, S., Kumar, A., and Lal, N., 2000, Timing, quantification and tectonic modelling of Pliocene- Quaternary movements in the NW Himalaya: evidence from fission track dating: Earth and Planetary Science Letters, v. 179, p. 437-451.

Jamieson, R.A., Beaumont, C., Nguyen, M.H., and Lee, B., 2002, Interaction of metamorphism, deformation and exhumation in large convergent orogens: Journal of Metamorphic Geology, v. 20, p. 9-24.

John, B.E., and Foster, D.A., 1993, Structural and thermal constraints on the initiation angle of detachment faulting in the Southern Basin and Range - the Chemehuevi Mountains case-study: Geological Society of America Bulletin, v. 105, p. 1091-1108.

Jolivet, L., and Goffe, B., 2000, Extensional metamorphic domes in mountains belts, syn-orogenic and post-orogenic extension: Comptes Rendus De L Academie Des Sciences Serie Ii Fascicule a-Sciences De La Terre Et Des Planetes, v. 330, p. 739-751.

Ketcham, R.A., Donelick, R.A., and Carlson, W.D., 1999, Variability of apatite fission-track annealing kinetics: III. Extrapolation to geologic time scales: American Mineralogist, v. 84, p. 1235-1255.

Ketcham, R.A., Donelick, R.A., and Donelick, M.B., 2003, AFTSolve: A program for multi-kinetic modeling of apatite fission-track data: American Mineralogist, v. 88, p. 929-929.

Klootwijk, C.T., Conaghan, P.J., and Powell, C.M., 1985, The Himalayan arc - large-scale continental subduction, oroclinal bending and back-arc spreading: Earth and Planetary Science Letters, v. 75, p. 167-183.

Klootwijk, C.T., Gee, J.S., Pierce, J.W., Smith, G.M., and McFadden, P.L., 1992, An early India-Asia contact: Paleomagnetic constraints from Ninetyeast Ridge, ODP Leg 121: Geology, v. 20, p. 395-398.

Koons, P.O., 1989, The topographic evolution of collisional mountain belts: A numerical look at the Southern Alps, New Zealand: American Journal of Science, v. 289, p. 1041-1069.

Koons, P.O., 1990, The two-sided orogen: collision and erosion from the sand box to the Southern Alps: Geology, v. 18, p. 679-682.

Koons, P.O., 1995, Modeling the topographic evolution of collisional belts: Annual Review of Earth and Planetary Sciences, v. 23, p. 375-408.

Koons, P.O., Zeitler, P.K., Chamberlain, C.P., Craw, D., and Meltzer, A.S., 2002, Mechanical links between erosion and metamorphism in Nanga Parbat, Pakistan Himalaya: American Journal of Science, v. 302, p. 749-773.

Kumar, A., Lal, N., Jain, A.K., and Sorkhabi, R.B., 1995, Late Cenozoic-Quaternary thermo-tectonic history of Higher Himalayan Crystalline (Hhc) in Kishtwar-Padar-Zanskar region, NW Himalaya - evidence from fission-track ages: Journal of the Geological Society of India, v. 45, p. 375-391.

Kutzbach, J.E., Prell, W.L., and Ruddiman, W.F., 1993, Sensitivity of Eurasian climate to surface uplift of the Tibetan Plateau: Journal of Geology, v. 100, p. 177-190.

Kwatra, S.K., Singh, S., Singh, V.P., Sharma, R.K., Rai, B., and Kishor, N., 1999, Geochemical and geochronological characteristics of the Early Paleozoic granitoids from the Sutlej-Baspa Valleys, Himachal Himalaya, *in* Jain, A.K., and Manickavasagam, R.M., eds., Geodynamics of the NW Himalaya, Volume Memoir No. 6: Trivandrum, Gondwana Research Group, p. 145-158.

Lacassin, R., Valli, F., Arnaud, N., Leloup, P.H., Paquette, J.L., Haibing, L., Tapponier, P., Chevalier, M.-L., Guillot, S., Maheo, G., and Zhiqin, X., 2004, Large-scale geometry, offset and kinematic evolution of the Karakorum fault, Tibet.: Earth and Planetary Science Letters, v. 219, p. 255-269.

Lal, N., Mehta, Y.D., Kumar, D., Kumar, A., and Jain, A.K., 1999, Cooling and exhumation history of the Mandi granite and adjoining tectonic units, Himachal Pradesh, and estimation of closure temperature from external surface of zircon, *in* Jain, A.K., and Manickavasagam, R.M., eds., Geodynamic of the NW Himalaya, Volume Gondwana Research Group Memoir 6: Gondwana: Osaka, Gondwana Research Group, Japan, p. 207-216.

Lanphere, M.A., and Dalrymple, G.B., 1978, The use of 40Ar/39Ar data in evaluiation of disturbed K-Ar systems: U. S. Geological Survey Open-File Report, v. 78-701, p. 241-243.

Lee, J., Hacker, B.R., Dinklage, W.S., Wang, Y., Gans, P., Calvert, A., Wan, J.L., Chen, W.J., Blythe, A.E., and McClelland, W., 2000, Evolution of the Kangmar Dome, southern Tibet: Structural, petrologic, and thermochronologic constraints: Tectonics, v. 19, p. 872-895.

Lefort, P., 1975, Himalayas - collided range - present knowledge of continental arc: American Journal of Science, v. A275, p. 1-&.

Leland, J., Reid, M.R., Burbank, D.W., Finkel, R., and Caffee, M., 1998, Late Pleistocene history of bedrock incision and differential uplift along the Indus River near Nanga Parbat, Pakistan Himalaya, from ^{10}Be and ^{26}Al exposure age dating of bedrock straths: Earth and Planetary Science Letters, v. 54, p. 93-105.

Linker, M.F., Kirby, S.H., Ord, A., and Christie, J.M., 1984, Effects of compression direction on the plasticity and rheology of hydrolytically weakened synthetic quartz crystals at atmospheric-pressure: Journal of Geophysical Research, v. 89, p. 4241-4255.

Maheo, G., Guillot, S., Blichert-Toft, J., Rolland, Y., and Pecher, A., 2002, A slab breakoff model for the Neogene thermal evolution of South Karakorum and South Tibet: Earth and Planetary Science Letters, v. 195, p. 45-58.

Mancktelow, N.S., and Grasemann, B., 1997, Time-dependent effects of heat advection and topography on cooling histories during erosion: Tectonophysics, v. 270, p. 167-195.

Mancktelow, N.S., and Pavlis, T.L., 1994, Fold-fault relationships in low-angle detachment Systems: Tectonics, v. 13, p. 668-685.

Masek, J.G., Isacks, B.L., Gubbels, T.L., and Fielding, E.J., 1994, Erosion and tectonics at the margins of continental plateaus: Journal Geophysical Research, v. B99, p. 12941-13956.

McCaffrey, R., and Nabelek, J., 1998, Role of oblique convergence in the active deformation of the Himalayas and southern Tibet plateau: Geology, v. 26, p. 691-694.

McClelland, W.C., and Gilotti, J.A., 2003, Late-stage extensional exhumation of high-pressure granulites in the Greenland Caledonides: Geology, v. 31, p. 259-262.

McDougall, I., and Harrison, T.M., 1999, Geochronology and Thermochronology by the 40Ar/39Ar Method, 2nd ed.: New York, Oxford University Press, 269 p.

Meigs, A., Burbank, D.W., and Beck, R.A., 1995, Middle-Late Miocene (pre-10 Ma) initiation of the Main Boundary Thrust in the western Himalaya: Geology, v. 23, p. 423-426.

Merrihue, C., and Turner, G., 1966, Potassium-argon dating by activation with fast neutrons: Journal of Geophysical Research, v. 71, p. 2852-2857.

Metcalfe, R.P., 1993, Pressure, temperature and time constraints on metamorphism across the Main Central Thrust zone and high Himalayan slab in the Garhwal Himalaya., *in* P., T.P.J.S.M., ed., Himalayan tectonics, Volume 74: London, Geological Society Special Publications. Pages 485-509, p. 485-509.

Metivier, F., Gaudemer, Y., Tapponnier, P., and Klein, M., 1999, Mass accumulation rates in Asia during the Cenozoic: Geophysical Journal International, v. 137, p. 280-318.

Métivier, F., Guademer, Y., Tapponier, P., and Klein, M., 1999, Mass accumulation rates in Asia during the Cenozoic: Geophysical Journal International, v. 137, p. 280-318.

Miller, C., Klotzli, U., Frank, W., Thoni, M., and Grasemann, B., 2000, Proterozoic crustal evolution in the NW Himalaya (India) as recorded by circa 1.80 Ga mafic and 1.84 Ga granitic magmatism: Precambrian Research, v. 103, p. 191-206.

Mohindra, R., and Bagati, T.N., 1996, Seismically induced soft-sediment deformation structures (seismites) around Sumdo in the lower Spiti valley (Tethys Himalaya): Sedimentary Geology, v. 101, p. 69-83.

Molnar, P., 1984, Structure and Tectonics of the Himalaya - Constraints and Implications of Geophysical-Data: Annual Review of Earth and Planetary Sciences, v. 12, p. 489-518.

Molnar, P., and Chen, W.P., 1983, Focal depths and fault plane solutions of earthquakes under the Tibetan Plateau: Journal of Geophysical Research, v. 88, p. 1180-1196.

Molnar, P., and England, P., 1990, Late Cenozoic uplift of mountain ranges and global climatic change: chicken or egg?: Nature, v. 346, p. 29-34.

Molnar, P., England, P., and Martinod, J., 1993, Mantle dynamics, uplift of the Tibetan Plateau, and the Indian monsoon: Reviews of Geophysics, v. 31, p. 357-396.

Molnar, P., and Lyon-Caen, H., 1988, Some simple physical aspects of the support, structure, and evolution of mountain belts, *in* Suppe, J., ed., Processes in Continental Lithospheric Deformation: Boulder, Colorado, The Geological Society of America, p. 179-207.

Molnar, P., and Lyon-Caen, H., 1989, Fault Plane Solutions of Earthquakes and Active Tectonics of the Tibetan Plateau and Its Margins: Geophysical Journal International, v. 99, p. 123-153.

Molnar, P., and Tapponier, P., 1975, Cenozoic tectonics of Asia: Effects of a continental collision: Science, v. 189, p. 419-426.

Molnar, P., and Tapponnier, P., 1978, Active Tectonics of Tibet: Journal of Geophysical Research, v. 83, p. 5361-&.

Montgomery, D.R., Balco, G., and Willett, S.D., 2001, Climate, tectonics, and the morphology of the Andes: Geology, v. 29, p. 579-582.

Murphy, M.A., Yin, A., Kapp, P., Harrison, T.M., Lin, D., and Guo, J.H., 2000, Southward propagation of the Karakoram fault system, southwest Tibet: Timing and magnitude of slip: Geology, v. 28, p. 451-454.

Murphy, M.A., Yin, A., Kapp, P., Harrison, T.M., Manning, C.E., Ryerson, F.J., Ding, L., and Guo, J.H., 2002, Structural evolution of the Gurla Mandhata detachment system, southwest Tibet: Implications for the eastward extent of the Karakoram fault system: Geological Society of America Bulletin, v. 114, p. 428-+.

Naeser, C.W., and Faul, H., 1969, Fission track annealing in apatite and sphene: Journal of Geophysical Research, v. 74, p. 705-710.

Najman, Y., Garzanti, E., Pringle, M., Bickle, M., Ando, S., and Brozovic, N., 2002, Exhumation and attainment of steady state in the Himalaya: insights from the detrital sediment record: EOS (Transactions of the American Geophysical Union), v. 83, p. F1302.

Najman, Y., Pringle, M., Bickle, M., Garzanti, E., Burbank, D., Ando, S., and Brozovic', N., 2003, Non-steady-state exhumation of the Higher Himalaya, N.W. India: Insights from a combined isotopic and sedimentological approach: Geophysical Research Abstracts, European Geophysical Society, Nice, v. 5.

Nelson, K.D., Zhao, W.J., Brown, L.D., Kuo, J., Che, J.K., Liu, X.W., Klemperer, S.L., Makovsky, Y., Meissner, R., Mechie, J., Kind, R., Wenzel, F., Ni, J., Nabelek, J., Chen, L.S., Tan, H.D., Wei, W.B., Jones, A.G., Booker, J., Unsworth, M., Kidd, W.S.F., Hauck, M., Alsdorf, D., Ross, A., Cogan, M., Wu, C.D., Sandvol, E., and Edwards, M., 1996, Partially molten middle crust beneath southern Tibet: Synthesis of project INDEPTH results: Science, v. 274, p. 1684-1688.

Neumayer, J., Wiesmayr, G., Janda, C., Grasemann, B., and Draganits, E., in press, Eohimalayan fold and thrust belt in the NW-Himalaya (Lingti-Pin Valleys): Shortening and depth to detachment calculation: Oesterreichsche Bergbau Studenten.

Ni, J., and Barazangi, M., 1984, Seismotectonics of the Himalayan Collision Zone - Geometry of the Underthrusting Indian Plate beneath the Himalaya: Journal of Geophysical Research, v. 89, p. 1147-1163.

Ni, J., and Barazangi, M., 1985, Active tectonics of the western Tethyan Himalaya above the underthrusting Indian plate - the Upper Sutlej River Basin as a pull-apart structure: Tectonophysics, v. 112, p. 277-295.

Ni, J., and York, J.E., 1978, Late Cenozoic tectonics of Tibetan Plateau: Journal of Geophysical Research, v. 83, p. 5377-5384.

Pan, Y., Copeland, P., Roden, M.K., Kidd, W.S.F., and Harrison, T.M., 1993, Thermal and unroofing history of the Lhasa area, Southern Tibet - evidence from apatite fission-track thermochronology: Nuclear Tracks and Radiation Measurements, v. 21, p. 543-554.

Pandey, M.R., Tandukar, R.P., Avouac, J.P., Lave, J., and Massot, J.P., 1995, Interseismic strain accumulation on the Himalayan crustal ramp (Nepal): Geophysical Research Letters, v. 22, p. 751-754.

Patriat, P., and Achache, J., 1984, Indo-Asia collision chronology and its implications for crustal shortening and driving mechanisms of plates: Nature, v. 311, p. 615-621.

Pavlis, T.L., Hamburger, M.W., and Pavlis, G.L., 1997, Erosional processes as a control on the structural evolution of an actively deforming fold and thrust belt: an example from the Pamir-Tien Shan region, central Asia: Tectonics, v. 16, p. 810-822.

Pecher, A., 1989, The Metamorphism in the Central Himalaya: Journal of Metamorphic Geology, v. 7, p. 31-41.

Peltzer, G., and Tapponnier, P., 1988, Formation and evolution of strike-slip faults, rifts, and basins during the India-Asia collision - an experimental approach: Journal of Geophysical Research-Solid Earth, v. 93, p. 15085-&.

Prell, W.L., and Kutzbach, J.E., 1992, Sensitivity of the Indian monsoon to forcing parameters and implications for its evolution: Nature, v. 360, p. 647-652.

Quidelleur, X., Grove, M., Lovera, O.M., Harrison, T.M., Yin, A., and Ryerson, F.J., 1997, Thermal evolution and slip history of the Renbu Zedong Thrust, southeasterm Tibet: Journal of Geophysical Research-Solid Earth, v. 102, p. 2659-2679.

Ratschbacher, L., Frisch, W., Liu, G.H., and Chen, C.S., 1994, Distributed deformation in southern and western Tibet during and after the India-Asia collision: Journal of Geophysical Research-Solid Earth, v. 99, p. 19917-19945.

Reiners, P.W., Ehlers, T.A., Garver, J.I., Mitchell, S.G., Montgomery, D.R., Vance, J.A., and Nicolescu, S., 2002, Late Miocene exhumation and uplift of the Washington Cascade: Geology, v. 30, p. 767-770.

Reiners, P.W., Ehlers, T.A., Mitchell, S.G., and Montgomery, D.R., 2003, Coupled spatial variations in precipitation and long-term erosion rates across the Washington Cascades: Nature, v. 426, p. 645-647.

Renne, P.R., 2000, K-Ar and 40Ar/39Ar Dating, *in* Noller, J.S., Sowers, J.M., and Lettis, W.R., eds., Quaternary Geochronology: Methods and Applications, Volume AGU Reference Shelf; 4: Washington, DC, American Geophysical Union, p. 77-100.

Robinson, D.M., DeCelles, P.G., Patchett, P.J., and Garzione, C.N., 2001, The kinematic evolution of the Nepalese Himalaya interpreted from Nd isotopes: Earth and Planetary Science Letters, v. 192, p. 507-521.

Robyr, M., Vannay, J.C., Epard, J.L., and Steck, A., 2002, Thrusting, extension, and doming during the polyphase tectonometamorphic evolution of the High Himalayan Crystalline Zone in NW India: Journal of Asian Earth Sciences, v. 21, p. 221-239.

Rowley, D.B., Pierrehumbert, R.T., and Currie, B.S., 2001, A new approach to stable isotope-bassed paleoaltimetry: implications for paleoaltimetry and the paleohypsometry of the High Himalaya since the Late Miocene: Earth and Planetary Science Letters, v. 188, p. 253-268.

Royden, L.H., Burchfiel, B.C., King, R.W., Wang, E., Chen, Z.L., Shen, F., and Liu, Y.P., 1997, Surface deformation and lower crustal flow in eastern Tibet: Science, v. 276, p. 788-790.

Ruddiman, W.F., and Kutzbach, J.E., 1989, Forcing of the late Cenozoic northern hemisphere climate by plateau uplift in southeast Asia and the American southwest: J. geophys. Res., v. 94, p. 18,409-18,427.

Safran, E.B., 2003, Geomorphic interpretation of low-temperature thermochronologic data: Insights from two-dimensional thermal modeling: Journal of Geophysical Research-Solid Earth, v. 108, p. art. no.-2189.

Scharer, U., Xu, R.H., and Allegre, C.J., 1986, U-(Th)-Pb systematics and ages of Himalayan leukogranites, South Tibet: Earth and Planetary Science Letters, v. 77, p. 35-48.

Schelling, D., 1992, The tectonostratigraphy and structure of the eastern Nepal Himalaya: Tectonics, v. 11, p. 925-943.

Schelling, D., and Arita, K., 1991, Thrust tectonics, crustal shorting, and the structure of the far-eastern Nepal Himalaya: Tectonics, v. 10, p. 851-862.

Schlup, M., Carter, A., Cosca, M., and Steck, A., 2003, Exhumation history of eastern Ladakh revealed by Ar-40/Ar-39 and fission-track ages: the Indus River-Tso Morari transect, NW Himalaya: Journal of the Geological Society, v. 160, p. 385-399.

Searle, M.P., 1996, Geological evidence against large-scale pre-Holocene offsets along the Karakoram Fault: Implications for the limited extrusion of the Tibetan plateau: Tectonics, v. 15, p. 171-186.

Searle, M.P., and Godin, L., 2003, The South Tibetan Detachment and the Manaslu Leucogranite: A structural reinterpretation and restoration of the Annapurna-Manaslu Himalaya, Nepal: Journal of Geology, v. 111, p. 505-523.

Searle, M.P., Noble, S.R., Hurford, A.J., and Rex, D.C., 1999, Age of crustal melting, emplacement and exhumation history of the Shivling leucogranite, Garhwal Himalaya: Geological Magazine, v. 136, p. 513-525.

Searle, M.P., Parrish, R.R., Hodges, K.V., Hurford, A., Ayres, M.W., and Whitehouse, M.J., 1997, Shisha Pangma leucogranite, south Tibetan Himalaya: Field relations, geochemistry, age, origin, and emplacement: Journal of Geology, v. 105, p. 295-317.

Searle, M.P., Simpson, R.L., Law, R.D., Parrish, R.R., and Waters, D.J., 2003, The structural geometry, metamorphic and magmatic evolution of the Everest massif, High Himalaya of Nepal-South Tibet: Journal of the Geological Society, v. 160, p. 345-366.

Searle, M.P., Weinberg, R.F., and Dunlap, W.J., 1998, Transpressional tectonics along the Karakoram fault zone, northern Ladakh: constraints on Tibetan extrusion, *in* Dewey, J.F., ed., Continental Transpressional and Transtensional Tectonics, Volume 135: London, Geological Society of London Special Publication, p. 307-326.

Seeber, L., and Gornitz, V., 1983, River profiles along the Himalayan arc as indicators of active tectonics: Tectonophysics, v. 92, p. 335-367.

Seeber, L., and Pecher, A., 1998, Strain partitioning along the Himalayan arc and the Nanga Parbat antiform: Geology, v. 26, p. 791-794.

Singh, S., Sinha, P., Jain, A.K., Singh, V.N., and Srivastava, L.S., 1975, Preliminary report on the January 19, 1975, Kinnaur earthquake in Himachal Pradesh: Earthquake Eng. Studies, v. 75, p. 1-32.

Sklar, L., and Dietrich, W.E., 1998, River longitudinal profiles and bedrock incision moderls" stream power and the influence of sediment supply, *in* Tinkler, K.J., and Wohl, E.E., eds., River over rock: Fluvial processes in bedrock channels, Volume Geophysical Monograph 107: Geophysical Monograph: Washington, D.C., American Geophysical Union, p. 237-260.

Sklar, L.S., and Dietrich, W.E., 2001, Sediment and rock strength controls on river incision into bedrock: Geology, v. 29, p. 1087-1090.

Snyder, N.P., Whipple, K.X., Tucker, G.E., and Merritts, D.J., 2003, Importance of a stochastic distribution of floods and erosion thresholds in the bedrock river incision problem (vol 108, pg 2117, 2003): Journal of Geophysical Research-Solid Earth, v. 108.

Sorkhabi, R.B., 1993, Time-temperature pathways of Himalayan and Trans-Himalayan crystalline rock: a comparison of fission-track ages: Nuclear Tracks and Radiation Measures, v. 21, p. 535-542.

Sorkhabi, R.B., Stump, E., and Foland, K.A., 2000, Late Pliocene Denudation Chronology ot the Main Central Thrust Hangingwall in Solu Himal, Nepal: Eos Trans. AGU, 81 (48) , Fall Meet. Suppl., v. T51C-05.

Sorkhabi, R.B., Stump, E., Foland, K.A., and Jain, A.K., 1996, Fission-track and Ar-40/Ar-39 evidence for episodic denudation of the Gangotri granites in the Garhwal Higher Himalaya, India: Tectonophysics, v. 260, p. 187-199.

Spicer, R.A., Harris, N.B.W., Widdowson, M., Herman, A.B., Guo, S.X., Valdes, P.J., Wolfe, J.A., and Kelley, S.P., 2003, Constant elevation of southern Tibet over the past 15 million years: Nature, v. 421, p. 622-624.

Spring, L., and Crespoblanc, A., 1992, Nappe tectonics, extension, and metamorphic evolution in the Indian Tehys Himalaya (Higher Himalaya, SE Zanskar and NW Lahul): Tectonics, v. 11, p. 978-989.

Srivastava, P., and Mitra, G., 1994, Thrust geometries and deep structure of the outer and lesser Himalaya, Kumoan and Garwhal (India): implications for evolution of the Himalayan fold-and-thrust belt: Tectonics, v. 13, p. 89-109.

Steck, A., 2003, Geology of the NW Indian Himalaya: Eclogae Geologicae Helvetiae, v. 96, p. 147-U13.

Steck, A., Epard, J.L., Vannay, J.C., Hunziker, J., Girard, M., Morard, A., and Robyr, M., 1998, Geological transect across the Tso Morari and Spiti areas: The nappe structures of the Tethys Himalaya: Eclogae Geologicae Helvetiae, v. 91, p. 103-122.

Steck, A., Spring, L., Vannay, J.C., Masson, H., Stutz, E., Bucher, H., Marchant, R., and Tieche, J.C., 1993, Geological Transect across the Northwestern Himalaya in Eastern Ladakh and Lahul (a Model for the Continental Collision of India and Asia): Eclogae Geologicae Helvetiae, v. 86, p. 219-&.

Strecker, M.R., Hilley, G.E., Arrowsmith, J.R., and Coutand, I., 2003, Differential structural and geomorphic mountain-front evolution in an active continental collision zone: The northwest Pamir, southern Kyrgyzstan: Geological Society of America Bulletin, v. 115, p. 166-181.

Strutt, R., 1905, On the radio-active minerals: Proceedings of the Royal Society of London, v. v. 76, p. 88-101.

Stuwe, K., White, L., and Brown, R., 1994, The Influence of Eroding Topography on Steady-State Isotherms - Application to Fission-Track Analysis: Earth and Planetary Science Letters, v. 124, p. 63-74.

Tapponnier, P., and Molnar, P., 1977, Active faulting and tectonics in China: Journal of Geophysical Research, v. 82, p. 2905-&.

Tapponnier, P., Xu, Z.Q., Roger, F., Meyer, B., Arnaud, N., Wittlinger, G., and Yang, J.S., 2001, Geology - Oblique stepwise rise and growth of the Tibet plateau: Science, v. 294, p. 1671-1677.

Taylor, M., Yin, A., Ryerson, F.J., Kapp, P., and Ding, L., 2003, Conjugate strike-slip faulting along the Bangong-Nujiang suture zone accommodates coeval east-west extension and north-south shortening in the interior of the Tibetan Plateau: Tectonics, v. 22, p. art. no.-1044.

Teyssier, C., and Whitney, D.L., 2002, Gneiss domes and orogeny: Geology, v. 30, p. 1139-1142.

Thiede, R., Bookhagen, B., Arrowsmith, J.R., Sobel, E., and Strecker, M., 2004, Climatic control on rapid exhumation along the Southern Himalayan Front: Earth and Planetary Science Letters, v. 222, p. 791-806.

Tippet, J.M., and Hovius, N., 2000, Geodynamic processes in the Southern Alps, New Zealand, *in* Summerfield, M.A., ed., Geomorphology and Global Tectonics: Chichester, John Wiley & Sons, p. 109-134.

Tucker, G.E., and Slingerland, R., 1997, Drainage basin responses to climate change: Water Resources Research, v. 33, p. 2031-2047.

Tullis, J., and Yund, R.A., 1987, Transition from cataclastic flow to dislocation creep of feldspar - mechanisms and microstructures: Geology, v. 15, p. 606-609.

Turner, G., Miller, J.A., and Grasty, R.L., 1966, The thermal history of the Bruderheim meteorite: Earth and Planetary Science Letters, v. 1, p. 155-157.

Valdiya, K.S., 1980a, The 2 Intracrustal Boundary Thrusts of the Himalaya: Tectonophysics, v. 66, p. 323-348.

Valdiya, K.S., 1980b, Geology of the Kumaun Lesser Himalaya: Dehra Dun, Wadia Institute of Himalayan Geology, 291 p.

Vanderhaeghe, O., Teyssier, C., and Wysoczanski, R., 1999, Structural and geochronological constraints on the role of partial melting during the formation of the Shuswap metamorphic core complex at the latitude of the Thor-Odin dome, British Columbia: Canadian Journal of Earth Sciences, v. 36, p. 917-943.

Vannay, J., and Grasemann, B., 2001a, Himalayan inverted metamorphism and syn-convergence extension as a consequence of a general shear extrusion: Geological Magazine, v. 3, p. 253-276.

Vannay, J.C., and Grasemann, B., 1998, Inverted metamorphism in the High Himalaya of Himachal Pradesh (NW India): phase equilibria versus thermobarometry: Schweizerische Mineralogische Und Petrographische Mitteilungen, v. 78, p. 107-132.

Vannay, J.C., and Grasemann, B., 2001b, Himalayan inverted metamorphism and syn-convergence extension as a consequence of a general shear extrusion: Geological Magazine, v. 138, p. 253-276.

Vannay, J.C., Grasemann, B., Rahn, M., Frank, W., Carter, A., and Baudraz, V., 2004, Miocene to Holocene exhumation of metamorphic crustal wedges in the Himalayan orogen: Evidence for tectonic extrusion coupled to fluvial erosion: Tectonics, v. 23.

Vannay, J.C., and Hodges, K.V., 1996, Tectonometamorphic evolution of the Himalayan metamorphic core between the Annapurna and Dhaulagiri, central Nepal: Journal of Metamorphic Geology, v. 14, p. 635-656.

Vannay, J.C., Sharp, Z.D., and Grasemann, B., 1999, Himalayan inverted metamorphism constrained by oxygen isotope thermometry: Contributions to Mineralogy and Petrology, v. 137, p. 90-101.

Wagner, G., 1968, Fission track dating of apatites: Earth and Planetary Science Letters, v. 4, p. 411-415.

Wagner, G., and Van den Haute, P., 1992, Fission track dating: Dordrecht, Netherlands, Kluwer Acad. Publ.. 285 p.

Wagner, G.A., and Reiner, G.M., 1972, The tectonic interpretation of fission track apatite ages: Earth and Planetary Science Letters, v. 14, p. 263-268.

Wänke, H., and König, H., 1959, Eine neue Methode zur Kalium-Argon-Altersbestimmung und ihre Anwendung auf Steinmeteorite: Z. Naturforsch., v. 14a, p. 860-866.

Warnock, A.C., Zeitler, P.K., Wolf, R.A., and Bergman, S.C., 1997, An evaluation of low-temperature apatite U-Th/He thermochronometry: Geochimica Et Cosmochimica Acta, v. 61, p. 5371-5377.

Wendt, I., and Carl, C., 1991, The Statistical Distribution of the Mean Squared Weighted Deviation: Chemical Geology, v. 86, p. 275-285.

Whipple, K.X., Hancock, G.S., and Anderson, R.S., 2000, River incision into bedrock: mechanics and relative efficacy of plucking, abrasion, and cavitation: Geological Society of America Bulletin, v. 112, p. 490-503.

Whipple, K.X., and Meade, B.J., 2004, Controls on the strength of coupling among climate, erosion, and deformation in two-sided, frictional orogenic wedges at steady state: Journal of Geophysical Research, v. 109, p. 1-24.

Whipple, K.X., and Tucker, G., 2002, Implications of sediment-flux-dependent river incision models for landscape evolution: Journal of Geophysical Research, v. 107.

Whipple, K.X., and Tucker, G.E., 1999, Dynamics of the stream power river incision model: implications for height limits of mountain ranges, landscape response timescales and research needs: Journal of Geophysical Research, v. 104, p. 17,661-17,674.

White, N.M., Pringle, M., Garzanti, E., Bickle, M., Najman, Y., Chapman, H., and Friend, P., 2002, Constraints on the exhumation and erosion of the High Himalayan Slab, NW India, from foreland basin deposits: Earth and Planetary Science Letters, v. 195, p. 29-44.

Wiesmayr, G., and Grasemann, B., 2002, Eohimalayan fold and thrust belt: Implications for the geodynamic evolution of the NW-Himalaya (India): Tectonics, v. 21, p. art. no.-1058.

Willett, S., Beaumont, C., and Fullsack, P., 1993, Mechanical model for the tectonics of doubly vergent compressional orogens: Geology, v. 21, p. 371-374.

Willett, S.D., 1999, Orogeny and orography: the effects of erosion on the structure of mountain belts: Journal of Geophysical Research, v. 104, p. 28,957-28,982.

Willett, S.D., and Brandon, M.T., 2002, On steady states in mountain belts: Geology, v. 30, p. 175-178.

Willett, S.D., Fisher, D., Fuller, C., En-Chao, Y., and Lu, C.Y., 2003, Erosion rates and orogenic-wedge kinematics in Taiwan inferred from fission-track thermochronometry: Geology, v. 31, p. 945-948.

Willett, S.D., Slingerland, R., and Hovius, N., 2001, Uplift, shortening, and steady state topography in active mountain belts: American Journal of Science, v. 301, p. 455-485.

Willgoose, G., Bras, R.L., and Rodriguez-Iturbe, I., 1991, Results from a new model of river basin evolution: Earth Surface Processes and Landforms, v. 16, p. 237-254.

Wobus, C.W., Hodges, K.V., and Whipple, K.X., 2003, Has focused denudation sustained active thrusting at the Himalayan topographic front?: Geology, v. 31, p. 861-864.

Wolf, R.A., Farley, K.A., and Silver, L.T., 1996, Helium diffusion and low temperature thermochronometry of apatitie: Geochimica et Cosmochimica Act, v. 60, p. 4231-4240.

Wu, C.D., Nelson, K.D., Wortman, G., Samson, S.D., Yue, Y.J., Li, J.X., Kidd, W.S.F., and Edwards, M.A., 1998, Yadong cross structure and South Tibetan Detachment in the east central Himalaya (89 degrees-90 degrees E): Tectonics, v. 17, p. 28-45.

Yeats, R.S., and Lillie, R.J., 1991, Contemporary tectonics of the Himlayan frontal fault system: folds, blind thrusts and the 1905 Kangra earthquake: J. Struct. Geol., v. 13, p. 215-225.

Yeats, R.S., Nakata, T., Farah, A., Fort, M., Mirza, M.A., Pandey, M.R., and Stein, R.S., 1992, The Himalayan frontal fault system: Annales Tectonicae, v. 6, p. 85-98.

Yin, A., and Harrison, T.M., 2000, Geologic evolution of the Himalayan-Tibetan orogen: Annual Review of Earth and Planetary Sciences, v. 28, p. 211-280.

Yin, A., Harrison, T.M., Murphy, M.A., Grove, M., Nie, S., Ryerson, F.J., Feng, W.X., and Le, C.Z., 1999, Tertiary deformation history of southeastern and southwestern Tibet during the Indo-Asian collision: Geological Society of America Bulletin, v. 111, p. 1644-1664.

Yin, A., Harrison, T.M., Ryerson, F.J., Chen, W.J., Kidd, W.S.F., and Copeland, P., 1994, Tertiary structural evolution of the gangdese thrust system, southeastern Tibet: Journal of Geophysical Research-Solid Earth, v. 99, p. 18175-18201.

Yuan, W.M., Hou, Z.Q., Wang, S.C., and Li, S.G., 2002, Apatite fission track dating evidence for tectonic movement of Yarlung Zangbo Thrust Zone: Chinese Science Bulletin, v. 47, p. 765-768.

Zeitler, P.K., 1985, Cooling history of the NW Himalaya, Pakistan: Tectonics, v. 4, p. 127-151.

Zeitler, P.K., Herczig, A.L., McDougall, I., and Honda, M., 1987, U-Th-He dating of apatite: a potential thermochronometer: Geochimica et Cosmochemica Acta, v. 51, p. 2865-2868.

Zeitler, P.K., Koons, P.O., Bishop, M.P., Chamberlain, C.P., Craw, D., Edwards, M.A., Hamidullah, S., Jan, M.Q., Khan, M.A., Khattak, M.U.K., Kidd, W.S.F., Mackie, R.L., Meltzer, A.S., Park, S.K., Pecher, A., Poage, M.A., Sarker, G., Schneider, D.A., Seeber, L., and Shroder, J.F., 2001a,

Crustal reworking at Nanga Parbat, Pakistan: Metamorphic consequences of thermal-mechanical coupling facilitated by erosion: Tectonics, v. 20, p. 712-728.

Zeitler, P.K., Meltzer, A.S., Koons, P.O., Craw, D., Hallet, B., Chamberlain, C.P., Kidd, W.S.F., Park, S.K., Seeber, L., Bishop, M., and Shroder, J., 2001b, Erosion, Himalayan Geodynamics, and the Geomorphology of Metamorphism: GSA Today, v. 11, p. 4-9.

Zhang, P., Molnar, P., and Downs, W.R., 2001, Increased sedimentation rates and grain sizes 2–4 Myr ago due to the influence of climate change on erosion rates: Nature, v. 410, p. 891-897.

Zhao, W., Nelson, K.D., and Team, P.I., 1993, Deep seismic reflection evidence of continental underthrusting beneath southern Tibet: Nature, v. 366, p. 557-559.